



Norwegian University of  
Science and Technology

# PIV measurement of the flow in the vaneless space of a Francis Turbine

**Steinar Gilberg Straume**

Mechanical Engineering

Submission date: July 2018

Supervisor: Pål Tore Selbo Storli, EPT

Co-supervisor: Kristian Sagmo, EPT

Norwegian University of Science and Technology  
Department of Energy and Process Engineering



EPT-M-2018-90

**MASTER THESIS**

for

Student Steinar Straume

Spring 2018

***PIV measurement of the flow in the vaneless space of a Francis Turbine****PIV-målinger av strømningsforhold i omdreiningshulrommet i en Francisturbin***Background**

The flow conditions in a Francis runner is highly important for how the turbine behaves. However, it can be difficult to predict how the flow field is, and experimental investigations are needed. One region where the flow has previously not been investigated in detail in open research is the vaneless space, the region between the outlet of the wicket gates and the inlet of the runner. It is hypothesized that the velocities in this region is root cause on several undesired dynamic phenomena in Francis runners. A measurement technique that can capture details in velocity distribution with respect to both time and space is Particle Image Velocimetry (PIV). It makes use of laser and high-speed cameras to track the movement of seeding particles in the flow, and based on that the data can be postprocessed into velocity vector fields. The Francis test rig at the Waterpower laboratory has recently been modified to allow for PIV measurements in the vaneless space.

**Objective:** Perform measurements and quantify the time resolved flow field in the vaneless space of the Francis test rig at the Waterpower laboratory.

**The following tasks are to be considered:**

1. Literature study on the flow in the vaneless space and PIV measurements techniques
2. Develop a measurement campaign for PIV measurements in the Francis test rig at the Waterpower laboratory
3. Execute the measurement campaign
4. Document the measurements and the postprocessing of image data for determination of the velocity field
5. If the student goes to Nepal for an excursion, earlier and further work will be presented as a publication and presented at the conference; 8<sup>th</sup> International symposium on Current Research in Hydraulic Turbines (CRHT-VIII) at Kathmandu University in March 2018

-- ” --

Within 14 days of receiving the written text on the master thesis, the candidate shall submit a research plan for his project to the department.

When the thesis is evaluated, emphasis is put on processing of the results, and that they are presented in tabular and/or graphic form in a clear manner, and that they are analyzed carefully.

The thesis should be formulated as a research report with summary both in English and Norwegian, conclusion, literature references, table of contents etc. During the preparation of the text, the candidate should make an effort to produce a well-structured and easily readable report. In order to ease the evaluation of the thesis, it is important that the cross-references are correct. In the making of the report, strong emphasis should be placed on both a thorough discussion of the results and an orderly presentation.

The candidate is requested to initiate and keep close contact with his/her academic supervisor(s) throughout the working period. The candidate must follow the rules and regulations of NTNU as well as passive directions given by the Department of Energy and Process Engineering.

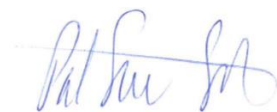
Risk assessment of the candidate's work shall be carried out according to the department's procedures. The risk assessment must be documented and included as part of the final report. Events related to the candidate's work adversely affecting the health, safety or security, must be documented and included as part of the final report. If the documentation on risk assessment represents a large number of pages, the full version is to be submitted electronically to the supervisor and an excerpt is included in the report.

Pursuant to "Regulations concerning the supplementary provisions to the technology study program/Master of Science" at NTNU §20, the Department reserves the permission to utilize all the results and data for teaching and research purposes as well as in future publications.

The final report is to be submitted digitally in DAIM. An executive summary of the thesis including title, student's name, supervisor's name, year, department name, and NTNU's logo and name, shall be submitted to the department as a separate pdf file. Based on an agreement with the supervisor, the final report and other material and documents may be given to the supervisor in digital format.

- Work to be done in lab (Water power lab, Fluids engineering lab, Thermal engineering lab)  
 Field work

Department of Energy and Process Engineering, 15. January 2018



---

Pål-Tore Storli  
Academic Supervisor

Co-supervisor: Kristian Sagmo

## Abstract

As the demand for green energy increases, so does the investment into clean energy sources. Especially the amount of solar and wind energy produced are growing at a rapid pace. While their cost is decreasing, they remain what is referred to as unreliable energy sources. This might emphasise hydropower's role as a power grid balancer, forcing turbines to operate at transient conditions. Both in the form of reoccurring start-stop cycles as well as part-load operations.

The most frequently used hydropower turbine, the Francis turbine, is sensitive outside of its design condition. Not only do minor changes quickly reduce efficiency, it also has a history of causing fatigue, noise and cracks in internal components. Several of these issues originate from pressure pulsations and vibrations stemming from distinct regions of the turbine. Among these are the *Rotor-Stator Interaction (RSI)* and shedding frequency.

There has previously been performed both pressure measurements and simulations throughout the Francis rig in the Waterpower Laboratory at NTNU. The area of interest in this thesis is the vaneless space, located between the guide vanes and turbine runner. The velocity field in the vaneless space was measured using *Particle Image Velocimetry (PIV)* equipment.

There is currently no available research using PIV equipment in this section of a Francis turbine. Consequently, a major part of this thesis was designing a full equipment setup procedure, as well as a measurement campaign. The solutions used is showcased throughout this project paper.

The velocity field was successfully measured for a range of guide vane openings, but due to time constraints the focus of this thesis is the *Best Efficiency Point (BEP)*. For this operating condition the velocity field was compared to computational fluid dynamics simulations. Additionally, both RSI and shedding frequency was identified in the vaneless space. A clear relation between these fluid phenomena was not found for BEP conditions.

**Keywords:** *NTNU, Hydropower, Francis turbine, Vaneless space, PIV, RSI, vortex shedding*

## Sammendrag

Med den stadig økende etterspørselen av grønn energi er investeringen i ren energi rekordhøy. Spesielt har mengden produsert sol- og vindenergi økt drastisk. Selv om kostnadene synker, fortsetter de å være upålitelige energikilder. Dette vil antakelig forsterke vannkraften sin posisjon som balanseblokk i kraftnettverket, noe fører til varierende driftstilstander. Både i form av hyppige start-stop sykluser i tillegg til drift under del-last.

Den mest bruke vannkraft turbinen, Francis turbinen, er sensitiv til forandringer i driftstilstander. Ikke bare fører små endringer fort til redusert effektivitet, det har også historisk sett ført til utmattelse, støy og sprekker i indre komponenter. Flere av disse problemene antas å stamme fra trykkpulsasjoner og vibrasjoner. Blant disse rotor-stator interaksjonen (*RSI*) og felling av virvler.

Det har tidligere blitt utført både trykkmålinger og simuleringer gjennom store deler av Francis-riggen i vannkraftslaboratoriet på NTNU. Interesseområdet i denne oppgaven er seksjonen mellom ledeskovlene og turbinbladene. Hastighetsfeltet i denne delen blir målt ved å bruke *Particle Image Velocimetry (PIV)*.

There er foreløpig ikke tilgjengelige studier som bruker PIV utstyr i denne seksjonen. Som følge av dette vil store deler av denne oppgaven beskrive oppsett og fremgangsmåte når man måler med PIV instrumenter. Løsningene som har blitt funnet og brukt er vist gjennom denne masteroppgaven.

Hastighetsfeltet ble målt for en rekke ledeskovlån timer, men på grunn av lite tid har *Best Efficiency Point (BEP)* fått hovedfokus. For denne driftstilstanden har hastighetsfeltet blitt sammenlignet med CFD simuleringer. I tillegg har både RSI og felling av virvler blitt identifisert i interesseområdet. Det ble ikke funnet en klar sammenheng mellom de to for BEP driftstilstanden.

**Nøkkelord:** NTNU, Hydropower, Francis turbine, Vaneless space, PIV, RSI, vortex shedding

## Acknowledgements

I would like to thank Pål-Tore Storli for his supervising throughout this year at the Waterpower Laboratory at NTNU. From creating an exciting thesis to providing equipment for the lab all his support has been hugely appreciated.

I would also like to thank Magne Bolstad, Chirag Trivedi and Einar Agnalt for their valuable assistance. The guys in the lab, especially Halvor Haugvik and Trygve Opland, has provided loads of support and knowledge which the experiment could not have been completed without.

A special thanks to my co-supervisor and lab companion Kristian Sagmo. Not only for the long hours and weekends put into this project, but also for his experience and knowledge, which has been invaluable.

Finally, I am grateful to the Waterpower Laboratory at NTNU for providing the opportunity to apply theoretical knowledge while working with high-end equipment.

# Table of contents

|  |             |
|--|-------------|
| <b>ABSTRACT</b> .....  | <b>I</b>    |
| <b>SAMMENDRAG</b> .....                                      | <b>II</b>   |
| <b>ACKNOWLEDGEMENTS</b> .....                                | <b>III</b>  |
| <b>TABLE OF CONTENTS</b> .....                               | <b>IV</b>   |
| <b>TABLE OF FIGURES</b> .....                                | <b>VI</b>   |
| <b>NOMENCLATURE</b> .....                                    | <b>VIII</b> |
| <i>Symbol:</i> .....   | <i>viii</i> |
| <i>Description:</i> .....                                    | <i>viii</i> |
| <i>Units:</i> .....  | <i>viii</i> |
| <b>1: INTRODUCTION</b> .....                                 | <b>1</b>    |
| 1.1: BACKGROUND.....   | 1           |
| 1.2: OBJECTIVE .....   | 2           |
| <b>2: THEORY</b> .....                                       | <b>3</b>    |
| 2.1: FRANCIS TURBINE.....                                    | 3           |
| 2.2: FLOW OVER FOILS .....                                   | 4           |
| 2.2.1: <i>Significant terms</i> .....                        | 5           |
| 2.2.2: <i>Foil basics</i> .....                              | 7           |
| 2.2.3: <i>Vortex shedding</i> .....                          | 8           |
| 2.2.4: <i>Von Kàrmàn vortex street</i> .....                 | 9           |
| 2.2.4: <i>Shedding frequency</i> .....                       | 10          |
| 2.2.5: <i>Lock-in</i> .....                                  | 11          |
| 2.3: SPECIFIC SHEDDING FREQUENCY AND STROUHAL NUMBER.....    | 12          |
| 2.3.1: <i>Leading edge</i> .....                             | 12          |
| 2.3.2: <i>Trailing edge</i> .....                            | 13          |
| 2.4: ROTOR-STATOR INTERACTION.....                           | 16          |
| 2.6 FOURIER TRANSFORMATION.....                              | 19          |
| 2.7 NYQUIST SAMPLING .....                                   | 20          |
| 2.8 ERROR AND UNCERTAINTY .....                              | 21          |
| <b>3: PARTICLE IMAGE VELOCIMETRY</b> .....                   | <b>22</b>   |
| 3.1: FUNDAMENTALS .....                                      | 22          |
| 3.2: A CLOSER LOOK .....                                     | 23          |
| 3.2.1: <i>Interrogation area</i> .....                       | 23          |
| 3.2.2: <i>Seeding</i> .....                                  | 24          |
| 3.2.3: <i>Laser and light sheet</i> .....                    | 24          |
| 3.2.4: <i>Optic</i> .....                                    | 25          |
| 3.3: CALIBRATION.....  | 25          |
| 3.3.1 <i>Particle shift</i> .....                            | 28          |
| 3.3.1 <i>Double frame imaging and pulse separation</i> ..... | 29          |
| 3.3.2 <i>Camera lens characteristics</i> .....               | 30          |
| 3.3.3 <i>Pre-processing</i> .....                            | 30          |
| 3.3.4: <i>Postprocessing</i> .....                           | 31          |
| 3.4: UNCERTAINTY AND ERROR IN PIV MEASUREMENTS .....         | 33          |
| <b>4. FRANCIS SETUP</b> .....                                | <b>35</b>   |
| 4.1 TEST SECTION.....  | 35          |
| 4.2 PIV EQUIPMENT.....                                       | 36          |
| 4.3 PARTICLE FEEDING.....                                    | 38          |
| 4.4 LASER OVERLAP .....                                      | 40          |
| 4.5 EXPERIMENTAL SETUP .....                                 | 41          |



|   |            |
|---|------------|
| 4.6 LASER SHEET / PLEXIGLAS INTERACTION .....               | 42         |
| 4.7 CALIBRATION .....                                       | 44         |
| 4.8 OPERATING PARAMETERS AND TEST PROCEDURE.....            | 47         |
| 4.8.1 PIV pre-processing settings .....                     | 49         |
| 4.8.2 PIV post-processing settings .....                    | 50         |
| 4.9 MEASURING EQUIPMENT AND UNCERTAINTY .....               | 51         |
| 4.9.1 Quantified uncertainty of operational parameters..... | 52         |
| 4.9.2 Quantified uncertainty for PIV .....                  | 53         |
| 4.9.3 Repeatability .....                                   | 54         |
| <b>5. RESULTS AND DISCUSSION .....</b>                      | <b>55</b>  |
| 5.1 VELOCITY FIELD.....                                     | 55         |
| 5.2 RSI.....  | 57         |
| 5.3 GUIDE VANE SHEDDING FREQUENCY .....                     | 59         |
| 5.4 DISCUSSION.....   | 61         |
| <b>6. CONCLUSION.....</b>                                   | <b>62</b>  |
| <b>7. FURTHER WORK.....</b>                                 | <b>63</b>  |
| <b>BIBLIOGRAPHY .....</b>                                   | <b>64</b>  |
| <b>APPENDIX A: PARTICLE FEEDING.....</b>                    | <b>I</b>   |
| <b>APPENDIX B: REPEATABILITY CHECK .....</b>                | <b>IV</b>  |
| <b>APPENDIX C: MEASUREMENT RESULTS.....</b>                 | <b>VI</b>  |
| <b>APPENDIX D: RISK ASSESSMENT .....</b>                    | <b>VII</b> |

# Table of Figures

|   |    |
|---|----|
| Figure 1: Overview of the main components in a Francis turbine. Geometry from Francis-99 workshop [15] .....  | 3  |
| Figure 2: streamlines around a horizontal plate, cylinder and vertical plate [17].....  | 4  |
| Figure 3: Illustration of the induced angular velocity on two separate points, from a simple line vortex centred at the origin. ....  | 6  |
| Figure 4: Common foil terms.....  | 7  |
| Figure 5: Flow separation and wakes produced by the hydrofoils at various angles of attack. These simulations are done for $Re = 750\,000$ . Adapted from [21] .....  | 7  |
| Figure 6: Flow around cylinders for increasing Reynolds numbers. ....   | 8  |
| Figure 7: The effect of Reynolds number on Kàrmàn vortex street for flow past cylinder [23] .....   | 9  |
| Figure 8: Measured Strouhal number behind a cylinder for different $Re$ [24] .....  | 10 |
| Figure 9: Graph showcasing $F_s$ , $F_n$ and $St$ for increasing flow velocity.....   | 11 |
| Figure 10: Sketch of rectangular, oval, oblique truncated and Donaldson TE geometry from top left to bottom right, respectively. ....   | 13 |
| Figure 11: Compilation of relative amplitude for different TE geometries [29] .....   | 14 |
| Figure 12: vibration amplitude measured versus $Re$ /velocity for three distinct TE geometries. [29]...   | 15 |
| Figure 13: Shedding frequency measured against $Re$ /velocity [29] .....  | 15 |
| Figure 14: Wake trajectory for three different guide vane angles. [31].....   | 16 |
| Figure 15: Left: Upstream velocity effect caused by the turbine blades. Middle: downstream velocity effect of guide vanes. Right: combination of the two. Adapted from [32] .....   | 16 |
| Figure 16: Static pressure distribution around stay vanes and guide vanes, neglecting runner [9] .....  | 17 |
| Figure 17: Normalized pressure oscillations at a point in the vanless space. Comparison of two turbulence model and experimental data. X-axis represents angle of runner blade. [9] .....   | 18 |
| Figure 18: A sample signal is turned into two single sinusoidal waves [38] .....  | 19 |
| Figure 19: Reproduced wave (black stippled) compared to the original signal (red) for 5 sample points (blue circles).....   | 20 |
| Figure 20: Main components of PIV setup [42] .....  | 22 |
| Figure 21: A picture and its corresponding interrogation areas. Adapted from [43] .....   | 23 |
| Figure 22: Interrogation areas, the right image has 4 times more IAs than the left one. [46].....   | 25 |
| Figure 23: Light sheet focusing [46].....   | 26 |
| Figure 24: Particles in and out of focus. In focus to the right. [46] .....   | 27 |
| Figure 25: In-plane motion of particles for two different IA sizes. Adapted from [42] .....   | 28 |
| Figure 26: Vector fields for different particle shifts. [46].....   | 28 |
| Figure 27: Distinction between camera frequency and pulse separation.....   | 29 |
| Figure 28: Raw image (left) compared to pre-processed image (right).....  | 30 |
| Figure 29: Left: Overview of possible new positions (black arrows) for a single particle, and actual particle movement (green arrows). Middle: Possible movements for one point. Right: Sum of all possible movements for every particle. [42] .....  | 31 |
| Figure 30: Window shifted based on previous vector calculation [42].....  | 32 |
| Figure 31: Left: Error as a function of background noise for various IAs. Middle: Cross correlation plane of particle images with background noise. Right: Cross correlation plane for the same images with background noise filtered out. Adapted from [52] [56] .....   | 33 |
| Figure 32: top left: Error due to out-of-plane motion for particle pixel size 1.5. top right: Error due to out-of-plane motion for particle pixel size 2.5. bottom left: Error caused by a constant out-of-plane motion of 10% varying with seeding density. bottom right: Error caused by a constant out-of-plane motion of 10% varying with particle size. [52] ..... | 34 |
| Figure 33: Fluid trajectory in the closed loop. Green from the pump to the turbine. Red from the turbine back to the pump.....  | 35 |
| Figure 34: Test section with its main components .....  | 37 |

|  |    |
|--|----|
| Figure 35: Feeding flow rate for various pressure and flowrates.....   | 38 |
| Figure 36: Burn marks for; A) laser 1 – 50% intensity, B) laser 2 – 50% intensity, C) laser 1 – 70% intensity, D) laser 2 – 70% intensity.....     | 40 |
| Figure 37: Laser and camera view, from the outside(left) and inside(right). .....  | 41 |
| Figure 38: Camera windowpane to the left, old and new guide vane to the right. ....  | 42 |
| Figure 39: Laser sheet for 4 degrees (left) and 14 degrees(right) guide vane openings. the marked FOV is an approximation for the 100mm lens. .... | 42 |
| Figure 40: FOV 2, using 50mm lens.....   | 43 |
| Figure 41: Calibration device and overlay pattern used in the Francis turbine.....   | 44 |
| Figure 42: Cross section view of the turbine where the interchangeable guide vanes have been replaced by the calibration device.....               | 45 |
| Figure 43: Attachment of the calibration device seen from the top of the Francis turbine .....   | 45 |
| Figure 44: Pre-calibrated image (left) and corrected image (right).....  | 46 |
| Figure 45: Calibration boxes mounted on the camera and laser sheet optic.....  | 46 |
| Figure 46: Simulated average velocity at BEP around guide vanes in our AOI.....  | 49 |
| Figure 47: A sample velocity field at BEP for IAs of 48x48, 32x32,24x24 and 16x16 from top left to bottom right.....                               | 50 |
| Figure 48: Pressure transducer ( $P_d$ ) measuring points along with indicated head region $H$ . ....  | 51 |
| Figure 49: Average velocity at BEP from PIV (left) simulated average velocity(right).....  | 55 |
| Figure 50: Cross wake velocity vectors .....   | 56 |
| Figure 51: Power spectrum for a point located at $x=-5\text{mm}$ , $y=7.5\text{mm}$ .....  | 57 |
| Figure 52: Power spectrum of entire FOV for static frequency = 166.64Hz .....  | 58 |
| Figure 53: Side by side comparison of average velocity field for for 4° (left) and 14°(right) vane opening. ....                                   | 58 |
| Figure 54: Two ways of showcasing vorticity for the same Instantaneous velocity field.....   | 59 |
| Figure 55: Vortex shedding frequency measured at $x=15\text{mm}$ , $y=10\text{mm}$ .....   | 60 |
| Figure 56: Vortex shedding frequency measure at $x=5\text{mm}$ , $y=10\text{mm}$ .....   | 60 |

## Nomenclature

| Symbol:        | Description:                                   | Units:      |
|----------------|--|-------------|
| $ds$           | Particle shift                                 | [pixels]    |
| $F_D$          | Drag force                                     | [ N ]       |
| $F_L$          | Lift force                                     | [ N ]       |
| $f_B$          | Guide vane passing frequency                   | [Hz]        |
| $f_n$          | Natural frequency of structure                 | [Hz]        |
| $f_{max}$      | Highest relevant signal frequency              | [Hz]        |
| $f_{GV}$       | Turbine blade passing frequency                | [Hz]        |
| $f_s$          | Vortex shedding frequency                      | [Hz]        |
| $f_{sampling}$ | Sampling frequency                             | [Hz]        |
| $g$            | Gravitational constant                         | [ $m/s^2$ ] |
| $H$            | Potential head                                 | [ m ]       |
| $IA_{size}$    | Interrogation area size                        | [pixels]    |
| $L$            | Characteristic length                          | [ m ]       |
| $N$            | Sample size                                    | [ - ]       |
| $P_i$          | Pressure at given location                     | [kPa]       |
| $Q$            | Fluid flow                                     | [ $m^3/s$ ] |
| $r$            | Distance from origin                           | [ - ]       |
| $Re$           | Reynolds number                                | [ - ]       |
| $S_{dev}$      | Standard deviation of a sample size N          | [ - ]       |
| $S_i$          | Standard deviation from a single error source  | [ - ]       |
| $S_{Tot}$      | Total standard deviation for a single variable | [ - ]       |
| $St$           | Strouhal number                                | [ - ]       |
| $t$            | Thickness                                      | [mm]        |
| $\Delta t$     | Time difference                                | [ s ]       |
| $U$            | Inlet flow                                     | [ $m/s$ ]   |
| $u_\theta$     | Angular velocity                               | [ $rad/s$ ] |
| $V_i$          | Velocity at given location                     | [ $m/s$ ]   |

|           |                           |             |
|-----------|---------------------------|-------------|
| $X$       | Value of sample N         | [ - ]       |
| $\bar{x}$ | Mean value of all samples | [ - ]       |
| $Z_B$     | Number of turbine blades  | [ - ]       |
| $Z_{GV}$  | Number of guide vanes     | [ - ]       |
| $\rho$    | Density                   | $[kg/m^3]$  |
| $\mu$     | Dynamic viscosity         | $[kg/s\ m]$ |
| $\Gamma$  | Circulation               | [ - ]       |

# 1: Introduction

## 1.1: Background

Hydropower has an extensive history, with the ancient Greeks harnessing water to grind wheat more than 2000 years ago. The systems used back then obviously looked a lot different, but some of the same principles still applied. Hydropower turbines more reminiscent of those used today started appearing during the late 1700s, and in 1849 the first Francis turbine was created. Even though the name has stayed the same since then, the turbine has undergone a lot of both minor and major changes. [1]

Hydropower has long reigned supreme as the cheapest energy source available given the appropriate landscape [2]. However, the room for improvements in hydro machinery are limited due to the technology being so mature. In comparison, the cost of solar and wind energy has dropped 80% and 40%, respectively, since 2009 [3]. Even though hydropower holds an obvious advantage in terms of reliability, keeping the turbine efficiency high and reducing maintenance cost will be crucial as solar and wind energy become more competitive.

In Norway the amount of electricity produced was 134 *TWh* for 2013, where hydropower was responsible for 96% of the entirety. This production volume was split between 1476 power plants [4]. When considering numbers of this magnitude it becomes apparent that even minor improvements can lead to major benefits.

Water turbines are designed to operate optimally for specific conditions, and prefer being run at a *steady state*, which is when variables stay the same as time passes. The demand for energy, however, varies both throughout the day and the seasons. In addition, hydropower plants tend to be used in combination with less reliable power sources to smoothen out grid parameters. This means the turbines cannot constantly stay at the optimal operating conditions. [5]

In this thesis we will focus on the Francis turbine, which has very high peak efficiency, but also high sensitivity towards changes in its surroundings. [6] When forced to operate for numerous off-design conditions the likelihood of hitting unwanted and even damaging frequencies increase. Pressure pulsations stemming from turbine blades and guide vanes has been the root cause of cracks and premature fatigue in multiple parts of Francis turbines. [7]

[8] It has been established that transient operating conditions in general put a heavy toll on Francis turbines [9].

## 1.2: Objective

The goal for this thesis is to find an effective way to utilize *Particle Image Velocimetry (PIV)* equipment in the vaneless space of a Francis turbine, which may provide a better understanding of the flow and pressure pulsations in this region. No previous research using PIV measurements in the vaneless space of a Francis turbine have been found. There are, however, a few studies conducted using PIV equipment on the draft tube of a Francis rig.

The making of a proper PIV setup for the vaneless space is challenging on its own, though a suggested setup has previously been drafted by Pål-Tore Storli and processed by Magne T. Bolstad, who also performed a site acceptance test. [10]

The Waterpower Laboratory at NTNU has a scaled model (1:5.1) of the Francis turbines operating at Tokke powerplant. This is to be used for the PIV measurements. There has previously been conducted studies using pressure gauges throughout this Francis turbine, as well as simulated results using *Computational Fluid Dynamics (CFD)*.

Acquiring accurate CFD results in such a complex system is difficult and time consuming. One of the, thus far, two workshops of the Francis-99 project have been devoted to improving simulations both for steady state and transient operating conditions, specifically on this rig. This means that both measured and simulated results are readily available for comparison. [11]

## 2: Theory

### 2.1: Francis Turbine

The Francis turbine is the most common of the hydraulic turbines, being responsible for approximately 60% of the hydropower generated worldwide [12]. They normally operate with head values  $H \in [30\text{m}, 750\text{m}]$  [13].

In hydro powerplants the water typically starts in a reservoir and run through a penstock until it reaches the spiral casing. The spiral casing is illustrated below and is designed to distribute the water evenly around the turbine. The fluid then travels past the stay vanes which has both its position and angle fixed. Their primary function is to steer the fluid toward the runner while converting some of the pressure to kinetic energy.

The second layer of vanes, called the guide vanes, have adjustable angles. In addition to directing the fluid on to the runner at an appropriate angle, they have the task of increasing or decreasing the flow rate  $Q$  through the turbine, as well as adjusting the turbine load [14].

These vanes can be depicted as a cascade of foils, commonly called the wicket gate. Figure 1 shows an overview of the Francis turbine used in the waterpower laboratory at NTNU.

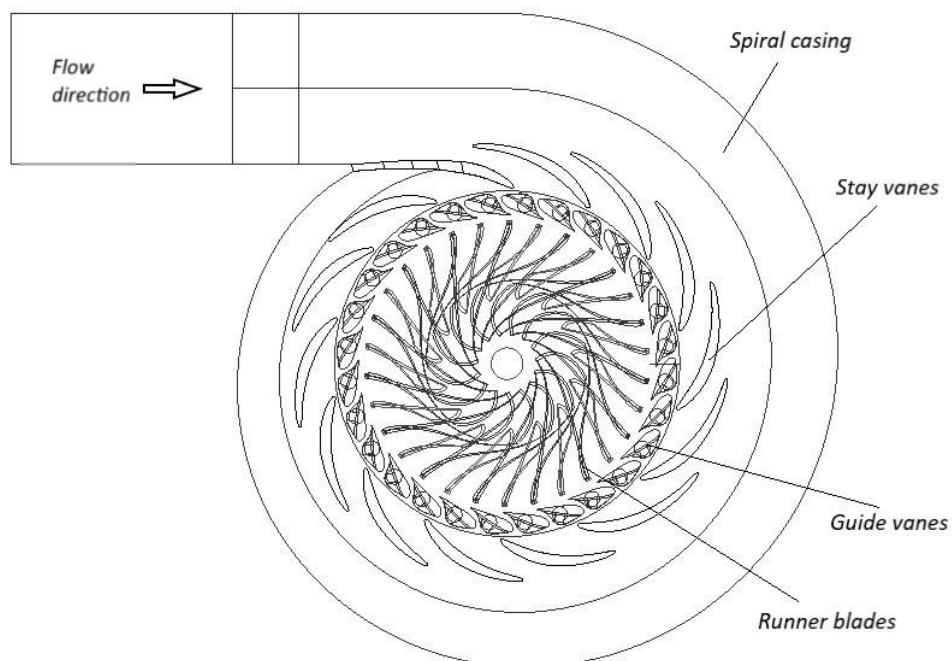


**FIGURE 1: OVERVIEW OF THE MAIN COMPONENTS IN A FRANCIS TURBINE. GEOMETRY FROM FRANCIS-99 WORKSHOP [15]**



Between the guide vanes and the runner blades there is a narrow gap referred to as the vaneless space. The width of this space is related to the angle of the guide vanes, and therefore also the flow rate. As the guide vanes open and the flow rate increases, their *trailing edge (TE)* move closer to the runner, causing the vaneless space to become narrower.

## 2.2: Flow over foils

It becomes apparent that the fluid has several hurdles to pass on its path through the Francis turbine, almost all of which affect the flow to some extent. Depending on the velocity, pressure and viscosity of the fluid, as well as the shape and roughness of objects it passes, these effects vary drastically. The figure below shows the streamlines and stream separation around some simple shapes. An area of recirculating and backflows occur where the streamlines no longer tightly follow the body, called wakes. Wakes are characterized by regions with altered velocities and pressure. [16]

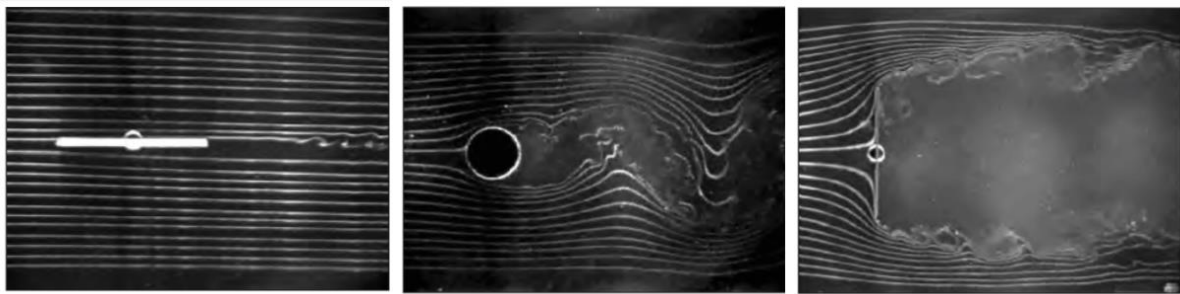


**FIGURE 2: STREAMLINES AROUND A HORIZONTAL PLATE, CYLINDER AND VERTICAL PLATE [17]**

Throughout this subsection the most influential factors will be touched upon, starting with some of the key words commonly used when trying to explain fluid phenomenon.

## 2.2.1: Significant terms

### 2.2.1.1: Reynolds number

For viscous flow the most influential parameter is the Reynolds number, defined as

$$Re = \frac{\rho UL}{\mu} \quad (2.1)$$

Here  $\rho$  represents the fluid density,  $U$  the velocity,  $L$  is a characteristic length and  $\mu$  is the dynamic viscosity. The Reynolds number describes to which degree a flow is laminar or turbulent, where higher values of  $Re$  correspond to more turbulence.

For flow around objects a laminar flow means that there is little or no flow separation. This means that from equation (2.1) we can see that for a given geometry and constant fluid density, a sufficiently low velocity or high viscosity will ensure that the flow follows the body. [18] Streamlined geometries, such as aerofoils or hydrofoils allow for fully attached flow at far higher Reynolds number than bluff bodies.

### 2.2.1.2: Surface roughness

Due to friction, higher surface roughness will in general produce more drag on bodies, this holds true for nearly all streamlined bodies. A side effect of higher roughness is, however, that flow more easily stay attached to surfaces. For blunt bodies, or bodies that otherwise would have experienced flow separation, a rougher surface can lead to a *decrease* in drag as it will result in smaller wakes. The effect of surface roughness on a body could therefore change depending on the amount of separation. [19]

### 2.2.1.3: Vortex line

When creating streamlines in fluid dynamics one of the main “building blocks” is the line vortex. Let us first look at a lone vortex with no outside influences. In figure 3 a cylindrical coordinate system, with the vortex centre located at the origin is showcased.

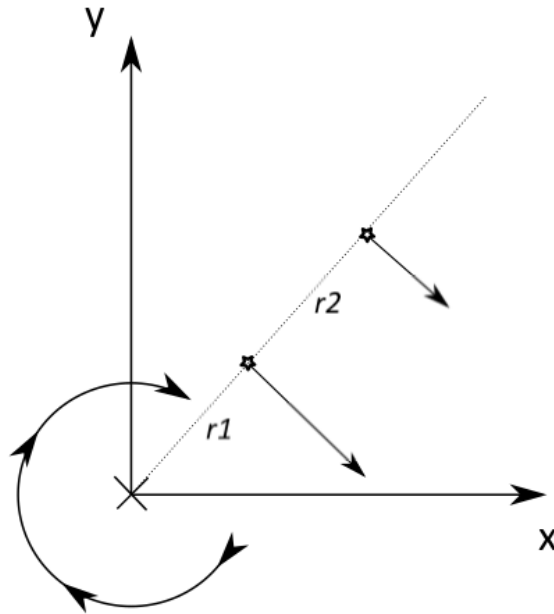


**FIGURE 3: ILLUSTRATION OF THE INDUCED ANGULAR VELOCITY ON TWO SEPARATE POINTS, FROM A SIMPLE LINE VORTEX CENTRED AT THE ORIGIN.**

The velocity induced by this type of vortex is always 0 in the radial direction, while the induced angular velocity  $u_\theta$  is defined as:

$$u_\theta = \frac{\Gamma}{2\pi r} \quad (2.2)$$

In equation (2.2)  $\Gamma$  is called the circulation or vortex strength, while  $r$  is the distance from the origin. This causes the induced velocity  $u_\theta \rightarrow \infty$  as we approach the origin. In other words, the effect from the vortex is stronger the closer we are. This function becomes discontinuous as we move through the centre of the line vortex, making it an inaccurate representation of real flow for small values of  $r$ . The reason for this is viscosity not being accounted for.  $\Gamma$  is defined as

$$\Gamma = 2\pi K \quad (2.3)$$

Where  $K$  represents the strength of the vortex. [20]

## 2.2.2: Foil basics

For foils, fluid flows will typically have no problem staying attached at the *leading edges (LE)*, due to pressure increasing from compression. At the *trailing edges (TE)* however, where the bodies narrow in, low-pressure regions appear. In these regions the flow is more likely to separate, and the streamlines will no longer tightly follow the body. A similar high- and low-pressure region can be seen on the lower and upper parts, respectively, of non-symmetrical foils. [19]

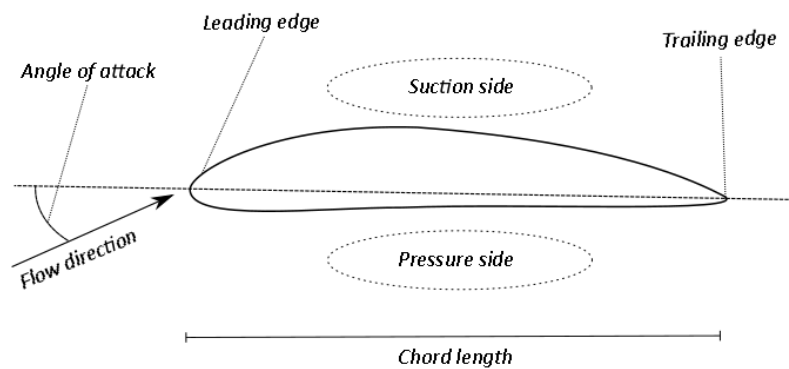


**FIGURE 4: COMMON FOIL TERMS**

The magnitude of the induced wakes will be highly dependent on the direction of the flow relative to the chord of the foil. The term *angle of attack*, illustrated in figure 4, is used to define this discrepancy. Some simulated examples for increasing angles can be seen in the figure below, where we can see that the flow separates from the low-pressure side. In this figure *LSB* is used as an acronym for laminar separation bubble, which at the TE can be detected even for the plane foil.

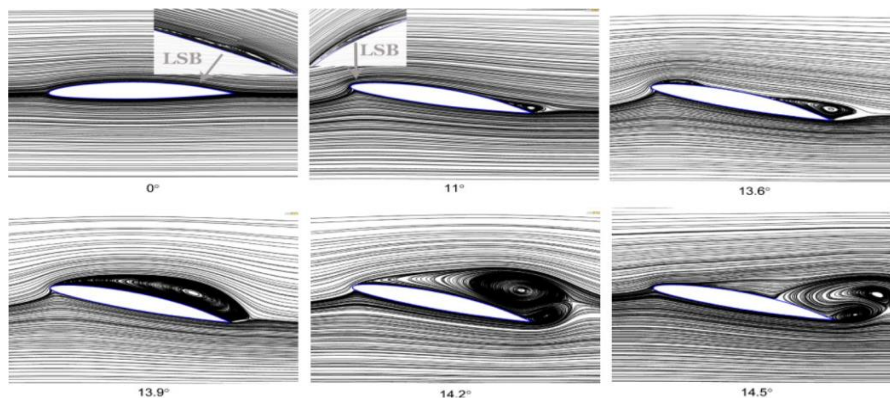


**FIGURE 5: FLOW SEPARATION AND WAKES PRODUCED BY THE HYDROFOILS AT VARIOUS ANGLES OF ATTACK. THESE SIMULATIONS ARE DONE FOR  $Re = 750\,000$ . ADAPTED FROM [21]**

### 2.2.3: Vortex shedding

As seen in figure 5 vortices start forming in regions where the flow is unable to stay attached to the body. Due to the velocity inside the wake being lower than outside, the free velocity stream crosses into the wake, accumulating vorticity at the junction points. These new velocity vectors will amplify the already existing perturbations [22]. Below is a sketch of how the flow around a cylinder evolve as the Reynolds number increase.

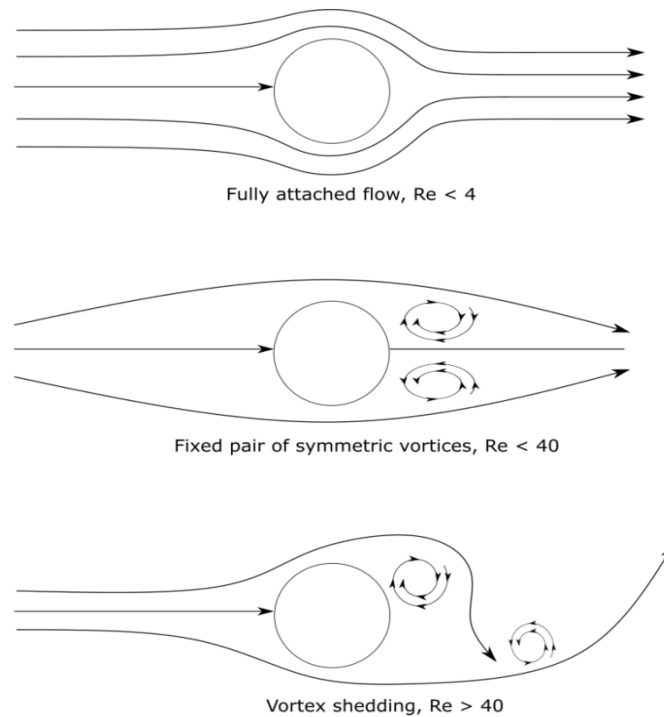


**FIGURE 6: FLOW AROUND CYLINDERS FOR INCREASING REYNOLDS NUMBERS.**

The imbalances in the flow causes the induced vortices to peel of the body, one side at the time. This means that if trying to simulate vortex shedding using a completely homogenous flow, it might yield the wrong result, or at the very least need more iterations to reach the correct solution.

## 2.2.4: Von Kàrmàn vortex street

A phenomenon called Kàrmàn vortex street appear over a wide range of Reynold numbers. The bodies start shedding vortices from the top and bottom in an alternating pattern, illustrated in figure 6.

For cylinders Von Kàrmàn vortex street can be detected for  $Re$  values as low as 40, all the way up to  $10^7$ . While exemplified using cylinders, this pattern is consistent for various shapes, even non-symmetrical ones. [22] [23]

As previously mentioned, vortices induce a velocity which is higher the closer you are to their centre. This means that for shedding bodies, a created vortex will exert a force on the body it was made by, gradually fading as it travels downstream. As illustrated in figure 6 the vortices being shed from the top and the bottom circulate in opposite directions. A ramification of this is that the shedding bodies will experience oscillating forces acting on them. This is of interest because it may lead to vibrations.

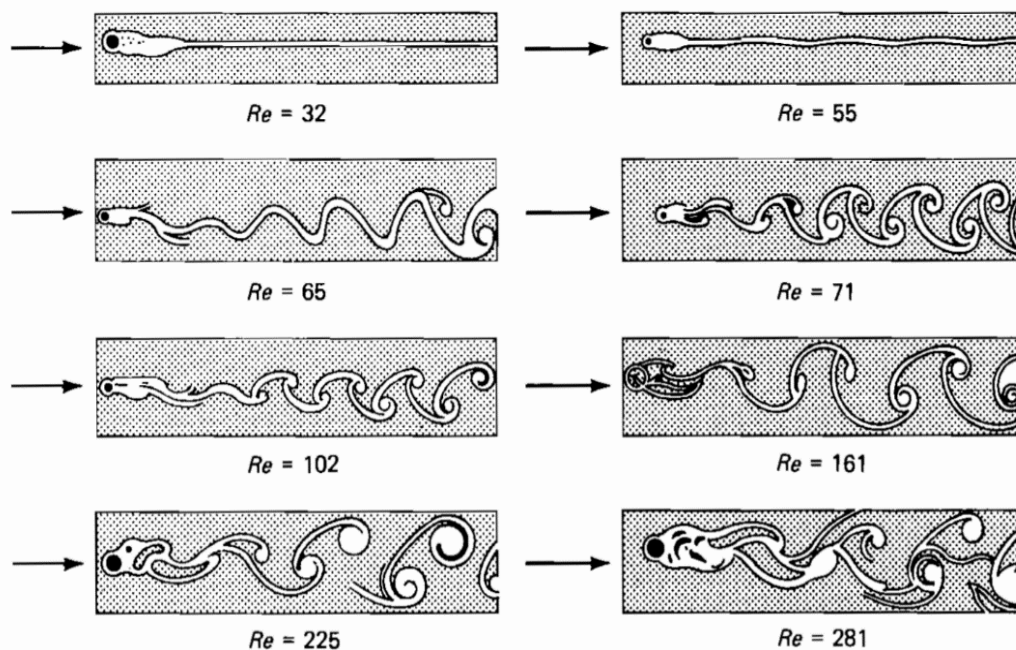


FIGURE 7: THE EFFECT OF REYNOLDS NUMBER ON KÀRMÀN VORTEX STREET FOR FLOW PAST CYLINDER [23]

### 2.2.5: Shedding frequency

The vortex shedding frequency is described by the dimensionless Strouhal number [ $St$ ], which has the definition:

$$St = \frac{f_s L}{U} \quad (2.4)$$

Where  $f_s$  is the shedding frequency,  $L$  a characteristic length, and  $U$  is velocity of the uniform flow. The Strouhal number plotted against the Reynolds number for a cylinder can be seen in figure 8. The highest and lowest values of the data spread is caused by smooth and rough surfaces, respectively. As we can see  $St \sim 0.2$  for a wide range of Reynolds numbers. A quick reorganizing of (4) for this value of  $St$  gives us:

$$f_s = St \frac{U}{L} = 0.2 \frac{U}{L} = \frac{U}{5L} \quad (2.5)$$

Meaning that one shedding cycle happens for each 5 diameters the uniform flow travels, which is more relatable. [23]

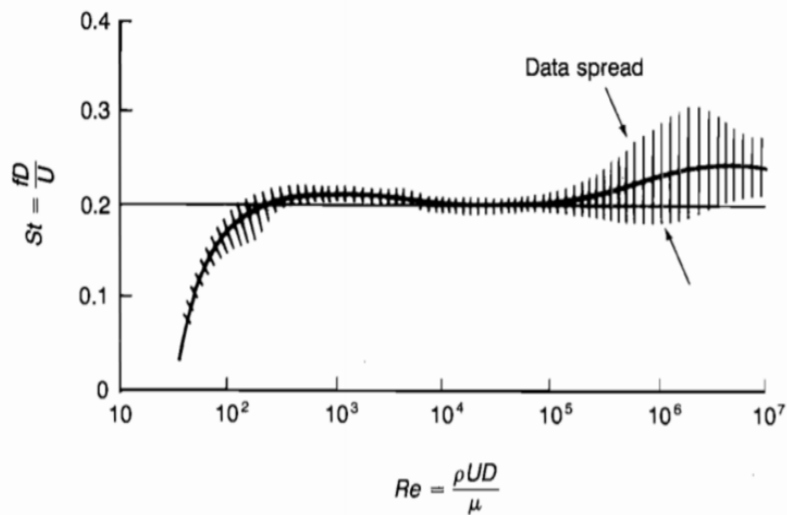


FIGURE 8: MEASURED STROUHAL NUMBER BEHIND A CYLINDER FOR DIFFERENT RE [24]

## 2.2.6: Lock-in

As mentioned earlier the induced vortices has an impact on the forces working on the body that created them. A sufficiently elastic structure will also vibrate with its own natural frequency  $f_n$ . When the frequency of the vortex shedding, and the natural frequency of the body are equal, we have what is called *lock-in*. In this case we will have a loop amplifying itself. The vibration of the body will influence both the strength and the frequency of the induced vortices, which in turn will make the amplitude of the oscillating forces working on the body greater. This is one of the main reasons for what is called *vortex-induced vibrations*. Operating at conditions where lock-in occurs has been shown to cause premature fatigue and cracks at several occasions. [8]

It is also of note that  $f_s$  can latch onto the natural frequency if in proximity. Meaning the body and the vortices may converge to a lock-in even if the frequencies are not exactly synchronized initially. This is sketched in figure 9. Strouhal's law is valid as long as there is no lock-in, during which the shedding frequency will flatline until the lock-off region. [25] [26]

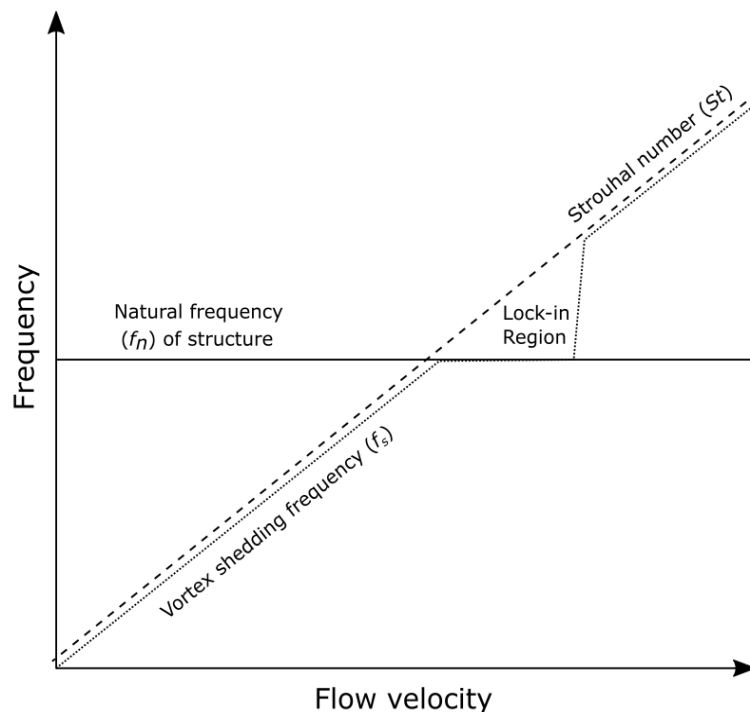


FIGURE 9: GRAPH SHOWCASING  $f_s$ ,  $f_n$  AND  $St$  FOR INCREASING FLOW VELOCITY



## 2.3: Specific shedding frequency and Strouhal number

### 2.3.1: Leading edge

Numerous studies have been conducted for vortex shedding induced by elongated bodies. Zachary J. Taylor examined, among other factors, the influence of the leading edge on the shedding frequency [27]. It is here shown that several LE geometries heavily affect the Strouhal number. Both triangular and rectangular shapes induce significant stream separation and vortex shedding at the LE, generally producing lower Strouhal numbers at the TE. From equation (2.5) we see that this will accordingly lead to a decrease in  $f_s$ . However, this is also reliant on other factors.

Depending on the  $\frac{c}{t}$  ratio, where  $c$  is the chord length and  $t$  the thickness, the way the leading edges affect the TE vortex shedding changes. An experiment done on rectangular shaped plates for  $Re \in [14800, 31100]$  found that there exist four different regimes for increasing  $\frac{c}{t}$  ratios. The highest ratio being  $\frac{c}{t} > 16$  where the Kàrmàn vortex street is no longer affected by the LE [28]. From this we can assume that for sufficiently elongated bodies the LE geometry does not affect the shedding.

For elliptical or cylindrical leading edges, which are the most relevant for vanes in Francis turbines, the reattachment length when  $Re = 5 * 10^5$  is close to zero with no vortex shedding [27]. With no induced vortices at the LE, the effects on the TE Strouhal number should be negligible. This will accordingly be valid for all lower Reynolds numbers.

### 2.3.2: Trailing edge

A range of authors have researched the effects of different trailing edge geometries on vortex shedding. [29] The earlier research mostly focused on the strength of the vortices and vibration amplitudes. A summary of some of the results are given in figure 11. They all used the blunt end as baseline, meaning relative amplitude 100, and the results are fairly consistent. If trying to reduce vibration amplitude, oblique endings in general outperforms the symmetrical ones. This is believed to be a consequence of the vortices emerging at different points in the chord direction, causing the vortices to somewhat cancel each other out. Illustrated in the figure below where it is also sketched how narrower wakes induce smaller vortices, and thus lower amplitudes.

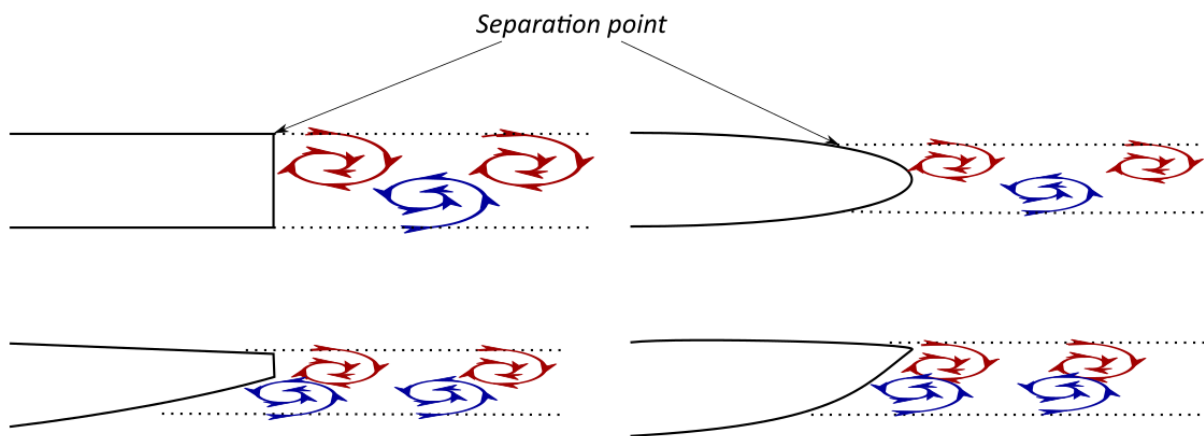


**FIGURE 10: SKETCH OF RECTANGULAR, OVAL, OBLIQUE TRUNCATED AND DONALDSON TE GEOMETRY FROM TOP LEFT TO BOTTOM RIGHT, RESPECTIVELY.**

Despite a lot of experimental research being done on the field, the physics are yet to be fully understood [29]. However, based on empirical data, several researchers have suggested modifications to the  $f_s$  equation to fit different TE geometries. A simplified variation presented by Brekke is as follows: [7]

$$f_s = 190 \frac{B}{100} \frac{U}{(t+0.56)} \quad (2.6)$$

Here  $B$  is a TE geometry dependant parameter, also described by frequency relative to the blunt edge,  $U$  is still the velocity and  $t$  is the thickness at the separation points for the plate or vane. Another variation which does not assume constant boundary layer thickness can be obtained from (2.6) by changing 0.56 to a variable  $\delta$ , dependent on chord length and Reynolds number. It has been suggested that the estimated Strouhal number of 0.19 is underestimating the shedding frequency relating to hydrofoils, with a more fitting estimate being in the range of 0.22-0.3. [30] [29]

When using these formulas, it important to stress that accurately measuring the thickness of the separation area is very hard, exemplified later. In addition, it seems reasonable to assume that with fluctuations in the flow the separation point will vary, causing the shedding frequency to not be a single number, but rather a distribution of frequencies.

| DONALDSON |           | HESKESTAD & OLBERTS |           | IPPEN    |           | BLAKE ET AL |           |              |                |
|-----------|-----------|---------------------|-----------|----------|-----------|-------------|-----------|--------------|----------------|
| GEOMETRY  | REL. AMP. | GEOMETRY            | REL. AMP. | GEOMETRY | REL. AMP. | GEOMETRY    | REL. AMP. | $\gamma t/h$ | $U_g/U_\infty$ |
|           | 360%      |                     | 380%      |          | 320%      |             |           |              |                |
|           | 260       |                     |           |          | 230       |             |           |              |                |
|           | 230       |                     | 190       |          |           |             |           |              |                |
|           | 100       |                     | 100       |          | 100       |             | 100       | 0.9          | 1.25           |
|           | 48        |                     | 43        |          |           |             |           |              |                |
|           | 22        |                     | 31        |          | 80        |             |           |              |                |
|           | 20        |                     | 38        |          | 70        |             |           |              |                |
|           | > 1       |                     | 3         |          | 60        |             | 0.3-1.5   | 0.5          | 1.05           |
|           | > 1       |                     | < 1       |          |           |             |           |              |                |
|           | > 1       |                     | < 1       |          |           |             | 1.0       | 0.5          | 1.03           |
|           |           |                     | < 1       |          |           |             | 0.5-1.7   | 0.8          | 1.2            |

FIGURE 11: COMPILATION OF RELATIVE AMPLITUDE FOR DIFFERENT TE GEOMETRIES [29]

Zobeiri measured vibration amplitude and  $f_s$  for a range of stream velocities, shown in figure 12 and 13 [29]. A contour of the three distinct TE geometries selected are shown in the top right of their respective graph in figure 12.

From Zobeiri's research it is clear the oblique non-truncated TE, labelled *Donaldson*, has the superior dampening capabilities of the three. Despite the large difference in vibration amplitude, the shedding frequency stay relatively equal. This causes the lock-in phenomenon to happen at approximately the same velocities, shown in both figure 12 and 13. From this we see that for a body vibrating with a known frequency, it should to a be possible to approximate where the lock-in will occur.

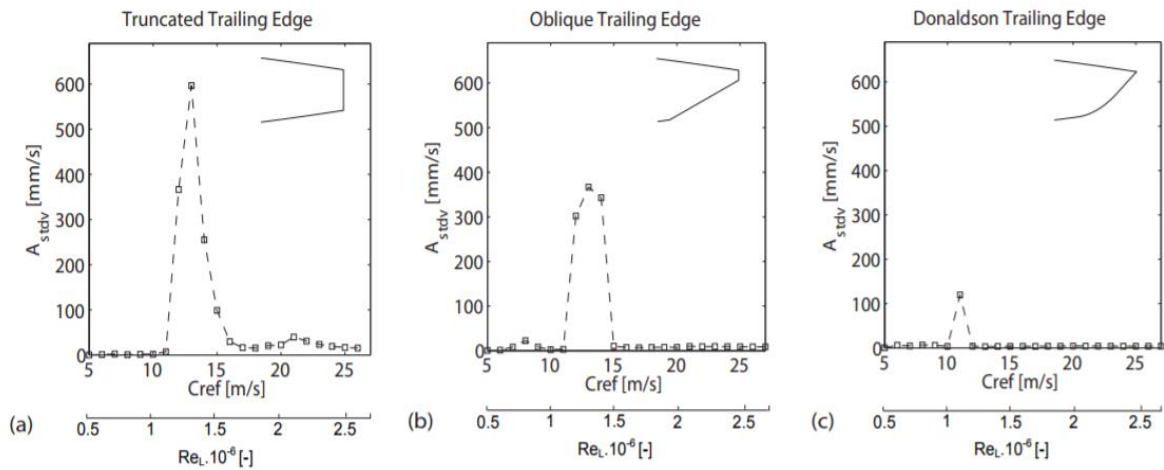


**FIGURE 12: VIBRATION AMPLITUDE MEASURED VERSUS RE/VELOCITY FOR THREE DISTINCT TE GEOMETRIES. [29]**

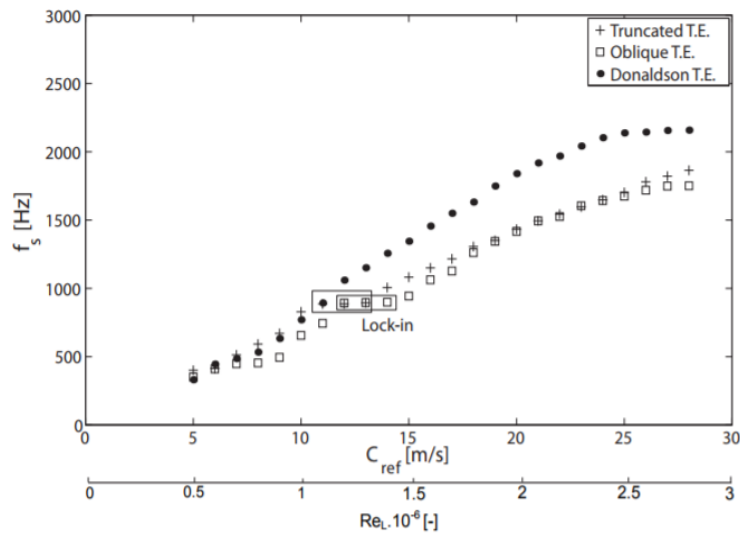


**FIGURE 13: SHEDDING FREQUENCY MEASURED AGAINST RE/VELOCITY [29]**

## 2.4: Rotor-stator interaction

Even though the turbine runner is located after the vanless space, some effects propagate upstream. The closer the guide vanes are to the turbine blades, the more apparent these effects become. This relationship between the rotational turbine blades and the stationary guide vanes is often referred to as the *Rotor-Stator interaction (RSI)*.

RSI is often split into two components. The first part is caused by the wake of the guide vane, which as previously explained has reduced velocity, and therefore also increased pressure. The runner blades notice these pressure inconsistencies every time it passes a wake, which in turn alters the inlet condition of the runner. This effect is believed to be increasing with guide vane angle, not only as a result of the proximity between the runner and vanes, but also because of the wake being more directed at the runner. Showcased in figure 14. [31]

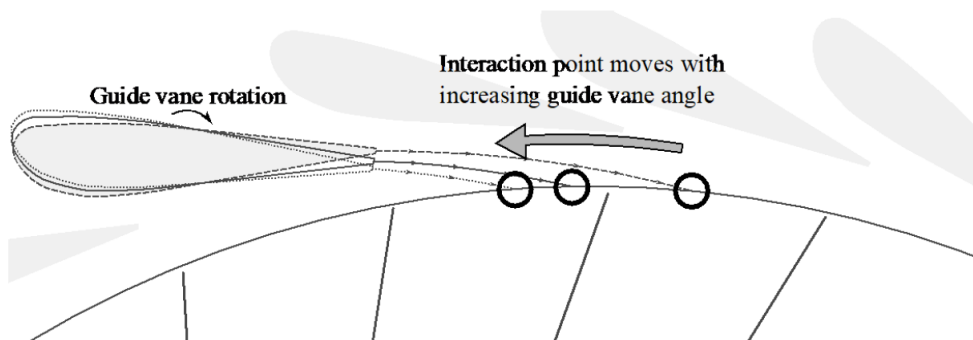


**FIGURE 14: WAKE TRAJECTORY FOR THREE DIFFERENT GUIDE VANE ANGLES. [31]**

The other effect is the potential flow interaction, which appears due to accelerated flow from the runner passing. If moving along with a turbine blade, we can imagine a stagnation point, or low velocity region in front of it, this will also mean a pressure peak which is noticeable by the guide vanes when passing. The effect on the velocity by runner blades and guide vanes is illustrated in figure 15.

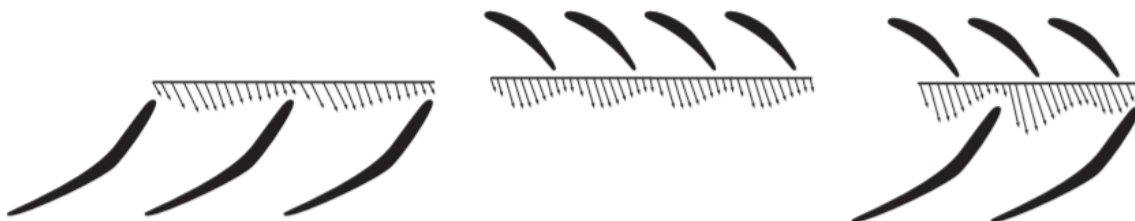


**FIGURE 15: LEFT: UPSTREAM VELOCITY EFFECT CAUSED BY THE TURBINE BLADES. MIDDLE: DOWNSTREAM VELOCITY EFFECT OF GUIDE VANES. RIGHT: COMBINATION OF THE TWO. ADAPTED FROM [32]**

Frequencies stemming from RSI have been shown to cause severe pressure pulsation throughout turbines, causing fatigue and cracks. It has also been shown that increasing the distance between the vanes and the runner lowers the amplitude of the pulsations, which is unfortunate since the hydraulic efficiency improves as the vaneless space becomes narrower. Dampening these effects by other means is therefore preferable. [33] [32]

Depending on our frame of reference, the frequency of the RSI generated pressure pulsations can be calculated by: [8]

$$f_s = n * Z_B \quad (2.7)$$

$$f_r = n * Z_{GV} \quad (2.8)$$

Here  $n$  is the runner speed in rotations per second, while  $Z_B$  and  $Z_{GV}$  are the number of runner blades and guide vanes, respectively. For a stationary domain, which is the most relevant for the scope of this thesis, equation (2.7) will be used. In other words, we will be looking from the perspective of the guide vane, where each passing of a turbine blade will cause a pressure excitation.

Trivedi [9] simulated the static pressure distribution around the stay vanes, guide vanes and in the vaneless space, not accounting for the runner. The pressure distribution in figure 16 was simulated at  $Q = 0.22 \frac{m^3}{s}$ , for the Francis turbine model located at the NTNU water power laboratory, which has a *best efficiency point (BEP)* at  $Q = 0.20 \frac{m^3}{s}$ .



**FIGURE 16: STATIC PRESSURE DISTRIBUTION AROUND STAY VANES AND GUIDE VANES, NEGLECTING RUNNER [9]**

In addition to simulations, measurements for several operating conditions in the Waterpower Laboratory at NTNU were conducted, which can be seen in full detail in [9]. The oscillating pressure at a point located in the vaneless space close to the trailing edge of a guide vane was measured. Both numerical and simulated data for this can be seen in figure 17, still for  $Q = 0.22 \frac{m^3}{s}$ . The peaks and valleys correspond to the guide vane being in- and out of line with the runner blades, which is in accordance the earlier study by Ciocan et al. [34]. For BEP the pressure oscillations were significantly lower, with the highest measured values being 1 kPa – less than half the effect showcased below. As a side note, the turbulence models also had less error in the BEP model.

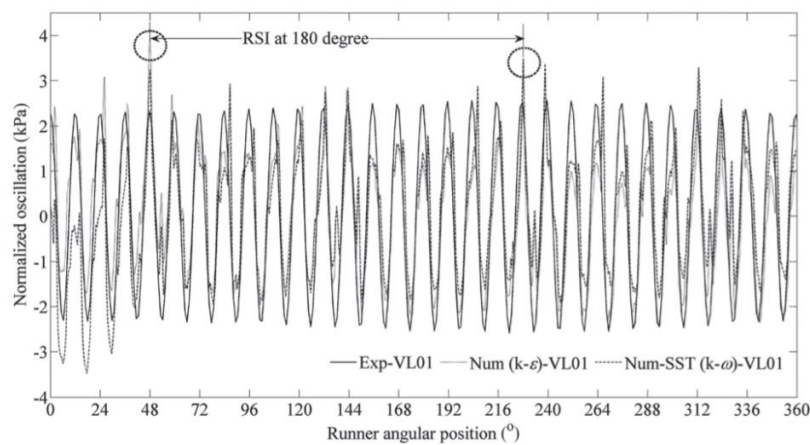


**FIGURE 17: NORMALIZED PRESSURE OSCILLATIONS AT A POINT IN THE VANLESS SPACE. COMPARISON OF TWO TURBULENCE MODEL AND EXPERIMENTAL DATA. X-AXIS REPRESENTS ANGLE OF RUNNER BLADE. [9]**

A smooth wake profile will cause smooth pressure oscillations. However, if the fluctuations in an unstable wake match the frequency of the runner blades, pulsations could get greatly amplified. [13]

## 2.6 Fourier transformation

Any continuous, periodic signal can be expressed as a sum of single sinusoidal waves with varying frequencies, phases and amplitudes. This is what is called a Fourier series. [35] Simple sine and cosine functions are a lot easier to process and distinguish than one composed function. Techniques for converting complex signals into Fourier series is widely used, for instance by post-processing programs.

Fourier transformation is one of these techniques which itself has several modified versions. A Fourier transformation will have a continuous periodic signal as input, which is decomposed into an array of single sinusoidal waves. The output will be given as a spectrum of the frequencies which made up the original signal, where the dominating frequencies will have the largest peaks. This is illustrated for a simple function in the figure below. Note that the domain after the transformation is now varying with frequency, not with time. When a *power spectrum* is utilized later, this is the corner stone of how it was built. [36] [37]

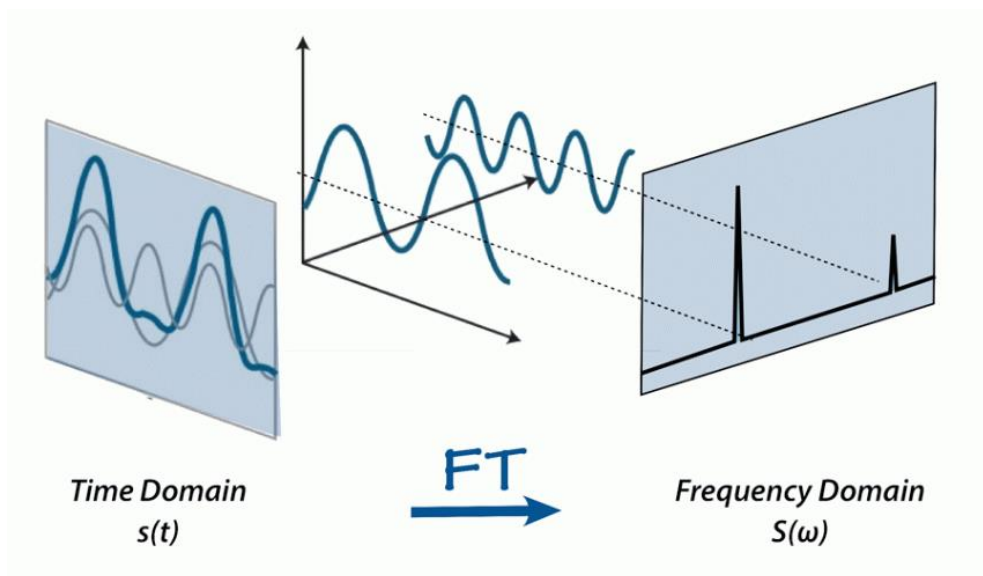


FIGURE 18: A SAMPLE SIGNAL IS TURNED INTO TWO SINGLE SINUSOIDAL WAVES [38]



## 2.7 Nyquist sampling

Nyquist's sampling theorem is commonly used when converting continuous (analog) signal to discrete (digital) signal. It states that to avoid information loss a sampling rate which is at least twice that of the highest frequency we are trying to capture should be used.

Mathematically this is easily expressed as:

$$f_{\text{sampling}} > f_{\text{max}} * 2 \quad (2.9)$$

Where  $f_{\text{sampling}}$  is our chosen sampling frequency and  $f_{\text{max}}$  is the highest frequency which we are trying to capture. When we do not have enough information to unambiguously reproduce a signal we might get what is called *aliasing*. Aliasing is the misidentification of a signal, causing distortion. Below we can see an illustration of how a signal might be wrongly reproduced when there are insufficient sampling points.

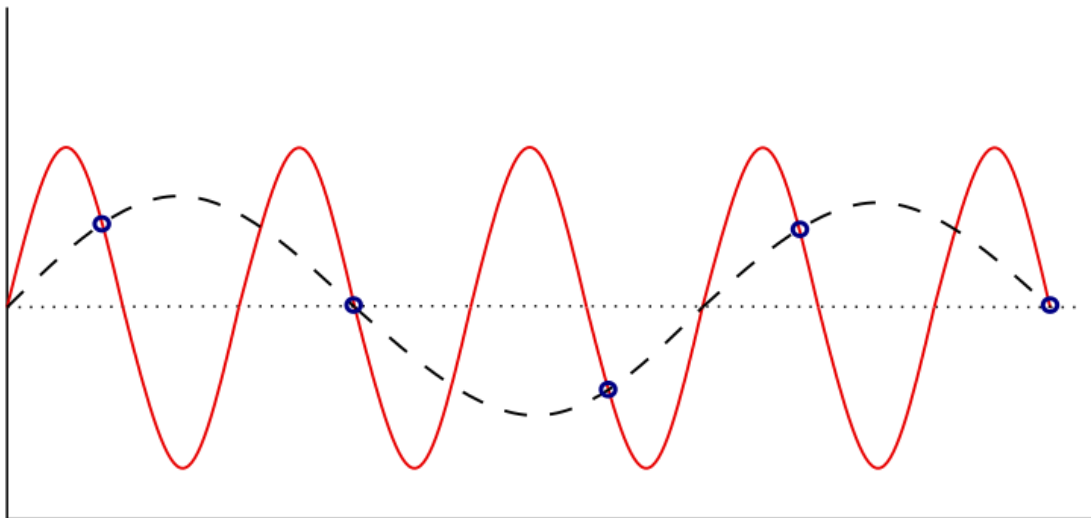


FIGURE 19: REPRODUCED WAVE (BLACK STIPPLED) COMPARED TO THE ORIGINAL SIGNAL (RED) FOR 5 SAMPLE POINTS (BLUE CIRCLES)

## 2.8 Error and uncertainty

Errors in scientific literature be separated into two main components. Firstly, we have what can be categorized as random uncertainty. These are errors which are present in any physical experiment and includes inaccuracies in measurement equipment and fluctuations in environmental conditions. Random uncertainties can be analysed statistically and are *Gaussian normal distributed*. We can estimate these errors by calculating the *standard deviation* of a dataset with sample size  $N$ , using the equation: [39] [40]

$$S_{dev} = \sqrt{\frac{1}{N-1} \sum_{i=1}^N (x_i - \bar{x})^2} \quad (2.10)$$

Where  $x_i$  is the value of a given sample and  $\bar{x}$  is the mean for the entire dataset. *student-t distribution* is used for smaller sample sizes. The only difference between t-distribution and the Gaussian normal distribution is the wider tails. However, as  $N$  increases the t-distribution approaches that of a Gaussian normal distribution. For sample sizes larger than 1000 a Gaussian distribution is typically assumed.

A *95% confidence interval* is often used in science literature and will also be used throughout this project. A 95% confidence interval simply means that a random sample value will have a probability of 95% to fall inside the given interval. For Gaussian distributed samples this is obtained by: [40] [41]

$$\bar{x} - 2 * S_{dev} < \bar{x} < \bar{x} + 2 * S_{dev} \quad (2.11)$$

In actuality this is a 95.45% confidence interval but is said to be 95% for simplicity's sake.

We can also note that an interval  $\bar{x} \pm S_{dev}$  would give a confidence level of 68% and  $\bar{x} \pm 3S_{dev}$  gives a confidence interval of 99.7%. Generally, there is more than one source of error for a single variable. We can estimate the total standard deviation  $S_{Tot}$  using: [40]

$$S_{Tot} = \sqrt{\sum_{i=1}^M (S_i)^2} \quad (2.12)$$

Where  $S_i$  is the standard deviation from a single source for a total of  $M$  error sources.

The second error source associated with measurements is called systematic error. Often identified as a set discrepancy in one direction. These errors are resistant to statistical analysis but can in theory be eliminated by using an offset or another appropriate form of correction. Spurious errors may be easier to notice when comparing repeated measurements. [39]

## 3: Particle image velocimetry

### 3.1: Fundamentals

PIV is a non-intrusive measuring technique, utilizing camera, laser and tracer particles to give an overview of a velocity field. The measurements are done in the following fashion: A certain amount of particles are seeded into a fluid moving towards an *area of interest (AOI)*. Here the laser will illuminate the particles at a preselected frequency. At the same time, a camera located perpendicular to the laser will take photos in rapid succession. An illustrated setup is shown in figure 20. It is crucial that the laser and camera are in phase, so that the particles will be highlighted in the photo series. Getting useful information from these photos on their own is close to impossible, which is why a suitable program is used for postprocessing. [42] Frame 1 and 2 in figure 20 serve as an example of how two pre-processed images look. Here  $t_0$  is the first timestep and  $\Delta t$  is the time difference between one step and the next. Now, if the software is able to identify the trajectory and distance travelled by the particles, in addition to the timesteps being known, calculating the velocity is elementary.

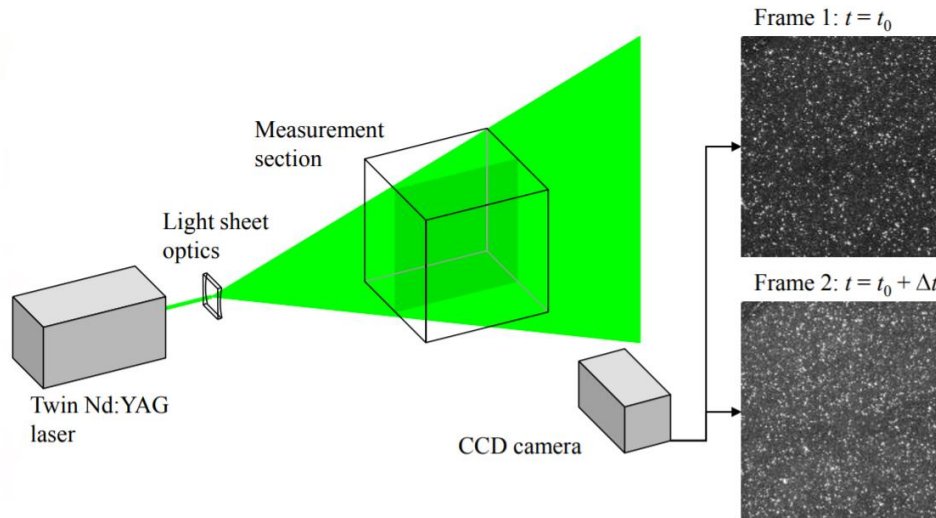


FIGURE 20: MAIN COMPONENTS OF PIV SETUP [42]

The core principles are easily understood, but getting accurate and reliable results can be difficult. It is also of note that this measuring technique is based in empiricism. Thus, the rules of thumb given may differ a bit from source to source.

## 3.2: A closer look

Even though postprocessing is the last step in the PIV-cycle, it is necessary to partially understand how the images are manipulated to create a velocity field before recognizing how other parameters are decided. Accordingly, a brief explanation of the image processing will be given initially.

### 3.2.1: Interrogation area

Every image will be split into several smaller sections called *interrogation areas (IA)* or interrogation windows, seen in figure 21. This sample picture is split into 8x8 by the solid lines, or 16x16 by the stippled ones. If we assume this picture has a resolution of 1024x1024 pixels, the respective lines would give interrogation areas of 124x124 and 64x64. Each IA will correspond to one velocity vector in a postprocessed image. Naturally, this means that a finer IA-grid will lead to a higher resolution vector field. While having a high resolution is convenient, and may even be necessary to showcase intricate flows, having a greater amount of interrogation areas will impose restrictions on other parameters. This will become apparent as we continue.

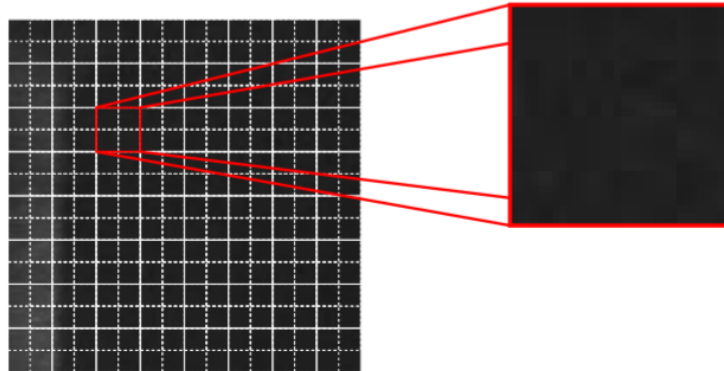


**FIGURE 21: A PICTURE AND ITS CORRESPONDING INTERROGATION AREAS. ADAPTED FROM [43]**

### 3.2.2: Seeding

It is necessary that the tracer particles selected for PIV measurement reflect light to some degree. Too great reflective capabilities cause clutter in the pictures and too little can make them undetectable for the postprocessing software. It is also desirable that the particles have comparable density to the fluid it is to be used in. This is to avoid floating or sinking which would be detrimental to a homogenous particle spread. The particles used for water applications are typically in the range  $\varnothing \in [5\mu m, 100\mu m]$ . In actuality, they may be of any size as long as they follow the flow without altering it and are of a suitable size compared to the fluid structure we are trying to expose.

If the particles do not influence the flow of interest, and can be distinguished from one another, there is no upper limit on the amount. The prevalent rule of thumb is that every IA should contain at least 10 particles. This means more interrogation areas; higher amount of tracer particles needed. Experience, however, shows that too many particles may be problematic, not due to the physical influence on the flow, but oversaturation may promote lumping. This may in turn cause severe clutter in the images. [42] [43] [44]

### 3.2.3: Laser and light sheet

Lasers typically provide a strong beam of light at one axisymmetric point, which is not what is needed for PIV measurements. A specialized optic is used to convert the beam into a planar light sheet, illuminating the AOI. Illustrated in figure 20. What this means is that the velocity fields are basically measured in 2D. There are other PIV variations available, such as stereo 2D and 3D, which will not be explained as they are not relevant for this project. [43]

It is common for PIV setups, including the one used in the Waterpower Laboratory at NTNU, that the apparatus with the lowest maximum frequency is the laser. The lasers associated with PIV are pulsed lasers, meaning they do not give a constant beam, but rather short pulses of light in the range of 5-10 ns. The lasers need some time to recharge between each pulse, which has led to the use of double pulsed lasers. As the name implies, these have two separate laser cavities, and can therefore discharge two pulses in rapid succession. This does mean that adjusting the separate beams so they overlap becomes important, but more on this later. [43] [44] [45]

### 3.2.4: Optic

The camera resolution heavily influences both the maximum *frames per second (fps)* and the IA resolution. As with regular cameras, there is a trade-off between picture quality and camera frame rate. Meaning that if we want a fine velocity field, we must accept a larger  $\Delta t$ . However, this is not the only factors we have to balance. The velocity of the flow will, along with the size of our IA, determine the maximum allowable value of  $\Delta t$ . This will be explained more in-depth in the calibration section.

### 3.3: Calibration

A calibration process must be completed before we can start measuring. The information presented will mostly be in accordance with the user manual provided by LaVision [46], using the Davis software.

The first step is to choose a suitable magnification factor, so that we are able to see the full fluid structure. In other words, we should strive to display a complete picture of the phenomenon we are about to investigate. That being said, a too large *field of view (FOV)* can cause problems since it forces us to use very small interrogation areas if we want to see details in the flow.

Figure 22 shows two images with different sized IAs. The picture to the left have multiple velocity directions inside one interrogation area, which will not reproduce the flow field correctly. The one to the right barely has enough areas to detect the flow structure.

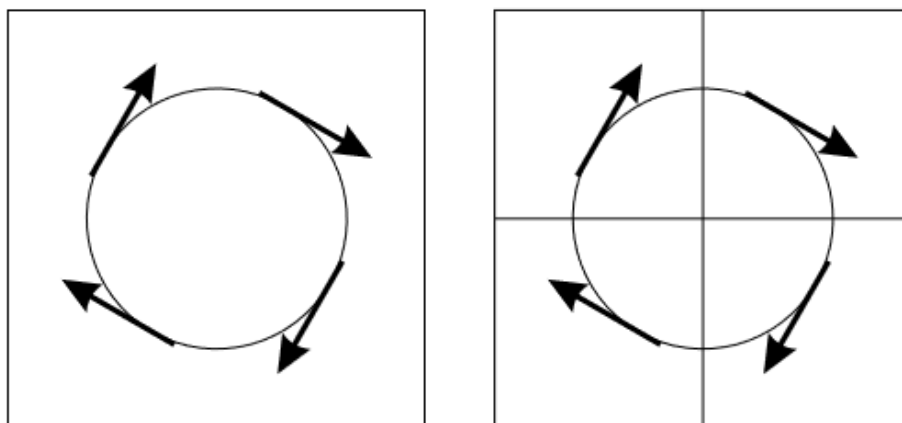


**FIGURE 22: INTERROGATION AREAS, THE RIGHT IMAGE HAS 4 TIMES MORE IAS THAN THE LEFT ONE. [46]**

Next, we have to relate pixels on the screen to actual dimensions. This is done by placing a calibration plate or ruler in plane of our AOI. Anything with distinguishable points and known sizes will do the trick, though it is easier using the calibration plate as it is recognizable by the software. If we then focus the camera and take a still picture, we may use the provided program and choose a couple of reference points on the screen. By afterwards inputting the real-world distances between these points the software will have a scale that remains valid until either the camera or AOI changes position.

With no distortions between the camera and area of interest, meaning the camera is angled completely perpendicular on the AOI, with no disturbance from outside sources, two calibration points are sufficient. However, this is very rarely the case. Especially when taking pictures through transparent materials or fluids which cause the light to break, more points are needed in both the vertical and horizontal direction. We should therefore strive to have evenly spread out calibration points throughout our AOI. This way the software can adjust for any distortions which may be present. Of course, this means inputting accurate information is highly important.

Afterwards we adjust the light sheet, which should be both parallel and in line with the area of interest. For PIV measurement we do not want particles moving in and out of the light sheet, referred to as *out-of-plane* motion. If new particles appear and disappear from our AOI when going from one timestep to the next, it will obviously cause errors in our results.

As is illustrated in figure 23, the sheet optic will produce a focal point. Since the goal is to measure in 2D, having the thinnest light sheet possible is preferable. Aiming the focal point close to the centre of our AOI is the easiest way of achieving this. LaVision suggests putting an orange piece of paper where our light sheet is supposed to be, manually observing and adjusting until the most illuminated part is in the middle. When doing this it is essential to wear specific goggles to avoid eye injuries.

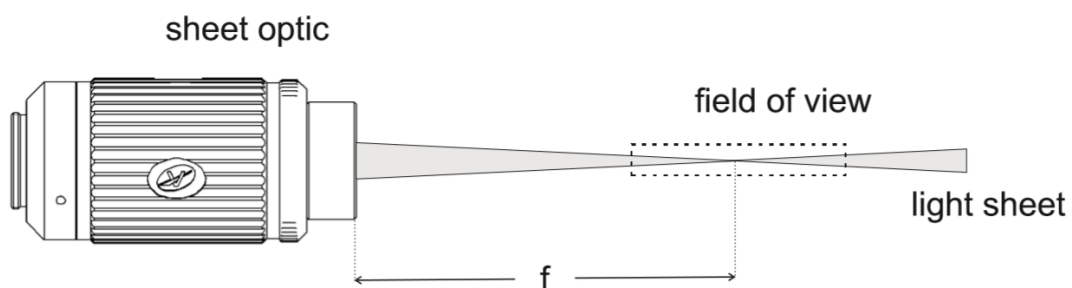
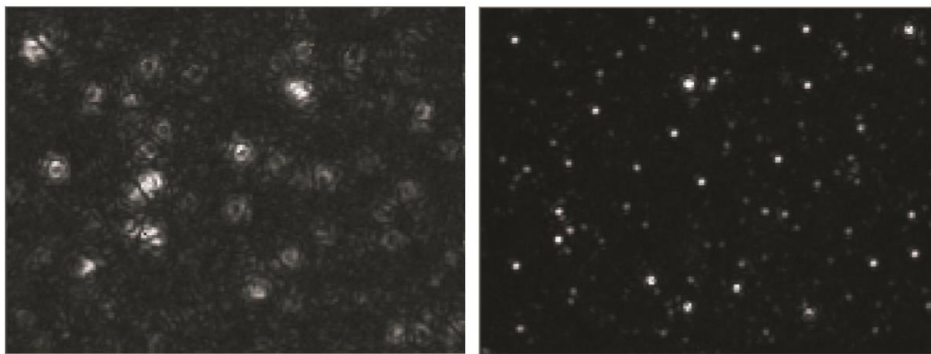


FIGURE 23: LIGHT SHEET FOCUSING [46]

Reflections may be produced in sections neighbouring the AOI. These are detrimental to the image quality since we want a sharp and thin 2D sheet. Therefore, it is recommended to cover areas near the AOI with non-reflective paint, e.g. black.

Following this, the light source settings in the software is adjusted. When tuning the power of the laser pulses, we should observe the particles. They should be clearly illuminated, but at the same time distinguishable from one another. Depending on the strength selected, the fluid may look like a sea of light or pitch black.

When that is done we should alter the focus of the camera. For a continuous series of images, the camera is adjusted until the particles are in focus, shown in the figure below.



**FIGURE 24: PARTICLES IN AND OUT OF FOCUS. IN FOCUS TO THE RIGHT. [46]**

As mentioned above the laser used has two alternating pulses. Checking the synchronization between laser and camera can be done by the following routine:

- Deactivating the first pulse and capturing two images – only the second image should be illuminated.
- Deactivating the second pulse and capturing two images – only the first image should be illuminated.
- Having both pulses active – both images should be illuminated.

When choosing an appropriate  $\Delta t$  there are as mentioned several factors to consider. Among these are the physical constraints; maximum possible pulse frequency for laser and maximum camera fps for an adequate resolution. Other parameters to look at are the interrogation area size in combination with stream velocity. Two IAs of different size is shown in figure 25.

Here the black particles represent position for timestep one  $t_1$ , and the red particles timestep two  $t_2$ , where  $t_2 = t_1 + \Delta t$ . As we can imagine, if the velocity was higher, the particles would



travel further for the given  $\Delta t$ . We should also acknowledge that making a velocity vector of an IA where the original particles have all moved out, and been replaced with new ones, do not represent the velocity in that area. Referred to as *in-plane pair loss*. It is natural to assume that the left IA in figure 25 would provide the more accurate vector representation, also showcased later on.

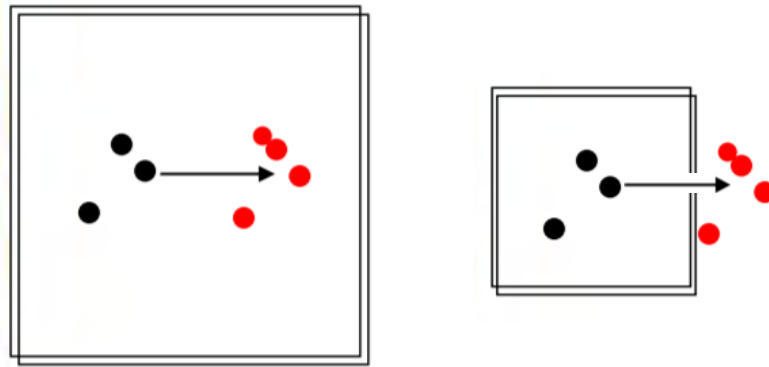


**FIGURE 25: IN-PLANE MOTION OF PARTICLES FOR TWO DIFFERENT IA SIZES. ADAPTED FROM [42]**

### 3.3.1 Particle shift

Particle shift ( $ds$ ) refers to how far the particles travel from one timestep to the next, measured in pixels on the screen. Several methods for evaluating correct  $\Delta t$  has been suggested.  $0.1\text{pixel} < ds < \frac{1}{4}IA_{size}$  is one of the most widely used approaches, which means at least a 75% overlap between two frames. LaVision suggests the  $ds$  to be  $\sim 5$  pixels. This calibration method is based purely on trial-and-error. By taking two pictures and moving back-and-forth between them, the particles should move  $\sim 5$  pixels on the screen. If the gap is longer  $\rightarrow$  reduce  $\Delta t$ , for shorter gaps  $\rightarrow$  increase  $\Delta t$ . Figure 26 shows the impact of a properly chosen timestep.

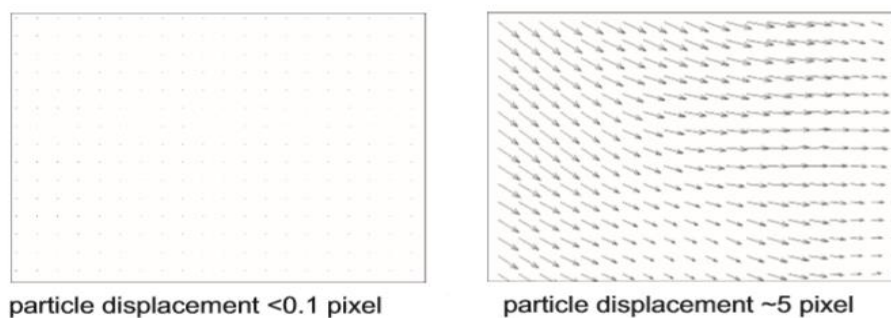


**FIGURE 26: VECTOR FIELDS FOR DIFFERENT PARTICLE SHIFTS. [46]**

### 3.3.2 Double frame imaging and pulse separation

Modern PIV systems have the option of single-frame (regular) or *double-frame* image capturing. Double frame imaging came to light when cameras with specialized shutter mechanisms started appearing. Simply explained cameras with a *double shutter function* will be able to briefly hold on to one image while simultaneously capturing the next. After an image pair is acquired there is a short downtime while the readout is happening. [47] These pairs are saved as single image files in the post-processing program and used together to form velocity vectors. More thoroughly explained in the postprocessing section.

For PIV measurements this means we can set pulse separation time and camera capturing frequency independent of one another. As explained earlier we typically want to set  $\Delta t$  for the laser pulses so that the particles travels  $\sim 5\text{px}$ . The camera frequency on the other hand should adhere to Nyquist sampling theorem. Therefore, it is a huge advantage to be able to adjust these parameters relatively independent of one another.

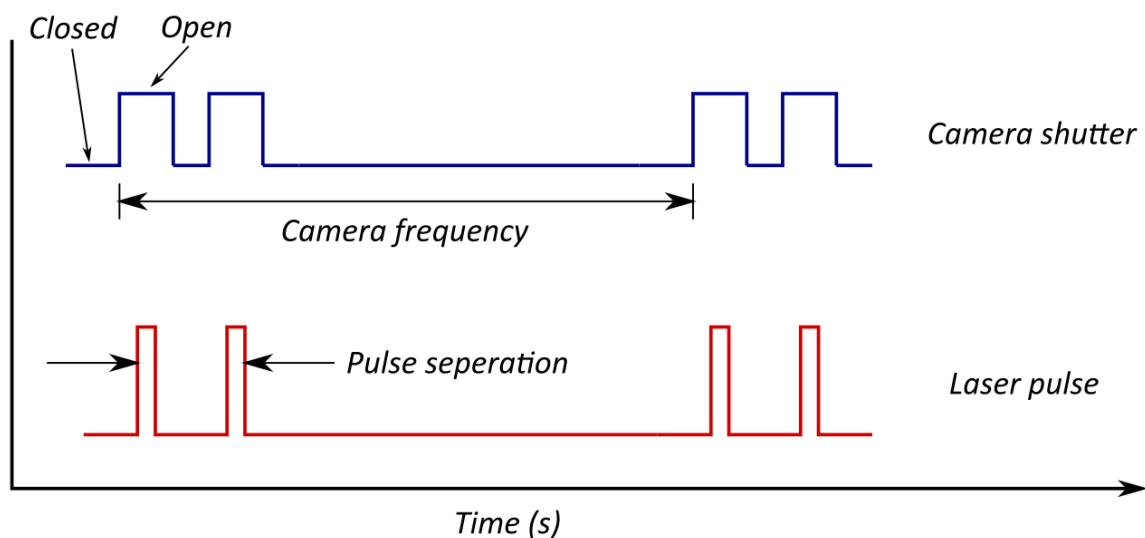


FIGURE 27: DISTINCTION BETWEEN CAMERA FREQUENCY AND PULSE SEPARATION

In figure 27 it is illustrated how camera fps and laser pulse are detached from one another. Note that the speed of the double shutter will solely rely on the pre-set pulse separation time. It is also important to remember that lower shutter times means less light exposure for the camera, leading to darker images. If adjusting the shutter times it is important to check if the laser intensity needs tuning as well.

### 3.3.3 Camera lens characteristics

Later on, the two lenses used in this experiment will be mentioned along with two key characteristics. A brief explanation of the two will be given in this section.

The first one is the denoted objective length. Where a longer lens in general corresponds to a higher magnification factor. Moving the camera closer or further away from our AOI could in theory produce the same result as changing to a bigger or smaller objective, respectively. This is obviously dependant on the lens' ability to focus from the given distance. [48]

The other characteristic is the *f-ratio*, which is calculated by taking the focal length of the lens and dividing it by the maximum aperture opening. What this means in a PIV context is that a lower f-ratio allows for more light exposure. Furthermore, a lower number will provide a stronger out-of-focus effect, which is beneficial since we only want the particles in one exact plane to be visible. [49]

### 3.3.4 Pre-processing

A wide range of pre-processing options are available in the Davis software. Their function is to optimize the data set before the velocity vectors are calculated. Attaining the perfect PIV setup is close to impossible, which is why some degree of particle lumping, unwanted reflection and background noise will always be present. Having the option to filter out some of the undesirable effects is accordingly a huge benefit.

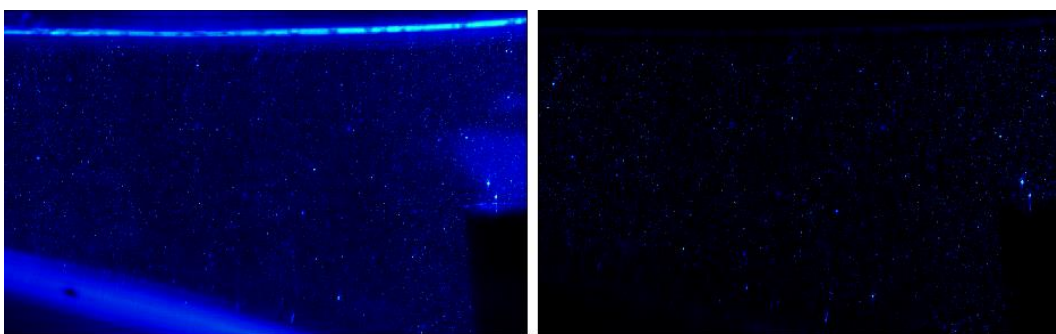
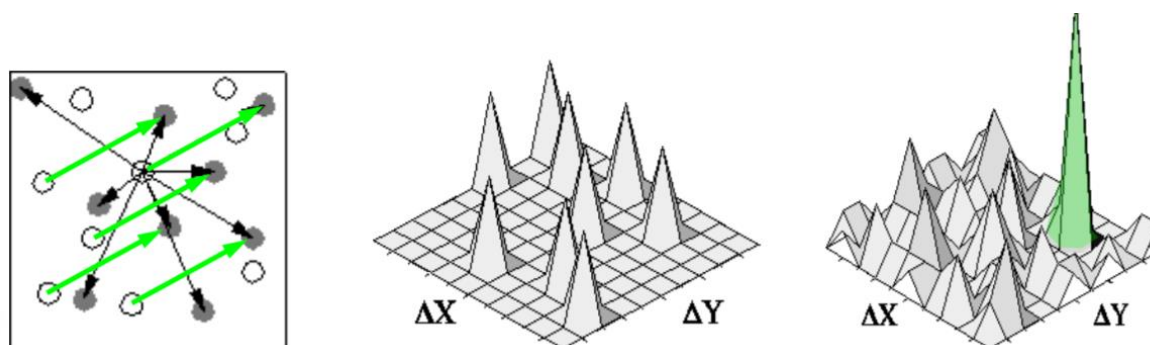


FIGURE 28: RAW IMAGE (LEFT) COMPARED TO PRE-PROCESSED IMAGE (RIGHT)

### 3.3.4: Postprocessing

PIV software does not track single particles when comparing positions in an image pair, instead it heavily relies on *cross-correlation*. Cross-correlation is used to find the distance the whole particle pattern inside an IA has moved from one timestep to the next. As shown in figure 29, there will be a lot of “wrong” assumptions, which cause noise. However, with every possibility taken into account, the true displacement will dominate in general. From this peak, seen to the right in figure 29, a velocity vector will be generated, representing the interrogation area as a whole.



**FIGURE 29: LEFT: OVERVIEW OF POSSIBLE NEW POSITIONS (BLACK ARROWS) FOR A SINGLE PARTICLE, AND ACTUAL PARTICLE MOVEMENT (GREEN ARROWS). MIDDLE: POSSIBLE MOVEMENTS FOR ONE POINT. RIGHT: SUM OF ALL POSSIBLE MOVEMENTS FOR EVERY PARTICLE. [42]**

The more particles we have inside an IA, the higher the signal-to-noise ratio will be [42]. This is also illustrated in figure 29, where in the middle figure we only consider movements for one particle. If looking at a single particle it is impossible to know what the true movement is.

This is merely the cornerstone of how velocity vectors are produced. As the PIV measurement technique has matured several approaches to reduce statistical error has been implemented. Most noticeably overlapping adjacent IAs, multi-passing and the more recent adaptive shapes IAs. Interrogation area overlapping is at this point well-researched and the ability for the user to choose the overlapping factor is standard. [50] [51] [52] [53]

By overlapping adjacent IAs and using the particles of nearby areas, the error induced by in-plane motion can be heavily reduced. This implementation was especially beneficial for smaller IAs which typically are more prone to in-plane errors, as illustrated in figure 25. [42] [50]

The multi-pass and adapting size approach typically starts with a larger rectangular shaped IA. The larger IAs are more robust due to having more particles/area and an overall lower sensitivity towards several types of error, which will be touched upon in the next section. A general velocity vector for this area will be produced and used as a “guideline” for the shifting of the smaller IAs as the images are processed for a second time. If we look at the figure below, we can image the left figure being an example of a first “pass”, and the right figure a second run through.

In postprocessing software, we can choose how many passes we want for the various IA sizes. More passes do not always equal better results, but it does always increase processing time. There is currently no guideline for how much the IAs should overlap, or how many passes should be used. This varies depending on the flow. [53] It is probably advisable to spend some time experimenting with different combinations and see what gives the most reasonable velocity fields.

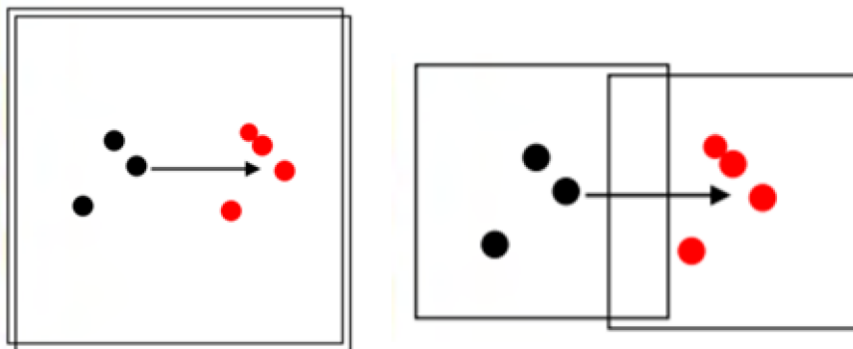


FIGURE 30: WINDOW SHIFTED BASED ON PREVIOUS VECTOR CALCULATION [42]

### 3.4: Uncertainty and error in PIV measurements

There are several sources of error specific to PIV measurements, many of which are hard to quantify. The systematic errors will be related to mistakes during setup and calibration and will not be possible to rectify after acquiring the images. [54]

On the other hand, there are several sources of random errors. which it is possible to estimate, and sometimes reduce, by statistical means. The total random error was previously quoted as somewhere in the range of 0.05-0.1pixels, without much research to back it up. [55] The last few years several studies have been conducted trying to relate errors of various parameters to each other. [52] [56] [54] [57]

In the earlier pre-processing section, figure 28 shows a comparison of an un-filtered and a filtered image. While it is easier to separate the particles with your own eyes, it might be hard to quantify how much difference it makes for the postprocessing software. In figure 31 we can see the how noise affects the cross-correlation process and how it relates to IA sizes for various amounts.

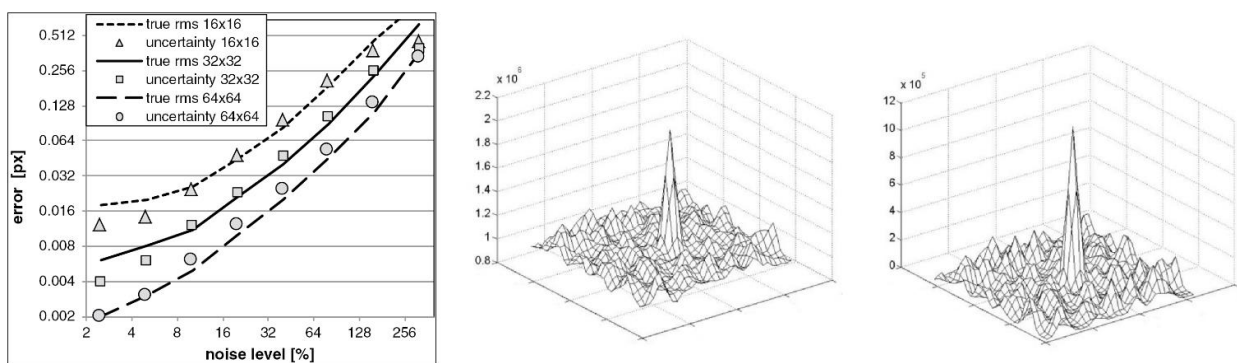


**FIGURE 31: LEFT: ERROR AS A FUNCTION OF BACKGROUND NOISE FOR VARIOUS IAs.**

**MIDDLE: CROSS CORRELATION PLANE OF PARTICLE IMAGES WITH BACKGROUND NOISE.**

**RIGHT: CROSS CORRELATION PLANE FOR THE SAME IMAGES WITH BACKGROUND NOISE FILTERED OUT. ADAPTED FROM [52] [56]**

Through the last decade out-of-plane motion has been found to be the dominant source of PIV error. [54] [55] Wieneke carried out a study relating several parameters to out-of-plane motion, depending on IA size. Some of the data is shown in figure 32, where rms is the widely used root-mean-square. As with most PIV error research the images are synthetically made, meaning that the true displacement is known. The *true rms* displayed in the graphs are therefore calculated by the differences from all the vectors to the true displacement. The total uncertainty is in accord with equation (2.12) [55]

In figure 32 the top left graph shows out-of-plane motion for a constant particle size of 1.5 pixels, while the top right graph is for 2.5 pixels. It seems apparent that larger sized particles are more prone to out-of-plane errors. This is reinforced by the bottom right graph which has a constant out-of-plane motion of 10%, with increasing pixel sizes. Here we see that the lowest errors are found for pixels  $\sim [1, 1.5]$ , which holds true for every IA size. However, for particles as small as this we need to be careful of a phenomenon called *peak-locking*, which is when the pixel-placing is rounded to the nearest integer. This is a systematic error which can cause discrepancies up to 0.1 pixels and cannot be accounted for. [54]

From the last graph, seen to the bottom left, we can read how different sized IAs affect error for different seeding densities, measured in *particles per pixel (ppp)*. This is also for a constant out-of-plane motion of 10%, where we can see the error is almost independent of the seeding density.

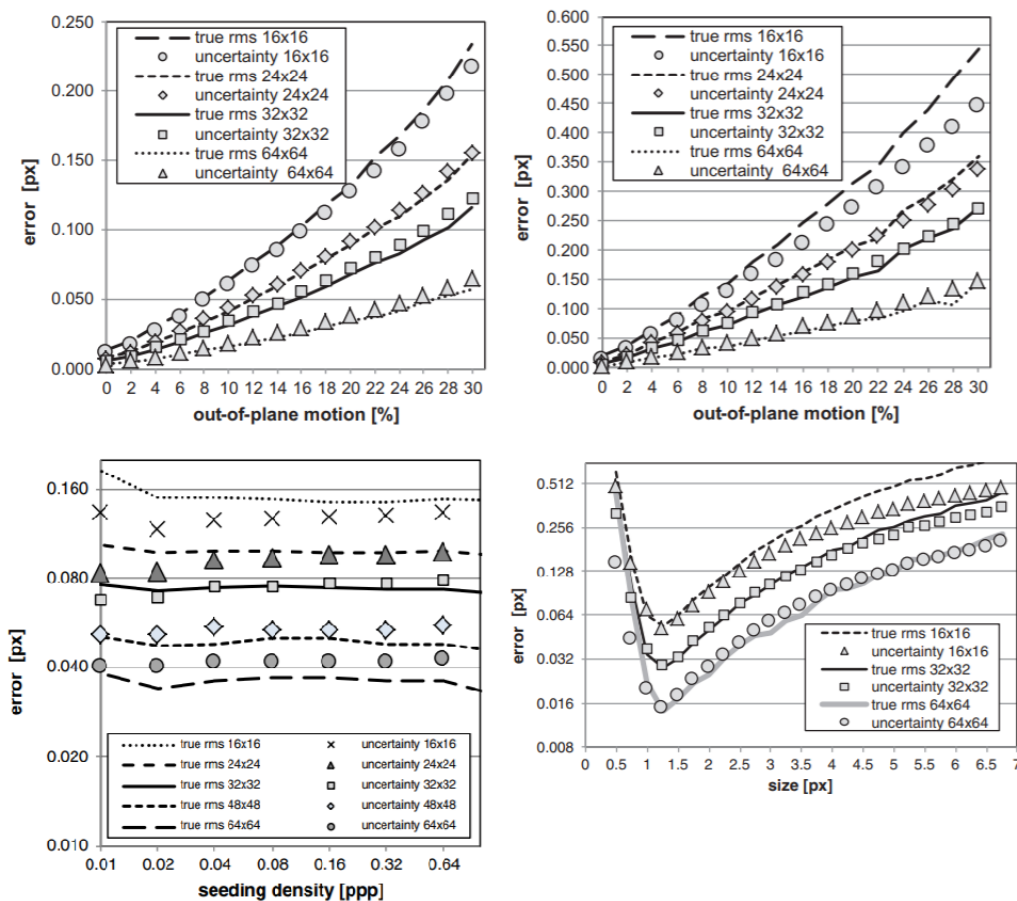


**FIGURE 32: TOP LEFT: ERROR DUE TO OUT-OF-PLANE MOTION FOR PARTICLE PIXEL SIZE 1.5. TOP RIGHT: ERROR DUE TO OUT-OF-PLANE MOTION FOR PARTICLE PIXEL SIZE 2.5. BOTTOM LEFT: ERROR CAUSED BY A CONSTANT OUT-OF-PLANE MOTION OF 10% VARYING WITH SEEDING DENSITY. BOTTOM RIGHT: ERROR CAUSED BY A CONSTANT OUT-OF-PLANE MOTION OF 10% VARYING WITH PARTICLE SIZE. [52]**

## 4. Francis setup

Since there is not any previous research available on 2D PIV measurements in the vaneless space of a Francis turbine, a considerable amount of work has gone into figuring out a potent setup. The AOI is located in a somewhat troublesome position both for calibration and stable high-speed picture acquiring. The applied solutions, along with an overview of the general layout, will be presented in this chapter, contributed by Bolstad, Sagmo and Storli. [10]

### 4.1 Test section

The measurements will be conducted using a closed loop, meaning there is no outlet to the atmosphere. Because of this we can freely regulate our drifting parameters. The rig at NTNUs waterpower laboratory is capable of producing and withstanding up to 100m head and flowrates reaching  $1 \text{ m}^3/\text{s}$  [58] The Francis turbine itself has 14 stay vanes, 28 guide vanes and 30 runner blades, 15 of which are splitter blades. The guide vanes can be adjusted to a maximum opening of 14 degrees, allowing a flowrate of  $0.263 \text{ m}^3/\text{s}$  The runner inlet and outlet diameters are 0.63m and 0.347m, respectively. An overview can be seen in figure 1.

In figure 33 we can see the section of the hydropower instalment which will be utilized for this thesis. The trajectory of the fluid is marked with green from the pump to the test section, and by red on its return to the pump.

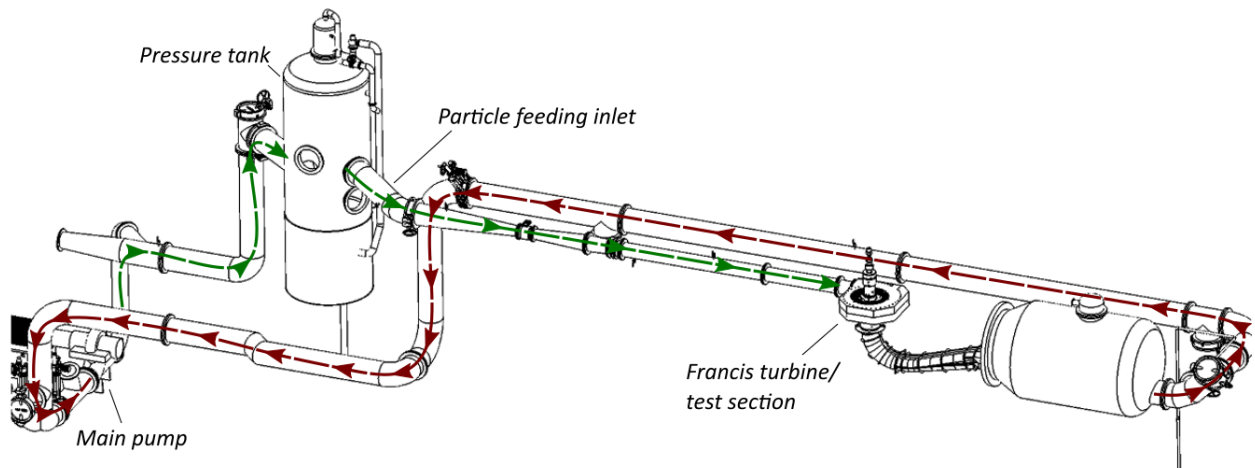


**FIGURE 33: FLUID TRAJECTORY IN THE CLOSED LOOP. GREEN FROM THE PUMP TO THE TURBINE. RED FROM THE TURBINE BACK TO THE PUMP.**



## 4.2 PIV equipment

In section 3 some of the main components in a PIV setup were mentioned, among these camera, laser, seeding particles and the postprocessing software. A run-through of the essential components will be given first, and an overview can be seen in table 4.1.

The Photron high-speed camera has a global electronic shutter mechanism which allows the previously mentioned double shutter function. In addition, the achievable fps can be significantly increased by cutting from the top and bottom of images, making the frames narrower. [59]

Lens 1, the primary lens for this thesis, has a 100mm objective with an f-ratio of 2.8. Lens 2 is a 50mm objective with an f-ratio of 1.2. The initial plan was to do all measurements points with both lenses. This way we could get different sized FOV without moving the camera. The benefit of having a static camera position will become evident in the calibration section. Due to an unanticipated interaction, which will be explained later, we chose to focus on the lens 1 – and thus a smaller FOV.

**TABLE 4. 1**

| Component:                   | Name/description:  |
|------------------------------|--|
| <i>Camera:</i>               | <i>Photron, FastCam Mini UX100</i>                           |
| <i>Lens 1:</i>               | <i>Tokina, AT-X Pro 100mm, f2.8</i>                          |
| <i>Lens 2:</i>               | <i>Nikon, Nikkor 50mm f1.2</i>                               |
| <i>Laser:</i>                | <i>Litron, LDY 300 PIV</i>                                   |
| <i>Synchronization unit:</i> | <i>LaVision, PTU X</i>                                       |
| <i>Timing stabilizer:</i>    | <i>LaVision LTS</i>  |
| <i>Software:</i>             | <i>Davis v. 8.4, CW, Diode client PIV v.1.0</i>              |
| <i>Seeding particles:</i>    | <i>LaVision, Glass hollow spheres, 9-13<math>\mu</math>m</i> |

Our AOI is illuminated by a Litron double cavity laser lead to the laser sheet optic by a guiding arm. The laser itself is connected to the operating computer through a separate power/cooling unit. This power unit is also connected to both a *programmable timing unit (PTU) X* and a *laser timing stabilizer (LTS)* unit. The PTU and LTS ensures that the input from the Davis software is interpreted and synchronized correctly. CW Diode client is used to

remote control the cooling/power unit of the laser, the laser intensity, as well as the laser shutter.

The seeding particles used for the experiment are LaVision glass hollow spheres, with an average diameter of  $11\mu\text{m}$  and a density of  $1.1\text{g}/\text{cm}^3$ , which is slightly higher than that of water. Residual particles from previous experiments will also be in the flow. These range from a size of  $20\mu\text{m}$  to  $55\mu\text{m}$ .

An overview of the main components can be seen in figure 34. In reality, a black fabric tent is surrounding the entire test section. The Litron LDY300 is a class 4 laser, which is hazardous to both the eyes and the skin. A thorough review of all the safety measures and health risks, along with models including the laser tent, can be found in appendix D.

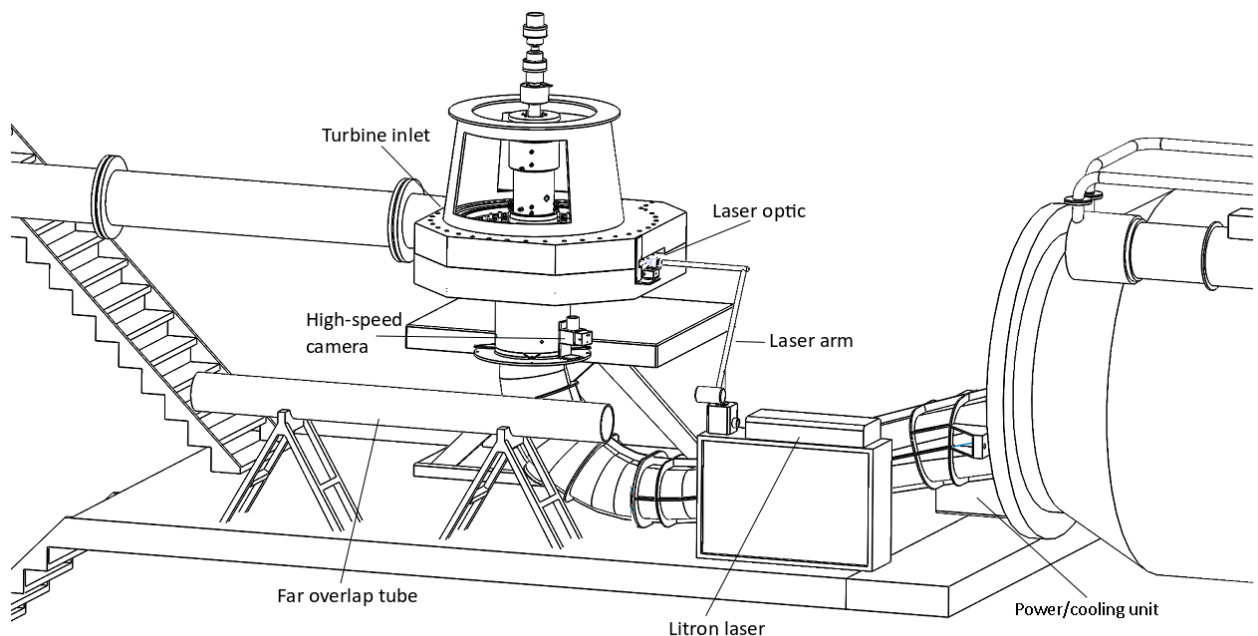


**FIGURE 34: TEST SECTION WITH ITS MAIN COMPONENTS**

### 4.3 Particle feeding

The particle feeding system has its outlet located right after the pressure tank, as indicated in figure 33. A 300l mixing tank, which has previously been levelled with the outlet, has been moved to the top floor, approximately 11.5m above. This was done to remedy a problem with the feeding rate as the head in the loop approached 10m. Some rough measurements for the new feeding flow rate was done for three various feeding pump RPMs. The results for the maximum output of 1800RPM is shown in the graph below. The RPM legend in this graph ties to the main pump RPM, dictating the volume flow in the entire loop. For the scope of this project the 280 RPM line is the most relevant as it resembles that of the BEP  $\sim 0.2m^3/s$ . The Y-axis displays how much of the total flow rate in the loop the feeding pump flow corresponds to. This means that the difference in values relates more to a higher overall flowrate, rather than an increase in dynamic pressure. An overview of all the graphs and numbers used can be seen in appendix A.

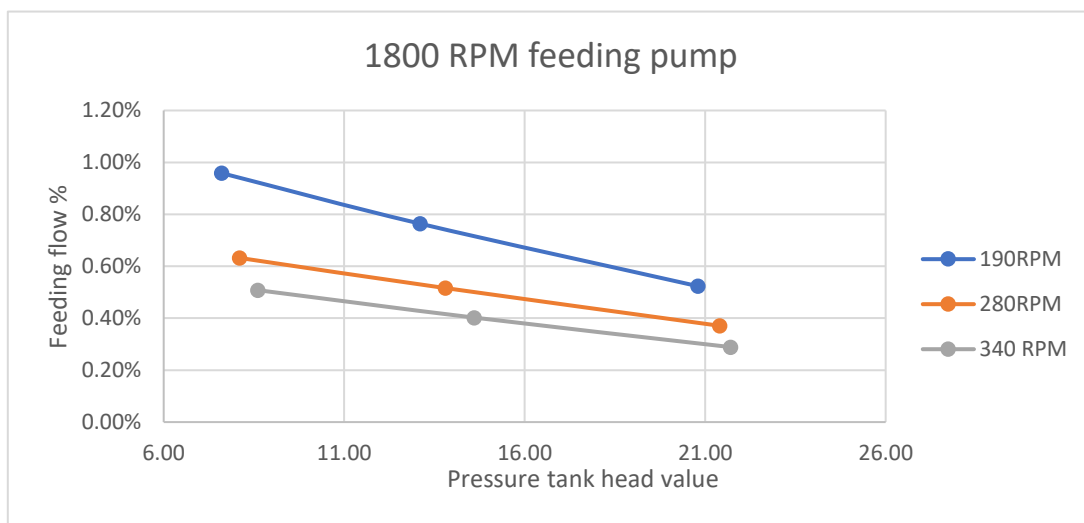


FIGURE 35: FEEDING FLOW RATE FOR VARIOUS PRESSURE AND FLOWRATES

The initial plan was to have a known water/particle concentration in the mixing tank and calculate an appropriate feeding rate depending on IA size, flowrate and pressure in the loop. However, the controlling unit for the pump broke down a few days before the PIV measurements took place, so these numbers will not be emphasized.

Fortunately, elevating the mixing tank gave us the alternative to saturate the entire loop with particles before ramping up the pressure. This was an iterative procedure done by alternating between feeding particles and taking pictures. When an IA of preselected size consistently

had a particle density  $\sim 10$  pixels/IA the loop was considered saturated. An advantage of this approach is that there is no interaction between feeding flow and the operating parameters. In addition, it ensures that the picture sets can be taken at any given time, we don't have to synchronize it with the particle feeding. However, if we were to do measurements for an open loop, there would be too much water to saturate.

## 4.4 Laser overlap

When the laser is physically moved, an overlap check of the two lasers is required. It is crucial that the overlap between the laser 1 and 2 are good since illuminating even slightly different planes in the flow would produce poor velocity vectors. As previously mentioned, PIV measurements are susceptible to out-of-plane motion, which an inaccurate laser overlap resembles.

The laser alignment is adjusted for two distances, a near field – just outside the laser, and a far field – ideally 3m away. [60] By removing the guiding arm along with the sheet optic, and letting the laser have a free path forward, the pipe in figure 34 was used for the far field testing. This is for safety reasons, and even though not in the model, there is fabric covering the tube exit as well as the test section at large.

Several carefully angled mirrors are located inside the Litron laser, which can be tweaked to adjust the path of the separate lasers. Some back and forth adjusting is required for both the near field and the far field overlap to coincide, as laser 1 and 2 do not originate from the same location. Some burn marks from the two lasers are presented in figure 36 to illustrate the end difference. It was done by hanging a stack of damp post-it notes ~1m from the laser outlet and peeling them off one at a time. It is possible to see a slight difference between them, where laser 2 has a minor tilt to the right compared to laser 1.

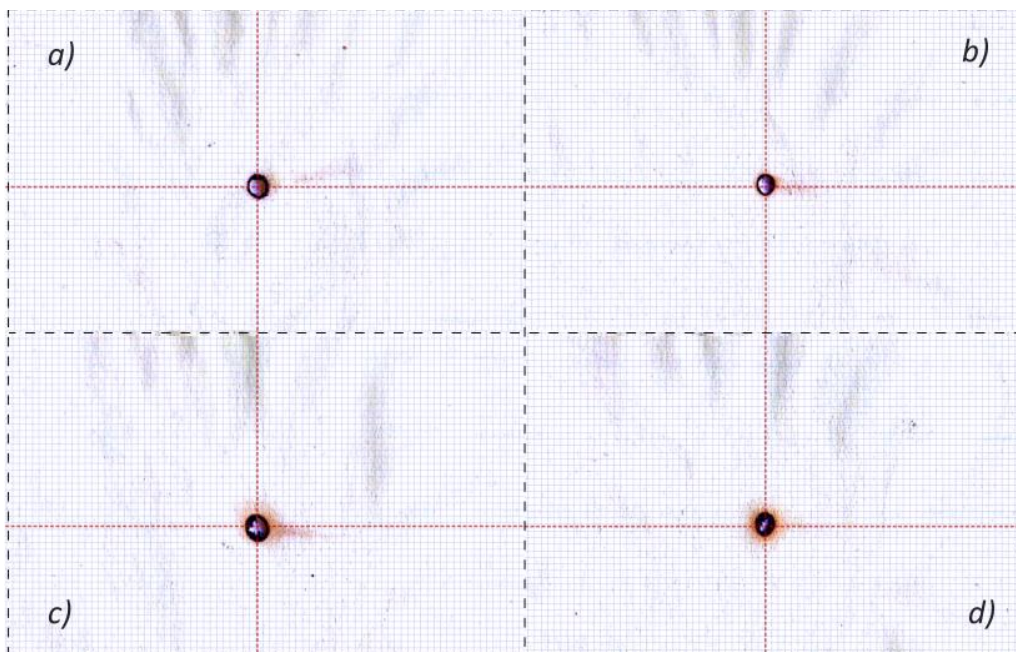


**FIGURE 36: BURN MARKS FOR; A) LASER 1 – 50% INTENSITY, B) LASER 2 – 50% INTENSITY, C) LASER 1 – 70% INTENSITY, D) LASER 2 – 70% INTENSITY.**

## 4.5 Experimental setup

To be able to do PIV measurements in the vaneless space of a Francis Turbine, some modifications to the turbine and the vanes are needed. Currently the laser sheet passes through a 30x550mm slice in the side of the Francis turbine, shown in figure 37. For this to be possible a section of the outer shell and spiral casing has been removed and replaced by Plexiglas. For the laser sheet to reach our AOI, which is the vaneless space, we can see to the right in the figure below that both the stay vanes and guide vanes needs to be translucent as well. At least those in the vicinity of our measurement region. Two of the stay vanes and three of the guide vanes have therefore been replaced by vanes made partially from Plexiglass. A side-by-side photo of an old and a new guide vane can be seen in figure 37.

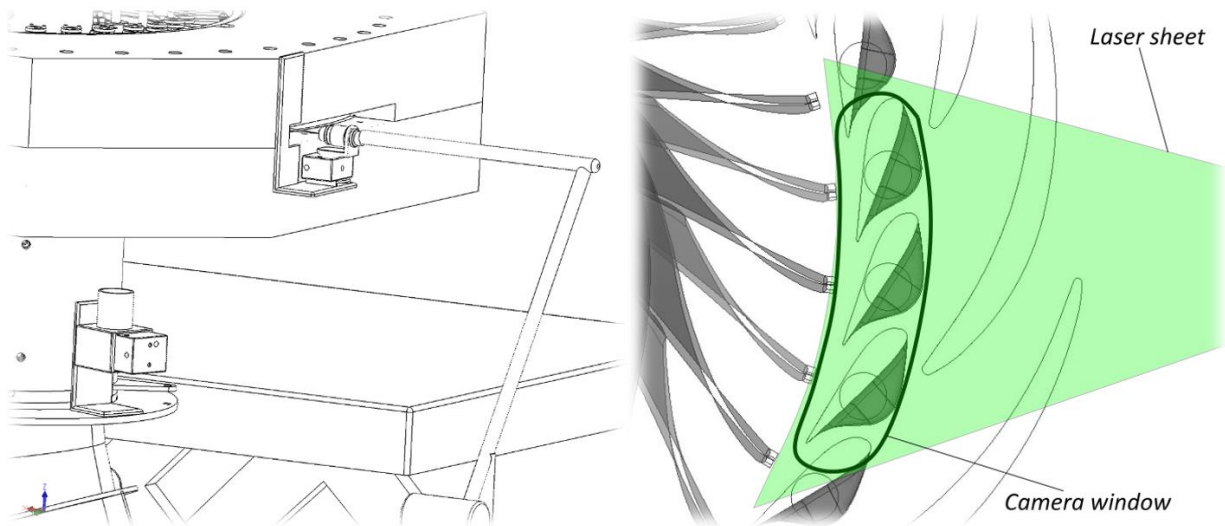


**FIGURE 37: LASER AND CAMERA VIEW, FROM THE OUTSIDE(LEFT) AND INSIDE(RIGHT).**

The camera is located right below the camera window, perpendicular to the laser sheet. Depicted in figure 37. We can see that the window covers three whole guide vanes and the TE of a fourth. A picture of the separate Plexiglas window can be seen in figure 38.

The guide vanes in the Francis turbine have a chord length of 105mm, and a height of 58.6mm. The TE shape is reminiscent of the earlier mentioned Donaldson geometry, and the thickness was measured to be 1.18mm by Bolstad [10], while 2.2mm was recently used by Trivedi. [61] As previously mentioned it is difficult to determine the position of the separation points. If we were to estimate the vortex shedding frequency using 1.18mm, 2.2mm and Brekke's formula (2.6) we would get 1430 Hz and 902 Hz, respectively, for a

flow velocity of 10 *m/s*. This is a huge discrepancy and considering we do not know the real Strouhal number for hydrofoils it is important to emphasise that these are just estimates.



FIGURE 38: CAMERA WINDOWPANE TO THE LEFT, OLD AND NEW GUIDE VANE TO THE RIGHT.

#### 4.6 Laser sheet / Plexiglas interaction

An even laser sheet is required for reliable PIV results. When looking at the laser spread through the camera pane for the first time, several ill-lighted regions were exposed. It seems both the LE and TE of the Plexiglas guide vanes and stay vanes cause light to scatter. This caused large unusable sections in our planned FOVs. Fortunately, both the laser and camera window allow for adjustment. After some modifications we found a camera position combined with a laser angle which gave an entire usable region for the 100mm lens. This is depicted in figure 39 where we can see the laser sheet for both 4 and 14 degrees guide vane opening. A raw image for this FOV was also shown in figure 28 for 10 degrees. It is important to stress that as the guide vanes move, so will the shadows.

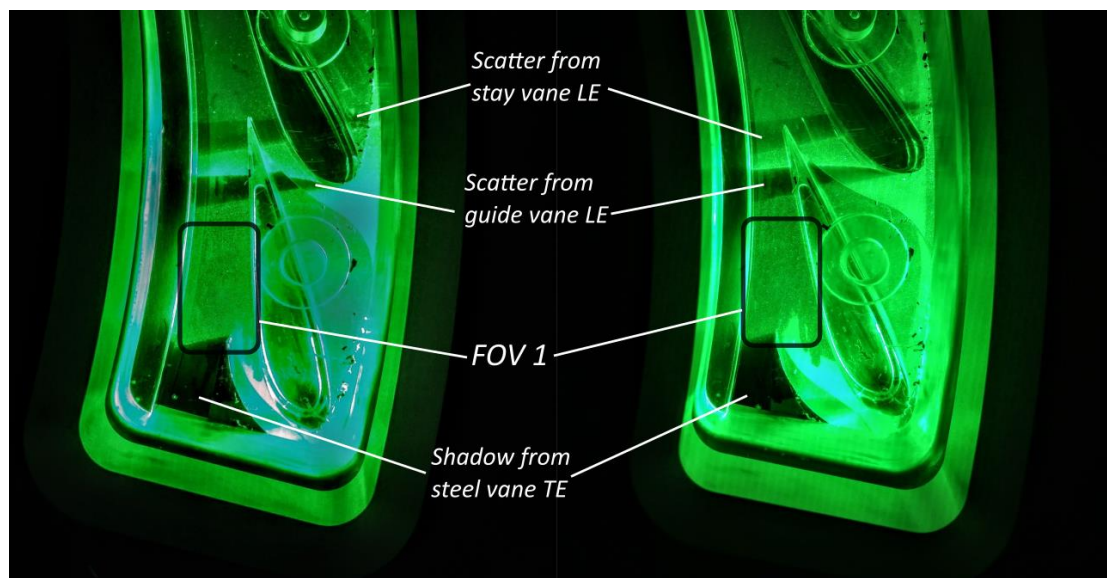
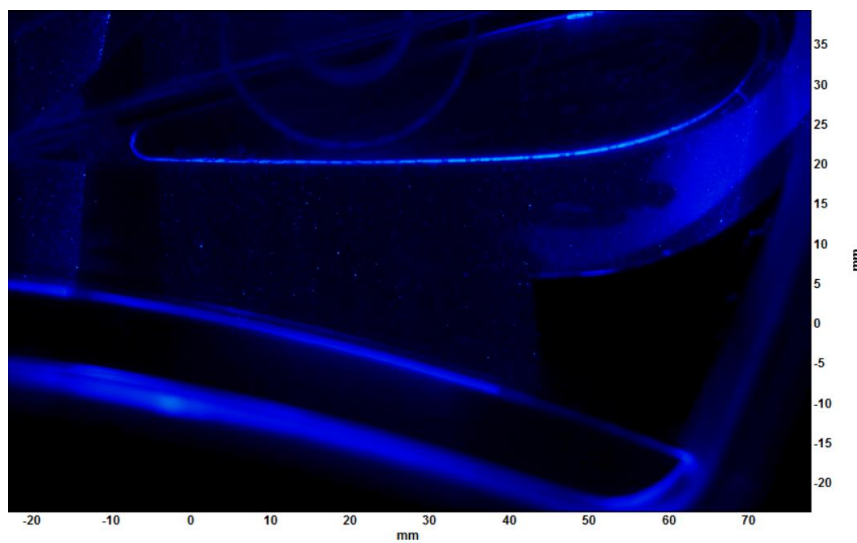


FIGURE 39: LASER SHEET FOR 4 DEGREES (LEFT) AND 14 DEGREES (RIGHT) GUIDE VANE OPENINGS. THE MARKED FOV IS AN APPROXIMATION FOR THE 100MM LENS.

A side effect of this adjustment was that lens 2, with the larger FOV, would now be redundant. A raw picture taken with lens 2 can be seen below. Here we can see that not much of interest is revealed compared to the smaller FOV. The region to the bottom right could have been interesting, but is not illuminated due to our FOVs being focused on the TE of a non-interchangeable steel vane. Additionally, the region to the top right is not accurately calibrated for, which will be explained later.

Note that figure 39/40 is looking from the perspective of the high-speed camera, while previous figures have been seen from above, causing seemingly reversed vane directions.



**FIGURE 40: FOV 2, USING 50MM LENS**



## 4.7 Calibration

Calibrating in the vaneless space required some custom devices. A picture of the calibration plate along with the overlay pattern is shown in figure 41. The Davis software can differentiate between dots and crosses, so both are used to avoid misinterpretation, as seen in the illustrated pattern. The distance is 10mm, 5mm and 2,5mm between the larger dots, crosses and smaller dots, respectively. This was done so the same overlay could be utilized for different sized FOVs. The rule of thumb often used for choosing correct “dot” size is approximately 10pixels in diameter and a total of ~25dots in the FOV. [37] The vertical and horizontal lines were aligned with premade points on the calibration plate to ensure a fixed coordinate system.

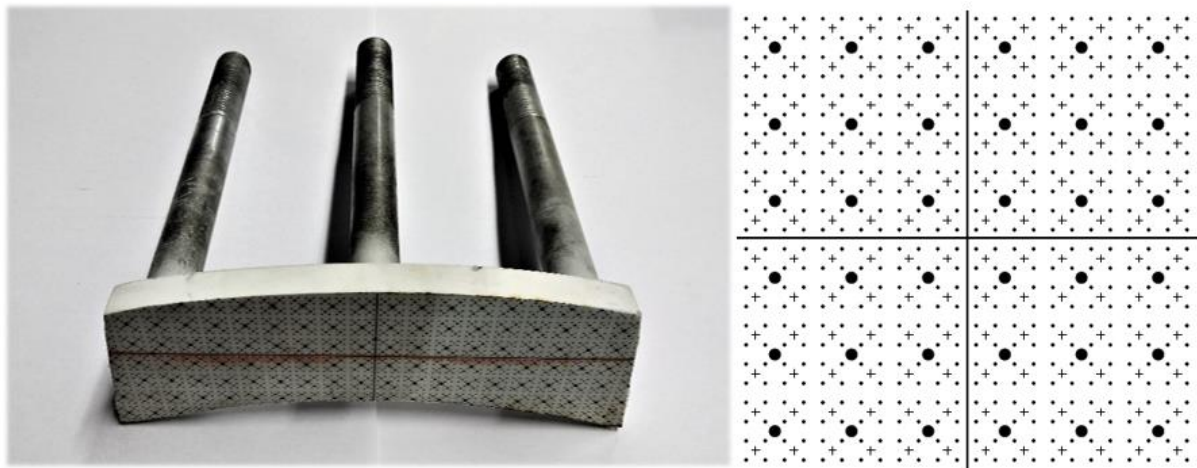


**FIGURE 41: CALIBRATION DEVICE AND OVERLAY PATTERN USED IN THE FRANCIS TURBINE**

The calibration device was made to fit the same attachments as the three guide vanes directly above the camera window. Accordingly, before mounting the calibration plate and window these vanes need to be removed. A cross sectional view of the turbine can be seen in figure 42, where the calibration plate is in its intended position. In figure 43 we can see how the rods attach to the top of the turbine. By pinpointing the location for which the bottom of the calibration device aligns with the bottom of the guide vanes, we can measure and adjust from the top of the turbine which plane the plate is located in. This is also indicated in figure 43. The customized “board” seen in this figure was machined to be completely horizontal, so that the measurement from this plane to the top of the rod would be more consistent.

When the calibration plate and window have been fixed, the test section is filled with water to best replicate the measurement conditions. The calibration device is adjusted to the plane we wish to measure in and the laser sheet is set to be parallel and at the same height. Following

this it is suggested by LaVision to retract the calibration plate before focusing the camera on the particles illuminated by the laser. When the focus is set, and the particles look sharp, the calibration plate is slowly moved back down until it is in focus. This is done to ensure that the camera is primarily fixated on the laser sheet, and not the calibration plate.

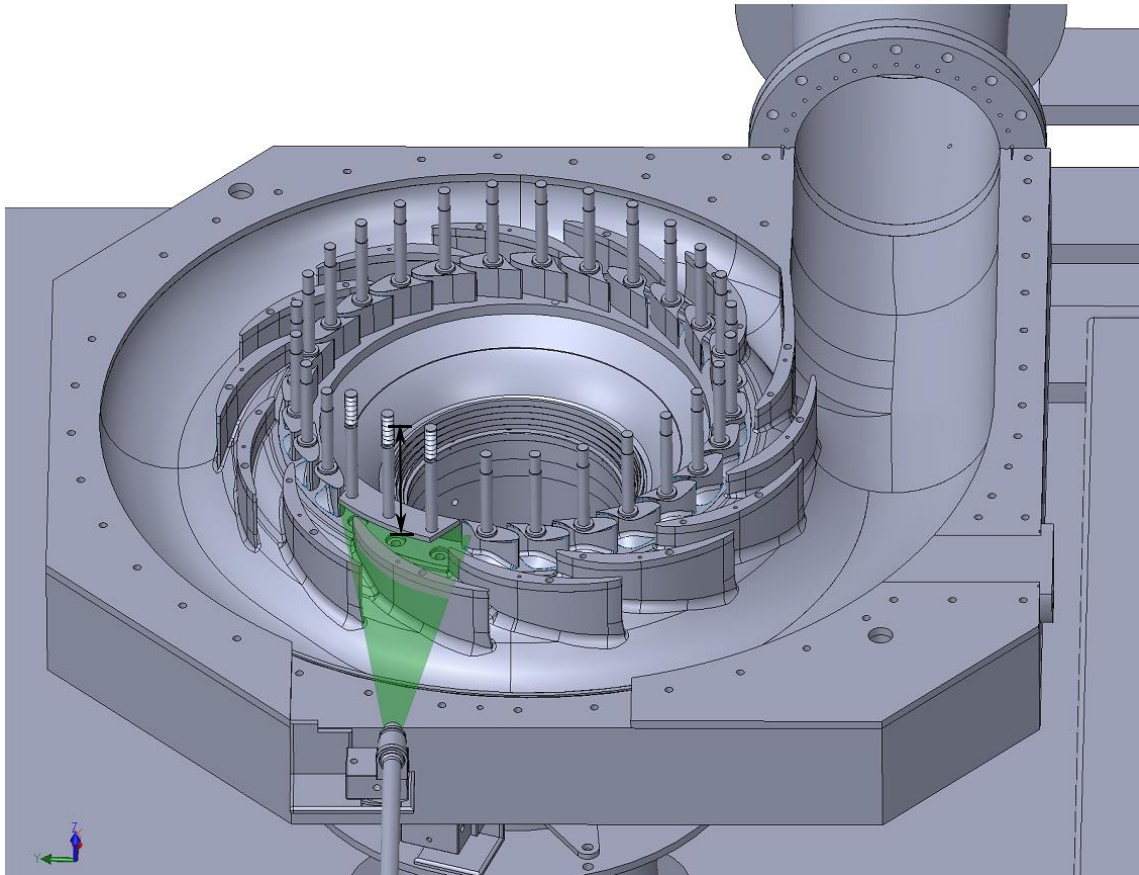


**FIGURE 42: CROSS SECTION VIEW OF THE TURBINE WHERE THE INTERCHANGEABLE GUIDE VANES HAVE BEEN REPLACED BY THE CALIBRATION DEVICE.**

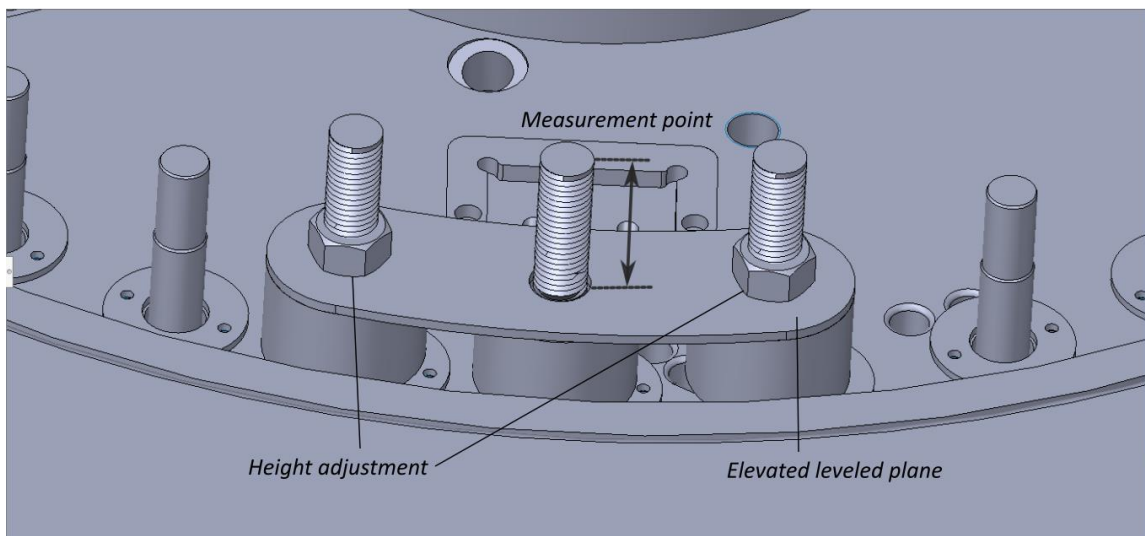


**FIGURE 43: ATTACHMENT OF THE CALIBRATION DEVICE SEEN FROM THE TOP OF THE FRANCIS TURBINE**

The Calibration for lens 1 can be seen in figure 44. Based on three chosen points, circled in the left image, other dots in a similar pattern and of comparable size are recognized, marked in green. The right image is a corrected image shown after the finished calibration. Here we can see the value of the axis has transformed to mm rather than pixels. The grid displayed in this image will be the foundation when calculating the magnitude of the velocity vectors. As previously mentioned the calibration plate does not reach the entire FOV, meaning the vectors generated to the far right in our images will in general be less accurate.

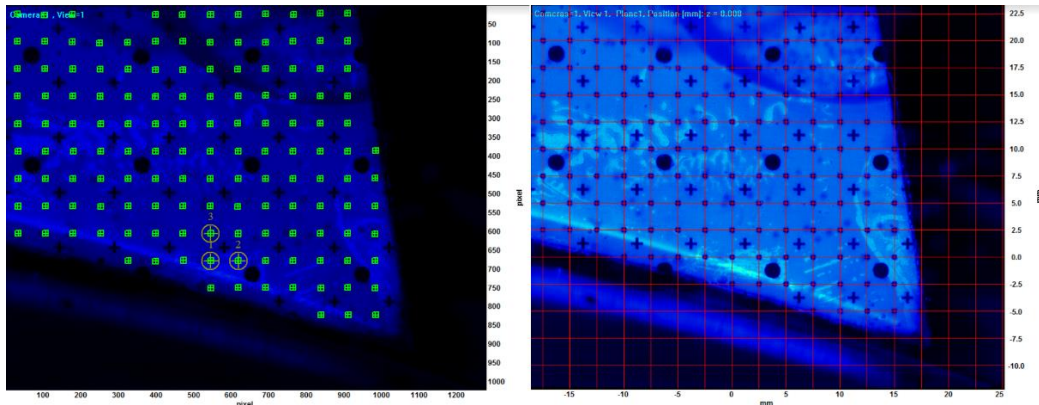


**FIGURE 44: PRE-CALIBRATED IMAGE (LEFT) AND CORRECTED IMAGE (RIGHT)**

Since the calibration process includes draining a section of the water loop and disassembling minor parts of the Francis turbine it is quite time-consuming. To avoid frequent recalibrations, a system was produced to check if the camera or laser had shifted. The system was simply a box with lasers facing multiple directions which could be attached to the camera and laser sheet optic. This is illustrated in figure 45. By marking positions on fixed surfaces after a calibration we could easily check if any of the critical components had moved.

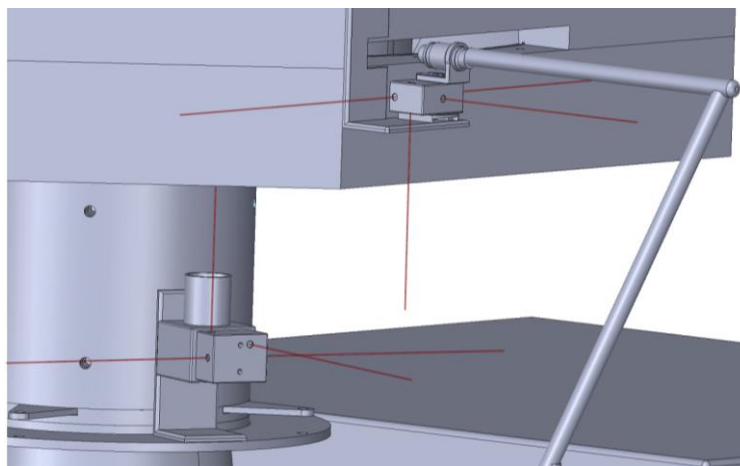


**FIGURE 45: CALIBRATION BOXES MOUNTED ON THE CAMERA AND LASER SHEET OPTIC.**

A theoretical secondary use of the system was for quickly adjusting camera position. By doing several calibrations at once for various camera locations and appropriately marking the surface areas where the beams hit, it might have been possible to realign the lasers with previously recorded positions. Since it is possible to switch to earlier calibrations in Davis, this could potentially save a lot of time in future measurements. A concern with this approach is that the lasers in the boxes themselves need to be focused. For various camera positions the beams might hit different surfaces, which means a refocusing is required. The lasers currently being used in the boxes do not maintain a steady trajectory when refocusing. This might make this application to unreliable for PIV measurements, but it has not yet been tested due to the static camera position used throughout this project.

## 4.8 Operating parameters and test procedure

The governing operating conditions will be the head value, guide vane opening and turbine RPM. Head and turbine RPM will be kept as constant as possible for the duration of our image acquisition. Due to time constraints BEP will be the main focus for this thesis. For the Francis turbine at NTNU this is specified as:

TABLE 4.2

| Parameter:                | Value:     | Unit:       |
|---------------------------|------------|-------------|
| <i>Head</i>               | $\sim 12$  | [m]         |
| <i>Turbine RPM</i>        | $\sim 333$ | [-]         |
| <i>Guide vane opening</i> | $\sim 10$  | [°]         |
| <i>Flowrate</i>           | $\sim 0.2$ | [ $m^3/s$ ] |

Datasets were also to be taken with the same head and RPM for guide vane openings of  $\sim [4^\circ, 6.7^\circ, 12,4^\circ, 14^\circ]$  corresponding to flowrates of  $\sim [0,081m^3/s, 0.137m^3/s, 0.24m^3/s, 0,263m^3/s]$ .

The newly acquired Francis parts had not been tested prior to the PIV measurements, where the guide vanes are likely the most fragile. It was therefore suggested by P. T. Storli to slowly ramp up the flowrate in the loop. Accordingly, the first dataset was acquired at  $4^\circ$  guide vane opening due to a prior torque test showing equilibrium for this opening. The torque increases on the guide vanes all the way up to BEP, from which it almost stays the same up to the maximum vane opening. [62]

The other points were chosen due to their frequent use in publications by NTNU researchers. Both  $4^\circ$  and  $6.7^\circ$  are used as part load conditions, whereas  $12.4^\circ$  is heavy load.  $14^\circ$  is not that commonly used but was included since it is the maximum opening, and thus has the narrowest vaneless space. Though not the focus of this thesis, having data from various openings may prove useful to accentuate differences in flow patterns.

As implied, the datasets were taken in the following order:

$4 \rightarrow 6.7 \rightarrow 10 \rightarrow 12.4 \rightarrow 14 \rightarrow 12.4 \rightarrow 10 \rightarrow 6.7 \rightarrow 4$

Resulting in two supposedly equivalent datasets for each guide vane opening, except for  $14^\circ$ . The first and second dataset of the day will later be denoted by *ramp-up* and *ramp-down*, respectively.

When opening the guide vanes, the measured head in the turbine will be reduced as the flow increases, showcased in the next section. This means that for each step the main pump RPM must be increased to keep the head at a static 12m during the image acquisition.

Consequently, when closing the vanes it is crucial to reduce the pump RPM beforehand to avoid throttling of the flow.

Measurements were done both on the ramp up and on the ramp down to ensure there was no influence from the order the operating parameters were set. This scheme was repeated a couple of days later to establish repeatability.

### 4.8.1 PIV pre-processing settings

The shedding frequency of the guide vanes was estimated using a simulated velocity field of our AOI for BEP conditions, provided by Trivedi. This was combined with the earlier mentioned TE thickness parameters used by Bolstad and Trivedi along with a Strouhal number of 2.2. From the Brekke equation (2.6) we get an interval [1044Hz - 1656Hz]

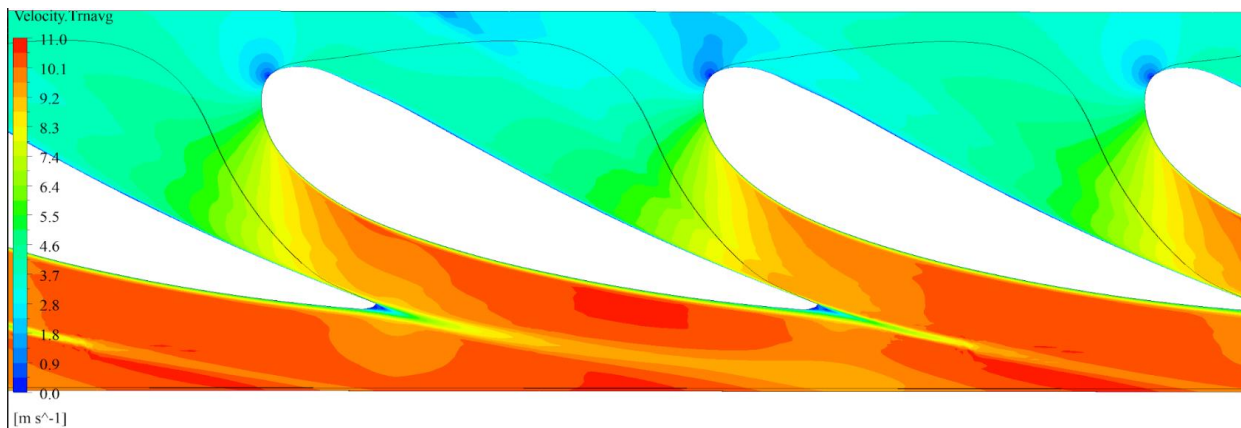


**FIGURE 46: SIMULATED AVERAGE VELOCITY AT BEP AROUND GUIDE VANES IN OUR AOI**

The camera has a maximum image resolution of 1280x1024 which allows a double frame image frequency of 2400Hz. Using Nyquist's theorem, we see that this is probably too low to showcase the entire shedding frequency spectre, which is assumed to be the highest frequency in the vaneless space. Since the estimates are so rough, datasets were taken for two different camera resolutions at every guide vane opening. The resolutions were set to 1280x800 and 1280x600, providing image rates of 3144Hz and 4166Hz, respectively. The memory capacity of the camera is 5589 image pairs and 7453 image pairs for these same respective image resolutions. This leads to a sample time of ~1.79s for both.

For a particle shift of ~5pixels the laser pulse separation was set to 14 $\mu$ s. This was done using the procedure explained in chapter 3.

The images were pre-processed using a time series subtraction, reducing background noise. Showcased in figure 28.

## 4.8.2 PIV post-processing settings

The scale factor after calibrating was 29.4px/mm. When feeding the water loop with particles an IA of size 24x24px was anticipated, meaning an area of 0.81x0.81mm should have roughly 10 particles. Other IA sizes have been tested along with various combinations of overlaps and passes. A compilation of different vector field resolutions is showcased in figure 47. The hydrofoil TE has been masked out, along with all other stationary components, but is located at approximately;  $x=20\text{mm}$ ,  $y=10\text{mm}$ . They have all been solved using multiple passes and decreasing IA sizes. The resolutions noted in the figure description is for the final pass. From this figure we can see that both 24x24 and 16x16 resolutions outline similar fluid structures. The 24x24px IA was chosen as larger IAs in general have less error, shown in section 3. It is also assumed that the fluid phenomenon observed in this thesis can be properly identified without using an even finer grid.

The PIV processing was performed using a decreasing IA size from  $64 \rightarrow 24$ , with 50% overlap and 2 passes for each size. Further increasing passes did not result in any noticeable difference.

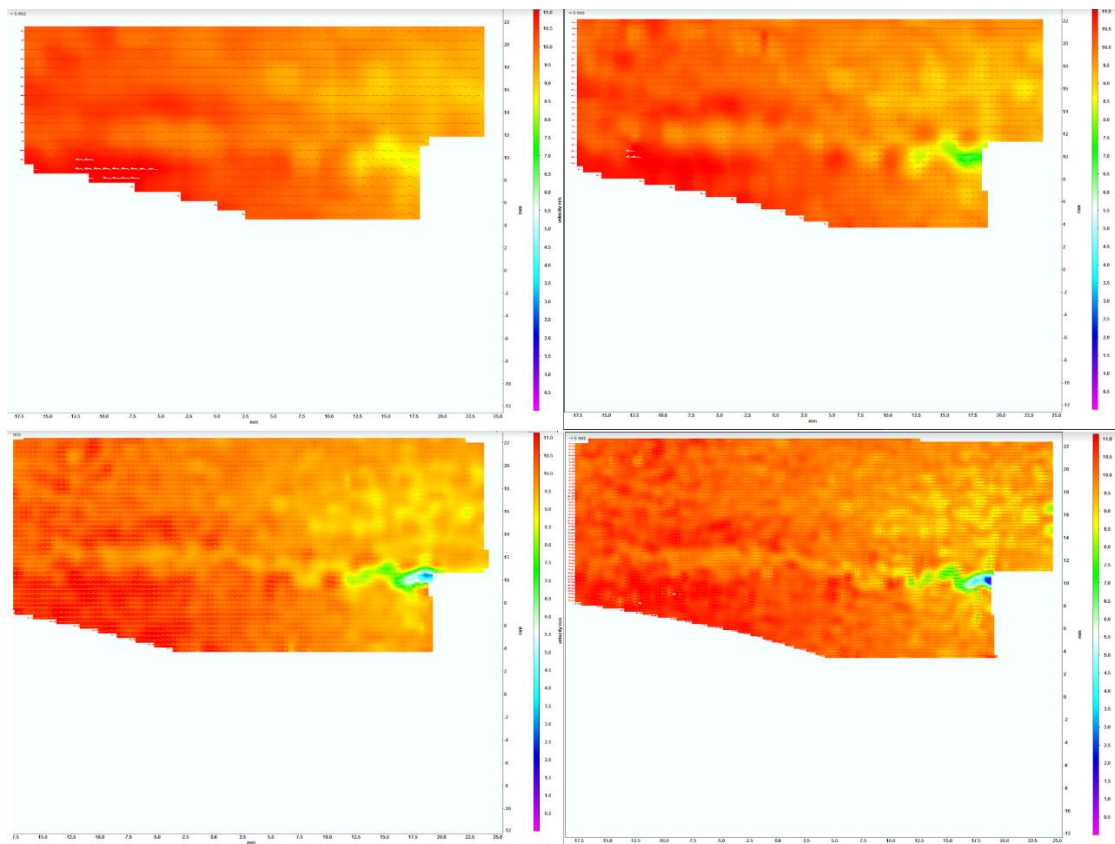


**FIGURE 47: A SAMPLE VELOCITY FIELD AT BEP FOR IAs OF 48x48, 32x32, 24x24 AND 16x16 FROM TOP LEFT TO BOTTOM RIGHT**

## 4.9 Measuring equipment and uncertainty

The primary focus of this subsection will be the uncertainty of the equipment used to calculate operating conditions, with focus on BEP running. The uncertainty calculations will be based on a thorough review of all the measuring equipment by E. Agnalt, [31] done a few months prior to the PIV measurements. As mentioned earlier; the Head, guide vane opening, and turbine runner speed will be used as the governing parameters. The flowrate and its effect on the head will also be touched upon.

The head is mainly measured by a differential pressure transducer  $P_d$ , with inputs stemming from the turbine inlet and outlet, indicated in figure 48 by  $P_1$  and  $P_2$ . There is also a contribution to the head by dynamic pressure. Using Bernoulli's equation, we can relate pressure, height and velocity by:

$$\frac{P_1}{\rho g} + \frac{V_1^2}{2g} + z_1 = \frac{P_2}{\rho g} + \frac{V_2^2}{2g} + z_2 + H \quad (4.1)$$

Where  $V_i$ ,  $P_i$  and  $z_i$  is the respective velocity, pressure and height at given locations. In this case 1 is the turbine inlet and 2 the draft tube.  $\rho$  is the density of the fluid and  $g$  is the gravitational constant. If we include relations for  $P_d$ ,  $P_1^*$  and  $P_2^*$  showcased in figure 48:

$$P_d = P_1^* - P_2^* \quad (4.2)$$

$$P_1^* = P_1 + \rho g z_1, P_2^* = P_2 + \rho g z_2 \quad (4.3)$$

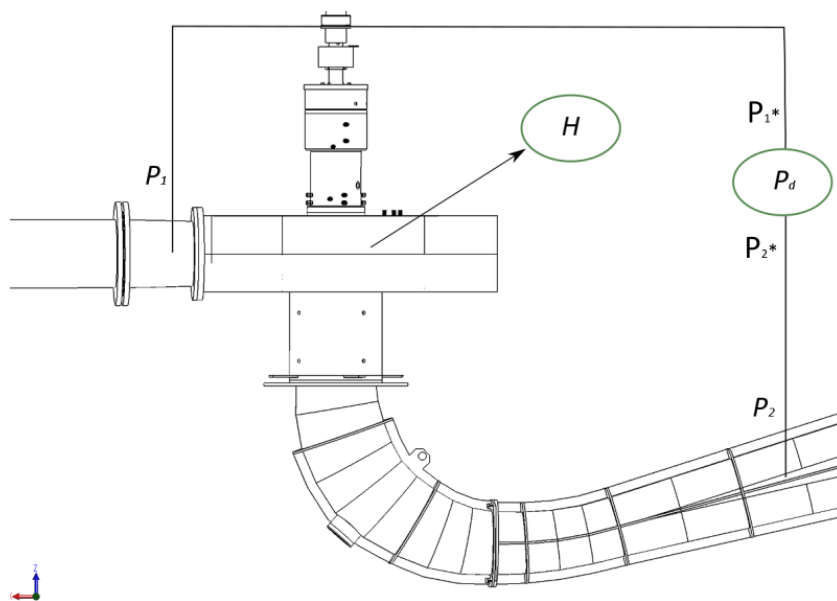


FIGURE 48: PRESSURE TRANSDUCER ( $P_d$ ) MEASURING POINTS ALONG WITH INDICATED HEAD REGION  $H$ .



We are now able to combine and manipulate these equations to:

$$H = \frac{Pd}{\rho g} + \frac{V_1^2 - V_2^2}{2g} \quad (4.4)$$

The flow velocities  $V_1$  and  $V_2$  are simply calculated from known area sizes at location 1 and 2, along with the measured flowrate. This leads to the relation;

higher guide vane openings  $\rightarrow$  higher flowrates  $\rightarrow$  higher dynamic impact on the head value.

This relates to the measurements for two reasons. The original flowmeter stopped working the day of our PIV measurements. The head values shown real time in the control room are calculated differently than the logged values, which was derived above. This discrepancy was not considered the first day of the PIV measurement, causing an error in head values equal to the dynamic pressure. The logged values for day 1 are still correct, but not exact BEP conditions. For the lowest flowrate the difference is almost negligible, but for guide vane openings of  $10^\circ$  and above it is apparent. The logged values, which are the accurate ones, show a deviation of approximately 0.35m head from the BEP. This can also be calculated using the second fraction on the right side of equation (4.4). A temporary flow meter was attached to the rig before the second day of measuring, making the operational parameters a lot more consistent.

This also relates to the calculated uncertainty for the head since we used a clamp-on flowmeter for the second day of measurements. The clamp-on flowmeter had a stated uncertainty of  $\pm 1\%$ , which is higher than the previous flow meter used in the calculations by Agnalt. However, for BEP condition the dynamic pressure only account for  $0.35/12 = 3\%$ . The original flowmeter had an uncertainty of 0.56%, equalling an increase in flowmeter uncertainty  $\sim 0.5\%$ . Considering the manufacturing uncertainty is usually on the high end the impact on the head uncertainty is deemed negligible.

#### 4.9.1 Quantified uncertainty of operational parameters

The head values, runner speed, guide vane angle and flowrate were all sampled and logged at a frequency of  $\sim 5\text{kHz}$ . An estimate of the total uncertainty will be given based on the sample uncertainty  $S_{dev}$  from equation (2.10), the sensor uncertainty  $S_A$  from Agnalt, and a total uncertainty  $S_{tot}$  from equation (2.12). An exception is for the flowrate, where the

manufacturer uncertainty will be provided in place of  $S_A$ . The sample uncertainty is based on the data logged during the image capturing  $\sim 1.8s$ , meaning a sample size of roughly 9000. Gaussian distribution and 95% interval is applied. The largest calculated  $2*S_{dev}$  for every parameter is used and converted to percentage values. The sample uncertainty of the guide vane angle is negligible, as it should be, since it stays fixed for the duration of the measurements.

**TABLE 4.3: BEP HEAD UNCERTAINTY**

| Uncertainty type: | Size:         |
|-------------------|---------------|
| $S_{dev}$         | $\pm 0.29 \%$ |
| $S_A$             | $\pm 0.20\%$  |
| $S_{tot}$         | $\pm 0.35 \%$ |

**TABLE 4.4: BEP FLOWRATE UNCERTAINTY**

| Uncertainty type: | Size:         |
|-------------------|---------------|
| $S_{dev}$         | $\pm 0.39\%$  |
| $S_A$             | $\pm 1\%$     |
| $S_{tot}$         | $\pm 1.06 \%$ |

**TABLE 4.5: BEP TURBINE RUNNER UNCERTAINTY**

| Uncertainty type: | Size:         |
|-------------------|---------------|
| $S_{dev}$         | $\pm 0.19 \%$ |
| $S_A$             | $\pm 0.33\%$  |
| $S_{tot}$         | $\pm 0.38 \%$ |

**TABLE 4.6: GUIDE VANE ANGLE UNCERTAINTY**

| Uncertainty type: | Size:         |
|-------------------|---------------|
| $S_{dev}$         | $\pm 0.004\%$ |
| $S_A$             | $\pm 1.41\%$  |
| $S_{tot}$         | $\pm 1.41 \%$ |

## 4.9.2 Quantified uncertainty for PIV

There is still much to learn when it comes to PIV uncertainty. The most thorough quantification of uncertainty to date was showcased in section 3, but it can still only serve as a rough outline for some relations. Additionally, it is widely accepted that synthetic data underestimate error because of too idealized conditions. [54] It will not be given an estimation of the uncertainty from errors caused by a combination of IA size, particle size, particle density and image settings as it would be speculation.

Davis provides an uncertainty estimate based on the calibration and cross-correlation. A lot of the data shown in the results stems from averages of oscillating velocities. The stronger the fluctuation in velocity is the more the standard deviation will be overestimated.

The original calibration plane height was measured to be 27.3mm from the bottom of the guide vane. This was measured using calliper which in itself has a reading error of ~0.1mm. The post-calibration was done after all measurements was concluded. This was done by reinserting the calibration device, and slowly adjusting the height until it was completely in focus. The post-calibration plane height was measured to be 29.5mm. Making the actual measurement plane  $28.4\text{mm} \pm 1.104\text{mm}$ .

### 4.9.3 Repeatability

Since the measurements from day one were executed for off-BEP conditions, the data will not be used to check repeatability. The showcased graphs in the result section will primarily stem from the ramp-up datasets from day two, while the ramp-down sets will be used to check repeatability. A replication of all reproduceable graphs, i.e. not instantaneous samples, seen in the result section can be seen in appendix C for the ramp-down dataset. Operational parameters for the ramp-down dataset is; turbine RPM 332.8, guide vane angle  $10,14^\circ$ , flowrate  $0.199\text{m}^3/\text{s}$  and a head value of 12,16m.

The values used in figure 50 was checked by *test-retest reliability*(*rtr*), shown in table 4.7

**TABLE 4. 7: VELOCITY WAKE REPEATABILITY**

| X-axis value: | Size:         |
|---------------|---------------|
| <i>15mm</i>   | $\pm 3.43 \%$ |
| <i>10mm</i>   | $\pm 1.88\%$  |
| <i>5mm</i>    | $\pm 1.48 \%$ |
| <i>0mm</i>    | $\pm 1.45 \%$ |

Due to time constraints the power spectrum values was not subdued to repeatability testing. The peaks and valleys are for the most part not exactly in phase, leading to very low correlation factors for the methods tested. There is surely a good way of checking reliability for these kinds of datasets, but it was not found.

## 5. Results and discussion

The results will be split into three parts. First, we will be looking at the overall velocity field in the FOV, checking the validity of the measurements compared to simulations. Afterwards we will look at RSI. Finally, a check of the shredding frequency of the guide vanes.

All stated operating conditions will be the average value of the logged data during the image acquisition, where the previously deduced uncertainty will apply, but it will not be written.

### 5.1 Velocity field

The velocity field shown to the left in figure 49 was calculated by averaging all samples for a dataset taken at turbine RPM 333.2, guide vane angle  $10,04^\circ$ , flowrate  $0.205\text{m}^3/\text{s}$  and a head value of 12,03m. The camera resolution used was 1200x600pixels meaning a sample size of 7453. Unless mentioned otherwise, this will be the sample used throughout the chapter.

Datasets were exported for vertical lines at x positions: 0mm, 5mm, 10mm and 15mm, indicated by the stippled lines. These values are shown in figure 50, where the x-axis corresponds to the y-axis in the velocity field.

Figure 46 has been transposed and cropped, seen to the right in figure 49, to easier compare the two averaged velocity fields. A glance shows that they compare well, both in terms of velocity magnitude and which regions has the higher and lower velocities. An exception is the recirculation area which is slightly underestimated for the PIV measurements. This is believed to be due to a combination of too low resolution to properly reproduce the area close to the trailing edge, as well as some of the recirculation area being masked.

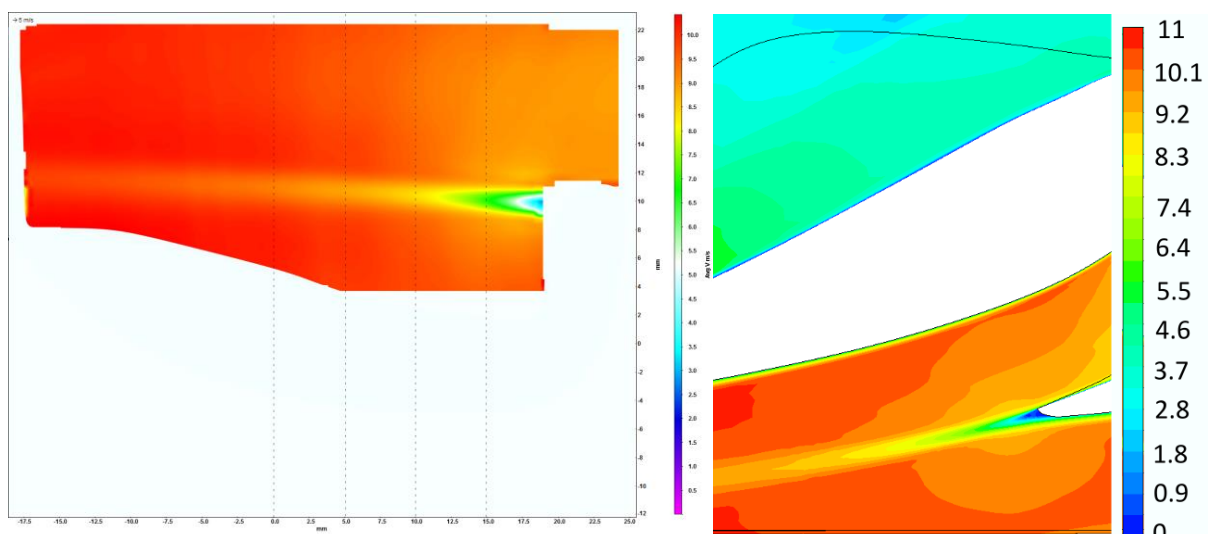


FIGURE 49: AVERAGE VELOCITY AT BEP FROM PIV (LEFT) SIMULATED AVERAGE VELOCITY (RIGHT)

An averaged velocity field using 16x16pixel IA sizes can be seen in appendix C, supporting the belief that resolution is at least partly to blame. Below that velocity field there is also a comparison of the velocity lines at  $x=15\text{mm}$  for the two applicable resolutions. This was included to show that the discrepancy is mostly limited to the recirculation area.

Figure 50 underlines the expected trend, where the wake gradually becomes weaker as the distance from the trailing edge increases.

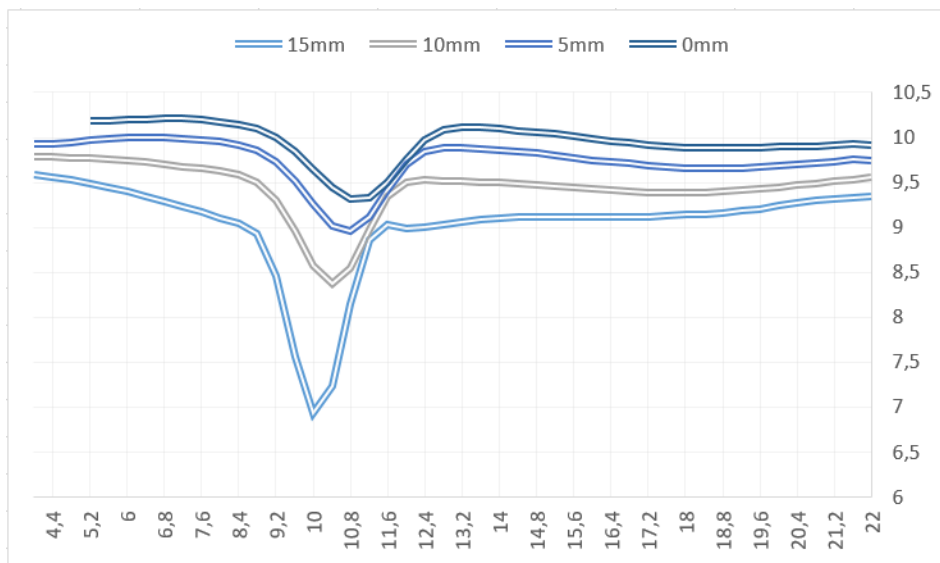


FIGURE 50: CROSS WAKE VELOCITY VECTORS

## 5.2 RSI

RSI is probably the easiest phenomenon to detect by itself. Using equation (2.7) we get an estimated value of 166.6Hz. This estimation is a lot more robust than the one used for shedding frequency as the number of times a turbine blade passes a guide vane is easily quantifiable.

We can set the software to recognize variations in *y-direction velocities* ( $V$ ). We choose to exclude the x-component since the flow in this direction is orders of magnitude larger. Additionally, the phenomenon we are trying to detect should produce flow variations in the y-direction

Below we can see a graph showcasing the power spectrum counts for a range of frequencies. This is done by a discrete Fourier transformation, which is a variation of the previously mention Fourier transformation. This graph is compiled from an entire dataset for a chosen point, in this case  $x = -5$ ,  $y = 7$ , highlighted in figure 52. The most persistent sinusoidal waves with the highest amplitudes will have the most defined peaks.

For this point we can see two distinct spikes. The largest manifestation is seen for  $\sim 166\text{Hz}$ , which fits the estimated value, and the other peak is very likely its second harmonica.

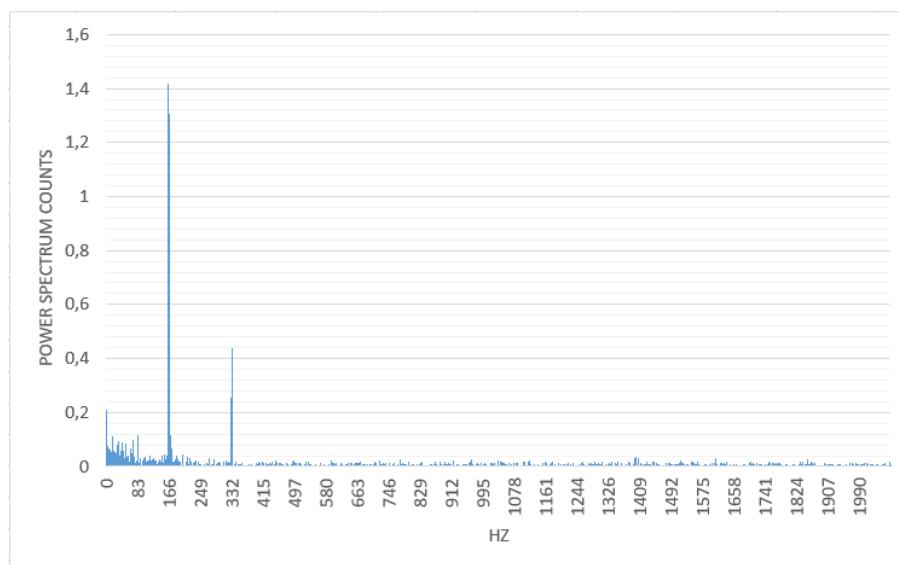


**FIGURE 51: POWER SPECTRUM FOR A POINT LOCATED AT  $x = -5\text{MM}$ ,  $y = 7.5\text{MM}$**

Another way of showcasing dominating frequencies is with a power spectrum of the entire FOV, seen in figure 52. This is a more time-consuming process, as the same data used in figure 51 is found for every IA. Instead of spikes in a graph the peaks are indicated by colour. Notice how these two representations have similar dimensions for the y-axis, even though

expressed differently. For complete a power spectrum, one picture corresponds to  $\sim 1\text{Hz}$ , meaning there is an array of pictures to scroll through.

For  $f=166.6\text{Hz}$ , which was found to be the peak intensity for this dataset, we can clearly see how the strength of the RSI tapers off as we move further away from the turbine runner. This induced velocity in the y-direction probably corresponds to the potential flow part of RSI, as mentioned in section 2. Due to changes in proximity it seems evident that this effect becomes more substantial as the guide vane angle increase.

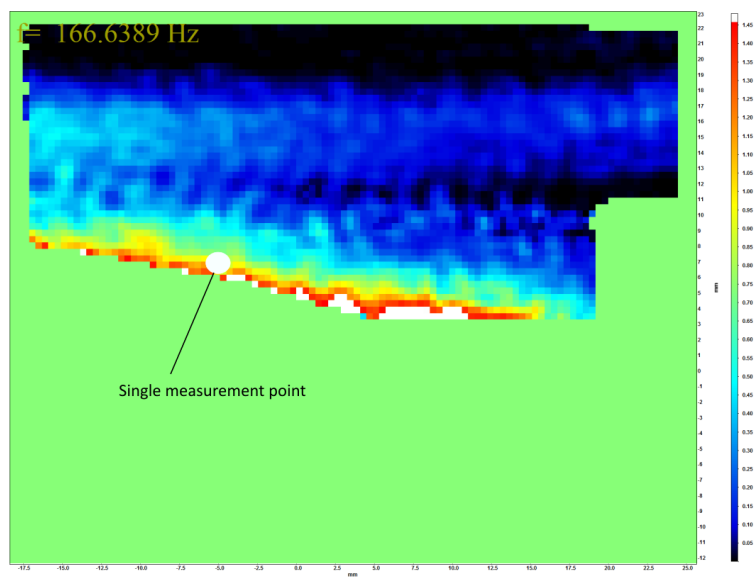


**FIGURE 52: POWER SPECTRUM OF ENTIRE FOV FOR STATIC FREQUENCY = 166.64HZ**

We saw in the velocity field part how wakes increase in strength as we move closer to the TE. To accentuate that the wake interaction from RSI also increase for an increasing guide vane angle, an averaged velocity field for guide vane angles of  $4^\circ$  and  $14^\circ$  have been included below. From these it is probably safe to assume that the wake interaction part of RSI is negligible for low guide vane openings.

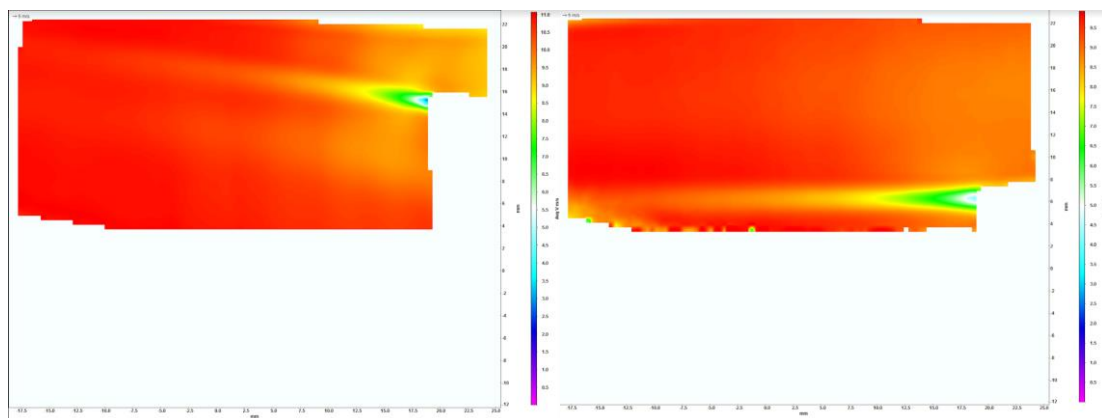


**FIGURE 53: SIDE BY SIDE COMPARISON OF AVERAGE VELOCITY FIELD FOR FOR  $4^\circ$  (LEFT) AND  $14^\circ$  (RIGHT) VANE OPENING.**

### 5.3 Guide vane shedding frequency

It is difficult to detect and correctly identify shedding from an unadopted velocity field. An instantaneous velocity field was shown in figure 46, where we can see that the shape of the wake resembles a Karman vortex shedding pattern, but since the planar velocity is so dominant, all velocity vectors point in the same direction, though to a lesser extent in some areas. It is also of note that the vortices travel downstream making any noticeable rotation unlikely. Two ways of checking for vorticity in a single snapshot can be seen in figure 54. For the image to the left we have changed the settings from velocity to vorticity, showing rotation in the flow, denoted by rotations/sec. From the colour scheme we see that the direction of the rotation depends on the shedding side, which is what it ideally should look like.

To the right we see a zoomed in image of the same timeframe. For this picture the velocity from a predetermined point has been subtracted for the entire FOV. This was done by using the left image as an indication of where the vortex centres are located. Afterwards the exact velocity in this point is found before the entire field is offset by this specific amount. For the right image the chosen “stagnation point” is located at  $x=12,5\text{mm}$ ,  $y=11\text{mm}$ . Surrounding this node we can clearly see a circular motion. From these two indicators we conclude that there is indeed vorticity in the flow.

Note that the velocity image used as example below is not what most images look like. The shedding seen here is a lot more structured than for most timesteps.

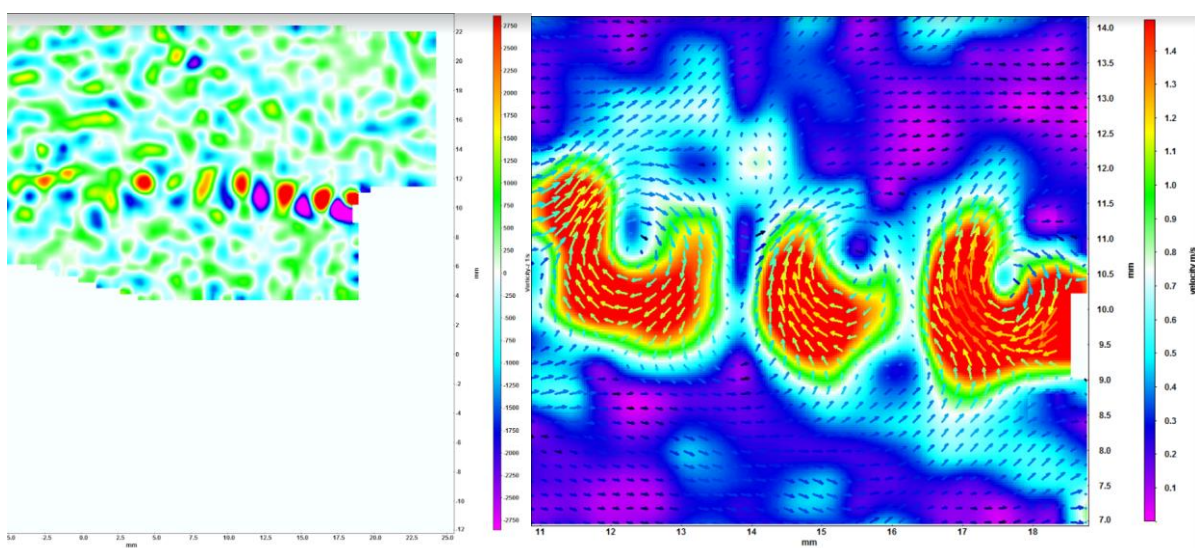
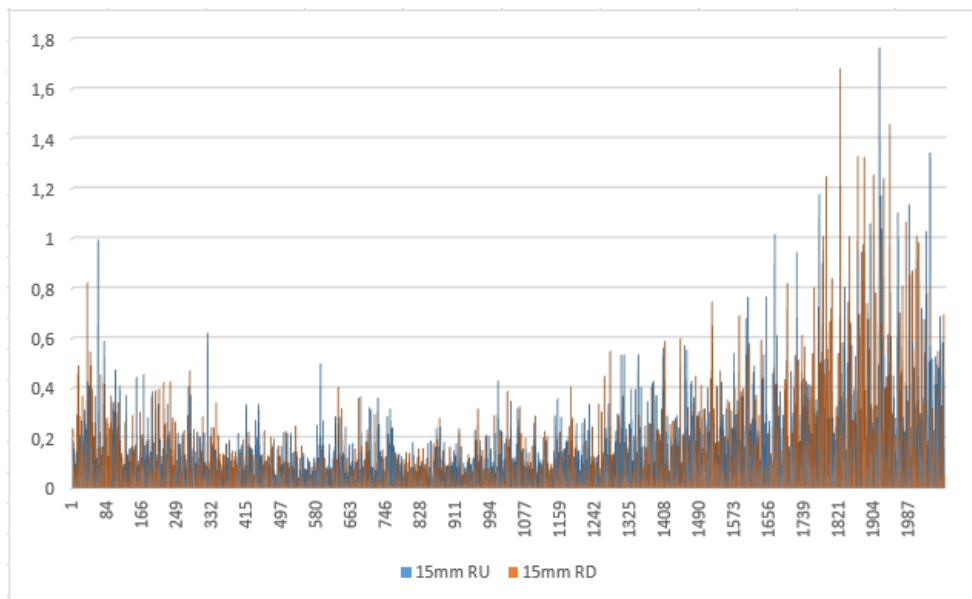


FIGURE 54: TWO WAYS OF SHOWCASING VORTICITY FOR THE SAME INSTANTANEOUS VELOCITY FIELD



The guide vane shedding frequency is plotted by the same procedure as the RSI. Where variance in  $V$  is measured. The shedding frequency is very spread, so data from both ramp up and ramp down will be used in an attempt to smoothen the distribution. The sampled points will for both datasets be  $x=15\text{mm}, y=10\text{mm}$  and  $x=5\text{mm}, y=10\text{mm}$ . The legends denoted RU and RD is for the ramp up and ramp down dataset, respectively.

As expected the intensity is higher for the dataset acquired closer to the TE, while the general trend is comparable. The RSI frequency has a distinct peak in figure 56, while in figure 55 it is not distinguishable from the random noise.



**FIGURE 55: VORTEX SHEDDING FREQUENCY MEASURED AT  $x=15\text{MM}, y=10\text{MM}$**

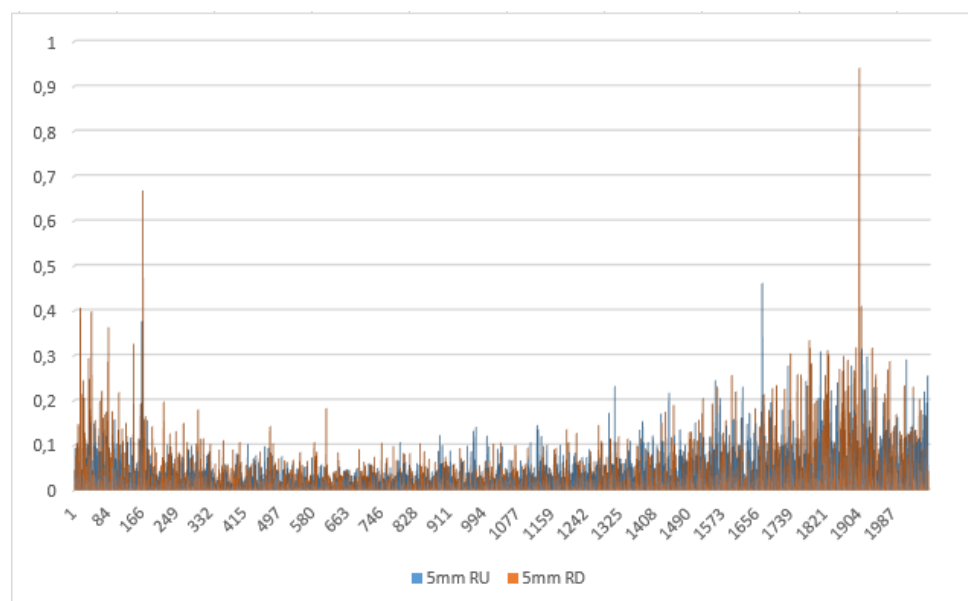


**FIGURE 56: VORTEX SHEDDING FREQUENCY MEASURE AT  $x=5\text{MM}, y=10\text{MM}$**

It seems apparent that the estimates from equation (2.6) were underestimating the vortex shedding frequency, even using two drastically different TE thickness values. From these datasets by themselves it is hard to estimate a peak value. It might look like it is located in the range of 1800Hz-2000Hz, but a definitive conclusion cannot be drawn. To properly map the guide vane frequency it is suggested to use a higher sample frequency for future measurements.

There was not found any interaction between the RSI frequency and shedding frequency. The sporadic peaks in measured shedding frequency did not have any apparent relationship with the RSI when looking at the intervals.

## 5.4 Discussion

BEP conditions is not generally a point of concern in Francis turbines. As explained throughout section 2 the pressure pulsations and fluid structure interactions are a lot stronger at various other operating conditions. This might be a part of the reason why no relationship was found between the detected fluid structures. Due to time constraints a more in-depth relationship analysis was not produced. Some suggestions for the future can be seen in the further work section.

## 6. Conclusion

In this thesis a PIV setup and measurement procedure for the vaneless space has been presented. Several modifications have been made to the Francis turbine, both inside and outside, to support the use of this measurement technique.

Measurements for various guide vane angles was successfully conducted, but only samples at BEP conditions was analysed, due to previous measurements and simulations at this condition being available for comparison. The samples at BEP condition displays a good correspondence with previously established results.

The produced velocity field was very resembling of widely accepted simulations and RSI was detected at the estimated frequency. The vortex shedding of the guide vanes was underestimated by the Brekke formula. For hydrofoils it appears a Strouhal number closer to 0.3 is more appropriate.

Several obstacles were faced during the setup of the experiment. This project can hopefully aid future research in bypassing some of these hindrances.

## 7. Further work

This thesis has to a large extent been about creating a measurement routine and examining the possibilities of PIV measurements in the vaneless space. The results showcased can serve as an outline for what can and cannot be detected in future research.

For overall velocity fields a larger FOV is probably. If the shedding frequency is not of any interest, there is a lot more freedom with regards to sampling frequency and IA size. A solution to the interaction between the TE and LE of the plexiglass stay vanes and guide vanes might have to be figured out beforehand. That being said, for an overall velocity field it might be sufficient to adjust the laser optic and mask the shaded areas.

An attempt was made to correlate runner position to the velocity field, similar to what was done in a paper by Trivedi [61]. A runner RPM of 333 is equivalent to  $1998^\circ$  per second. For a runner with 30 blades there is  $12^\circ$  between each blade. Utilizing that each timestep at a sample frequency of 4144Hz is close to  $0.5^\circ$  runner angle, it was assumed that for every 24 image-pair a runner blade would have moved  $\sim 12^\circ$ . It was therefore attempted to average velocity fields with 24 image increments for every  $3^\circ$ . This should in theory correspond to one velocity field for every runner position, with  $3^\circ$  intervals. A minor difference was seen but due to a lack of time the results were left out. PIV settings can easily be adjusted to specifically showcase this interaction. By setting the sampling frequency to for example the same or half the runner angle/sec it is possible to obtain large sample sizes for specific runner angles. For future researchers interested in observing this relationship it might be worth taking a couple of extra datasets with specific time spreads.

For observing guide vane shedding frequency, or even boundary layer separation points, an even smaller FOV is probably preferable. The  $24 \times 24$  pixel boundary is as previously mentioned  $\sim 0,8\text{mm} \times 0,8\text{mm}$  in size. The viscous boundary layer for the guide vanes' suction and pressure side has been found to be roughly 0.6mm and 0.2mm, respectively. [11]

To conclude, it seems to the author that a range of fluid phenomena and interactions can be observed using PIV equipment in the vaneless space. The measurement technique is still relatively young, so it is expected that the rapid advances will continue.

## Bibliography

- [1] "www.energy.gov," U.S Department of Energy, [Online]. Available: <https://energy.gov/eere/water/history-hydropower>. [Accessed 12 11 2017].
- [2] "www.irena.org/," International Renewable Energy Agency, [Online]. Available: <http://www.irena.org/costs/Power-Generation-Costs/Hydropower>. [Accessed 12 11 2011].
- [3] "www.irena.org," International Renewable Energy Agency, 2017. [Online]. Available: <http://www.irena.org/costs>. [Accessed 12 11 2017].
- [4] "Fakta, Energi- og vannressurser i Norge," Olje- og Energidepartementet, 2015.
- [5] R. Goyal, C. Bergan, M. J. Cervantes, B. K. Gandhi and O. G. Dahlhaug, "Experimental investigation on a high head model Francis," IOP Publishing, 2016.
- [6] H. Brekke, "Francisturbiner," in *Grunnkurs i Hydrauliske Maskiner*, NTNU, 2000, pp. 32-33.
- [7] H. Brekke, "12," in *A Review on Oscillatory Problems in Francis Turbine and Simulation of Unsteady Flow in Conduit Systems*, NTNU, 1994, pp. 219-222.
- [8] C. Trivedi and M. J. Cervantes, "Fluid-structure interactions in Francis turbines: A perspective review," NTNU, Trondheim, 2015.
- [9] T. C. Hasmukhlal, "Investigations of Transient Pressure Loading on a High Head Francis Turbine," Luleå University of Technology, Luleå, 2014.
- [10] M. T. Bolstad, "Experimental investigation and mitigation of vortex shedding," NTNU, Trondheim, 2017.
- [11] C. Trivedi, M. J. Cervantes and O. G. Dahlhaug, "Experimental and Numerical Studies of a High-Head Francis Turbine: A Review of the Francis-99 Test Case," NTNU, 2016.
- [12] R. Haas, M. Hiebert and E. Hoatson, "Francis Turbines, Fundamentals and Everything Else You Didn't Know You Wanted to Know," Colorado State University, 2014.
- [13] P. H. Finstad, "Mapping and analyzing dynamics in rotor-stator interaction and draft tube flow with novel methods," NTNU, 2012.
- [14] H. Brekke, "Ledeapparat," in *Pumper & Turbiner*, Trondheim, NTNU, 2003, pp. 63-66.
- [15] C. Trivedi, M. J. Cervantes and O. G. Dahlhaug, "Francis-99: A test-case on a high head Francis turbine," NTNU, Trondheim, 2019.
- [16] Y. A. Cengel and J. M. Cimbala, "External Flow: Drag and Lift," in *Fluid Mechanics: Fundamentals and Applications*, McGraw-Hill, 2010, pp. 590-593.
- [17] Y. A. Cengel and J. M. Cimbala, "External Flow: Drag and Lift," in *Fluid Mechanics: Fundamentals and Applications*, McGraw-Hill, 2010, p. 590.
- [18] F. M. White, "Preliminary Concepts," in *Viscous Fluid Flow Third Edition*, University of Rhode Island, 2006, p. 10.

- [19] Y. A. Cengel and J. M. Cimbala, "External Flow: Drag and Lift," in *Fluid Mechanics: Fundamentals and Applications*, McGraw-Hill, 2010, pp. 592-612.
- [20] Y. A. Cengel and J. M. Cimbala, "Approximate Solutions of the N-S EQ," in *Fluid Mechanics: Fundamentals and Applications*, McGraw-Hill, 2010, pp. 518-519.
- [21] A. Ducoin, J. A. Astolfi, F. Deniset and J. F. Sigrist, "Computational and experimental investigation of flow over a transient pitching hydrofoil," *European Journal of Mechanics - B/Fluids*, vol. Volume 28, no. Issue 6, pp. 728-743, 2009.
- [22] A. H. Techet, *Vortex Induced Vibrations*, Massachusetts Institute of Technology, 2005.
- [23] F. M. White, "Preliminary Concepts," in *Viscous Fluid Flow Third Edition*, University of Rhode Island, 2006, pp. 9-10.
- [24] F. M. White, "Preliminary Concepts," in *Viscous Fluid Flow Third Edition*, University of Rhode Island, 2006, p. 11.
- [25] J. Abhiroop, "Vortex Induced Vibrations," Indian Institute of Technology , Delhi, 2007.
- [26] P. Ausoni, M. Farhat, Y. A. Bouziad and J.-L. Kueny, "Kármán vortex shedding in the wake of a 2D hydrofoil: Measurement and numerical simulation," École polytechnique fédérale de Lausanne, 2006.
- [27] Z. J. Taylor, "Vortex shedding from elongated bluff bodies," University of Western Ontario, 2011.
- [28] Z. Liu and G. A. Kopp, "A Numerical Study of Geometric Effects on Vortex Shedding From Elongated Bluff Bodies," University of Western Ontario, London, 2009.
- [29] A. Zobeiri, "Effect of Hydrofoil Trailing Edge Geometry on the Wake Dynamics," École Polytechnique Fédérale de Lausanne, 2012.
- [30] Ø. Antonsen, "Unsteady flow in wicket gate and runner with focus on static and dynamic load on runner," NTNU, 2007.
- [31] E. Agnalt, "Measurement Report 2017 WP 1.3," NTNU (RESTRICTED), Trondheim, 2018.
- [32] C. Nicolet, N. Ruchonnet and F. Avellan, "One-Dimensional Modeling of Rotor Stator Interaction in Francis," École polytechnique fédérale de Lausanne, Lausanne, 2006.
- [33] C. Trivedi, "A review on fluid structure interaction in hydraulic turbines: A focus on hydrodynamic damping," NTNU, Trondheim, 2017.
- [34] G. D. Ciocan, F. Avellan and J. Kueny, "Optical measurement techniques for experimental analysis of hydraulic turbines rotor-stator interaction," in *Proceedings (CDRom) of the ASME Fluids Engineering Division Summer Meeting*, Boston, 2000.
- [35] E. W. Weisstein, "Fourier Series," MathWorld, [Online]. Available: <http://mathworld.wolfram.com/FourierSeries.html>. [Accessed 16 07 2018].
- [36] R. Fisher, "homepages.inf.ed.ac.uk," 2003. [Online]. Available: <https://homepages.inf.ed.ac.uk/rbf/HIPR2/fourier.htm>. [Accessed 16 07 2018].

- [37] in *DaVis 8.4 Software*, Göttingen, LaVision GmbH, 2017, p. 289.
- [38] "aavos.eu," aavos industrial, 11 2017. [Online]. Available: <https://aavos.eu/glossary/fourier-transform/>. [Accessed 16 07 2018].
- [39] I. Farrance and R. Frenkel, "Uncertainty of Measurement: A Review of the Rules for Calculating Uncertainty Components through Functional Relationships," *Clin Biochem Rev.*, pp. 49-75, 5 2012.
- [40] E. W. Weisstein, "Standard Deviation," MathWorld--A Wolfram Web Resource, [Online]. Available: <http://mathworld.wolfram.com/StandardDeviation.html>. [Accessed 18 07 2018].
- [41] E. W. Weisstein, "Confidence Interval," MathWorld--A Wolfram Web Resource, [Online]. Available: <http://mathworld.wolfram.com/ConfidenceInterval.html>. [Accessed 18 07 2017].
- [42] K. Kiger, "Introduction of Particle Image Velocimetry," [Online]. Available: <https://www2.cscamm.umd.edu/programs/trb10/presentations/PIV.pdf>. [Accessed 10 12 2017].
- [43] O. Törnblom, "https://www.mech.kth.se," 2004. [Online]. Available: [https://www.mech.kth.se/~olle/pivkurs/Intro\\_to\\_PIV.pdf](https://www.mech.kth.se/~olle/pivkurs/Intro_to_PIV.pdf). [Accessed 16 12 2017].
- [44] "https://www.dantecdynamics.com/," Dantec Dynamics, [Online]. Available: <https://www.dantecdynamics.com/measurement-principles-of-piv>. [Accessed 2017 12 16].
- [45] "https://www.lavision.de/en/," [Online]. Available: <https://www.lavision.de/en/download.php?id=319>. [Accessed 17 12 2017].
- [46] "Experimental Setup," in *Product-Manual: Flow Master Getting Started*, Göttingen, LaVision GmbH, 2015, pp. 9-22.
- [47] R. Geisler, "A Fast Multiple Shutter for Image-Based Metrology," Institute of Aerodynamics and Flow Technology, Göttingen, 2014.
- [48] "Understanding Microscopes and Objectives," edmundoptics, [Online]. Available: <https://www.edmundoptics.eu/resources/application-notes/microscopy/understanding-microscopes-and-objectives/>. [Accessed 20 07 2018].
- [49] "f/# (Lens Iris/Aperture Setting)," edmundoptics, [Online]. Available: <https://www.edmundoptics.com/resources/application-notes/imaging/lens-iris-aperture-setting/>. [Accessed 20 07 2018].
- [50] D. P. Hart, "PIV Error Correction," in *9th International Symposium on Applications of Laser Techniques*, Lisbon, 1998.
- [51] B. Wieneke and K. Pfeiffer, "Adaptive PIV with variable interrogation window size and shape," in *15th Int Symp on Applications of Laser Techniques to Fluid Mechanics*, Lisbon, 2010.
- [52] B. Wieneke, "PIV uncertainty quantification from correlation statistics," *Measurement Science and Technology*, vol. 26, no. 7, 5 6 2015.
- [53] R. Theunissen, "An adaptive sampling and windowing interrogation," *Measurement Science and Technology*, vol. 1, no. 18, 2007.

- [54] A. Sciacchitano, B. Wieneke and F. Scarano, "PIV uncertainty quantification by image matching," *Measurement Science and Technology*, vol. 24, no. 4, 2013.
- [55] B. Wieneke, "PIV uncertainty quantification from correlation statistics," *Measurement Science and Technology*, vol. 26, no. 7, 5 6 2015.
- [56] Z. Xue, J. J. Charonko and P. P. Vlachos, "Signal-to-noise ratio, error and uncertainty of PIV measurement," *Measurement Science and Technology*, 5 2014.
- [57] A. Sciacchitano and B. Wieneke, "PIV uncertainty propagation," *Measurement Science and Technology*, vol. 27, no. 8, 29 6 2016.
- [58] "Vannkraftlaboratoriet," NTNU, [Online]. Available: [https://www.ntnu.no/ept/om\\_vklab](https://www.ntnu.no/ept/om_vklab). [Accessed 18 07 2018].
- [59] "Datasheet," Photron, [Online]. Available: <https://photron.com/wp-content/uploads/2017/03/Mini-UX-REV17.03.03.pdf>. [Accessed 20 07 2018].
- [60] LaVision, "Maintenance & Care," in *Litron LDY series, Product-Manual*, Göttingen, LaVision GmbH, 2016, pp. 45-50.
- [61] C. Trivedi and O. G. Dahlhaug, "Interaction between trailing edge wake and vortex rings in a Francis turbine at runaway condition: Compressible large eddy simulation," *Physics of Fluids*, vol. 30, no. 7, 2018.
- [62] O. G. Dahlhaug, P. T. Storli and B. Aslak, "Tokke model test 2006-2007 NTNU reference runner," NTNU, Trondheim, 2007.

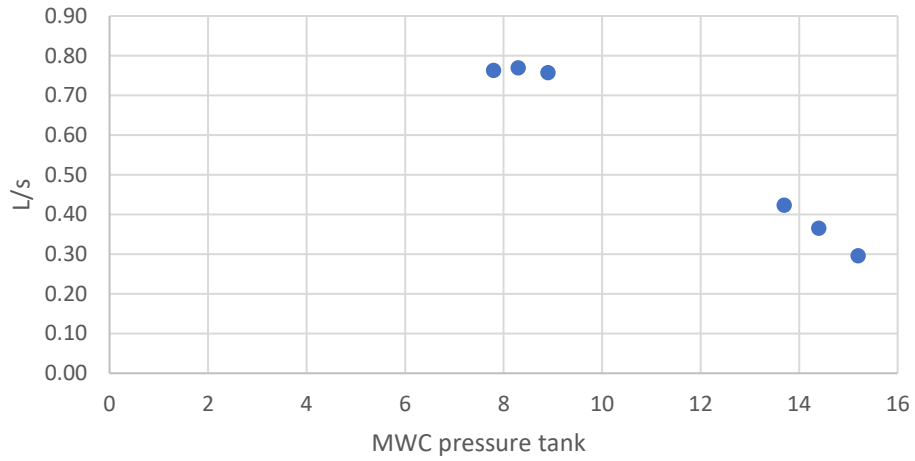


# Appendix A: Particle Feeding

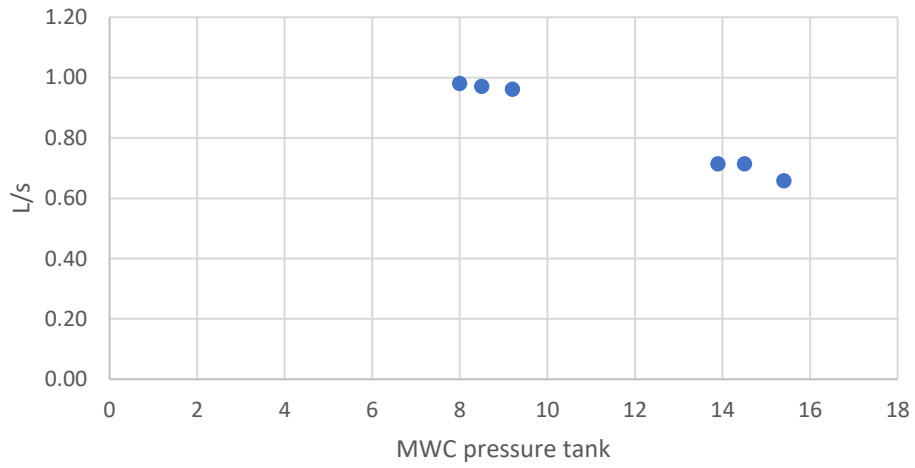
| Measurements                                 |                                   | 09/05/2018                         |  |                                      |                                       |                         |
|--|-----------------------------------|------------------------------------|--|--------------------------------------|---------------------------------------|-------------------------|
| Particle Feeding Pump Rotational Speed [rpm] | Test section Flow Pump (P1) [rpm] | Mean Measured Flow testsection [V] | Mean Measured Flow testsection [m <sup>3</sup> /s] | Mean Measured Flow testsection [L/s] | Mean Flow Velocity Test section [m/s] | MWC Pressure Tank [mWC] |
| 900  | 190                               | 3.571                              | 0.131834182  | 131.8                                | 5.86                                  | 7.8                     |
| 900  | 280                               | 4.357                              | 0.198048394  | 198.0                                | 8.80                                  | 8.30                    |
| 900  | 340                               | 4.893                              | 0.243202106  | 243.2                                | 10.81                                 | 8.90                    |
| 900  | 190                               | 3.575                              | 0.13217115   | 132.2                                | 5.87                                  | 13.70                   |
| 900  | 280                               | 4.359                              | 0.198216878  | 198.2                                | 8.81                                  | 14.40                   |
| 900  | 340                               | 4.898                              | 0.243623316  | 243.6                                | 10.83                                 | 15.20                   |
| 1350   | 190                               | 3.571                              | 0.131834182  | 131.8                                | 5.86                                  | 8.00                    |
| 1350   | 280                               | 4.36                               | 0.19830112   | 198.3                                | 8.81                                  | 8.50                    |
| 1350   | 340                               | 4.893                              | 0.243202106  | 243.2                                | 10.81                                 | 9.20                    |
| 1350   | 190                               | 3.572                              | 0.131918424  | 131.9                                | 5.86                                  | 13.90                   |
| 1350   | 280                               | 4.359                              | 0.198216878  | 198.2                                | 8.81                                  | 14.50                   |
| 1350   | 340                               | 4.898                              | 0.243623316  | 243.6                                | 10.83                                 | 15.40                   |
| 1800   | 190                               | 3.573                              | 0.132002666  | 132.0                                | 5.87                                  | 7.60                    |
| 1800   | 280                               | 4.353                              | 0.197711426  | 197.7                                | 8.79                                  | 8.10                    |
| 1800   | 340                               | 4.89                               | 0.24294938   | 242.9                                | 10.80                                 | 8.60                    |
| 1800   | 190                               | 3.575                              | 0.13217115   | 132.2                                | 5.87                                  | 13.10                   |
| 1800   | 280                               | 4.377                              | 0.199733234  | 199.7                                | 8.88                                  | 13.80                   |
| 1800   | 340                               | 4.898                              | 0.243623316  | 243.6                                | 10.83                                 | 14.60                   |
| 1800   | 190                               | 3.581                              | 0.132676602  | 132.7                                | 5.90                                  | 20.80                   |
| 1800   | 280                               | 4.359                              | 0.198216878  | 198.2                                | 8.81                                  | 21.40                   |
| 1800   | 340                               | 4.899                              | 0.243707558  | 243.7                                | 10.83                                 | 21.70                   |

| Measurements |     | Percentage Particle solution flow [%] | Particle Feeding Time [s] | Fed Volume of Particle Solution [L] | Mean particle feeding amount [L/s] | Particle Feeder Volumetric Flow rate [m <sup>3</sup> /s] |
|--------------|-----|---------------------------------------|---------------------------|-------------------------------------|------------------------------------|--|
| 900          | 190 | 0.58%                                 | 131                       | 100                                 | 0.76                               | 0.000763359  |
| 900          | 280 | 0.39%                                 | 130                       | 100                                 | 0.77                               | 0.000769231  |
| 900          | 340 | 0.31%                                 | 132                       | 100.00                              | 0.76                               | 0.000757576  |
| 900          | 190 | 0.32%                                 | 118                       | 50.00                               | 0.42                               | 0.000423729  |
| 900          | 280 | 0.18%                                 | 137                       | 50.00                               | 0.36                               | 0.000364964  |
| 900          | 340 | 0.12%                                 | 169                       | 50.00                               | 0.30                               | 0.000295858  |
| 1350         | 190 | 0.74%                                 | 102                       | 100                                 | 0.98                               | 0.000980392  |
| 1350         | 280 | 0.49%                                 | 103                       | 100.00                              | 0.97                               | 0.000970874  |
| 1350         | 340 | 0.40%                                 | 104                       | 100.00                              | 0.96                               | 0.000961538  |
| 1350         | 190 | 0.54%                                 | 70                        | 50.00                               | 0.71                               | 0.000714286  |
| 1350         | 280 | 0.36%                                 | 70                        | 50.00                               | 0.71                               | 0.000714286  |
| 1350         | 340 | 0.27%                                 | 76                        | 50.00                               | 0.66                               | 0.000657895  |
| 1800         | 190 | 0.96%                                 | 79                        | 100                                 | 1.27                               | 0.001265823  |
| 1800         | 280 | 0.63%                                 | 80                        | 100.00                              | 1.25                               | 0.00125  |
| 1800         | 340 | 0.51%                                 | 81                        | 100.00                              | 1.23                               | 0.001234568  |
| 1800         | 190 | 0.76%                                 | 99                        | 100.00                              | 1.01                               | 0.001010101  |
| 1800         | 280 | 0.52%                                 | 97                        | 100.00                              | 1.03                               | 0.001030928  |
| 1800         | 340 | 0.40%                                 | 102                       | 100.00                              | 0.98                               | 0.000980392  |
| 1800         | 190 | 0.52%                                 | 72                        | 50.00                               | 0.69                               | 0.000694444  |
| 1800         | 280 | 0.37%                                 | 68                        | 50.00                               | 0.74                               | 0.000735294  |
| 1800         | 340 | 0.29%                                 | 71                        | 50.00                               | 0.70                               | 0.000704225  |

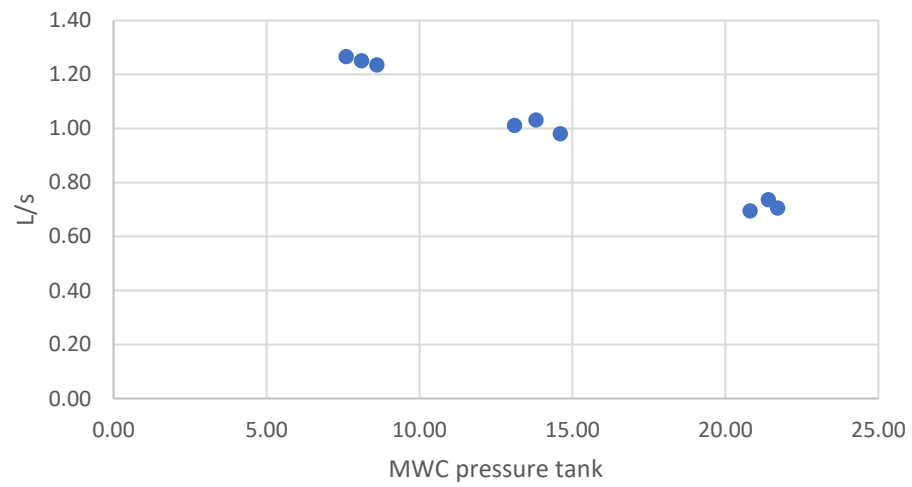
900 RPM feeding pump

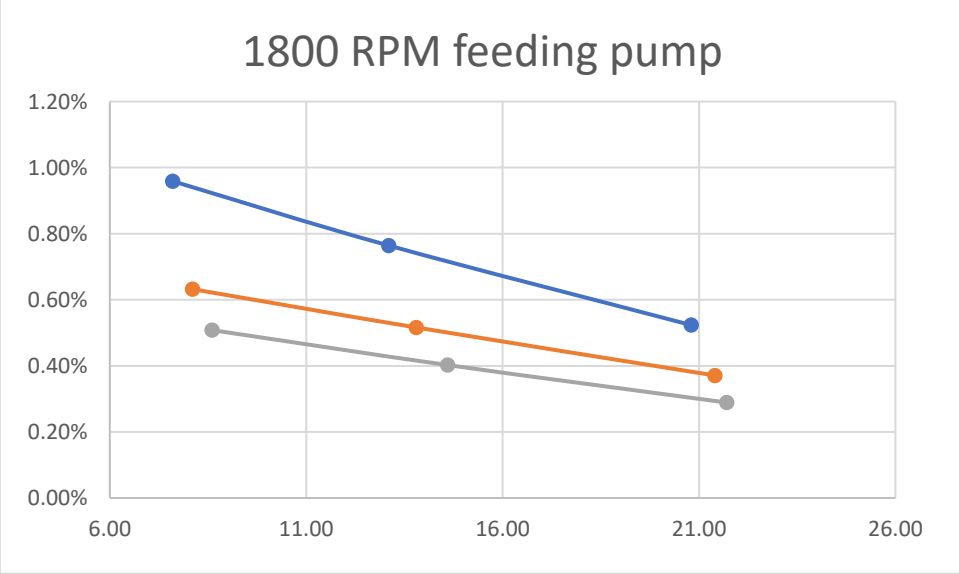
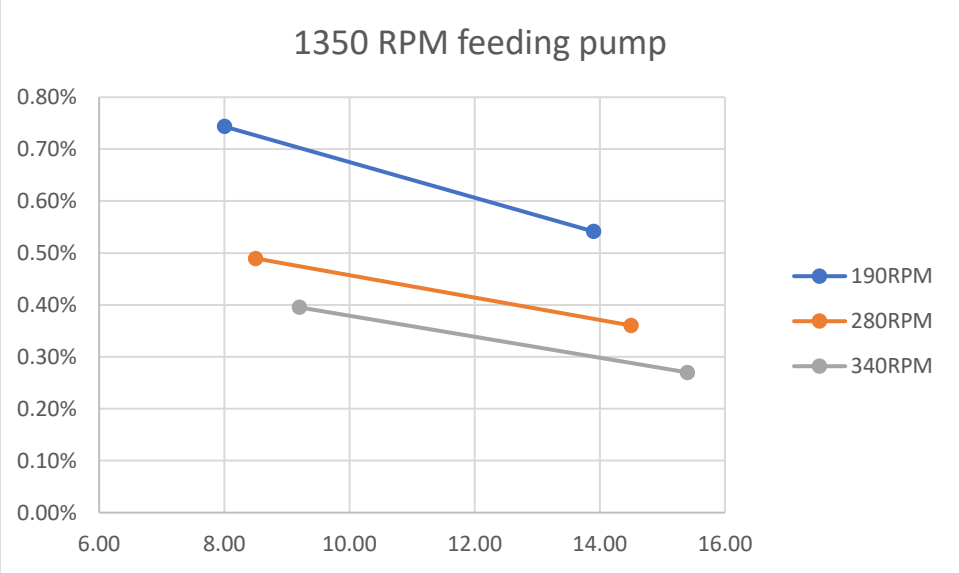
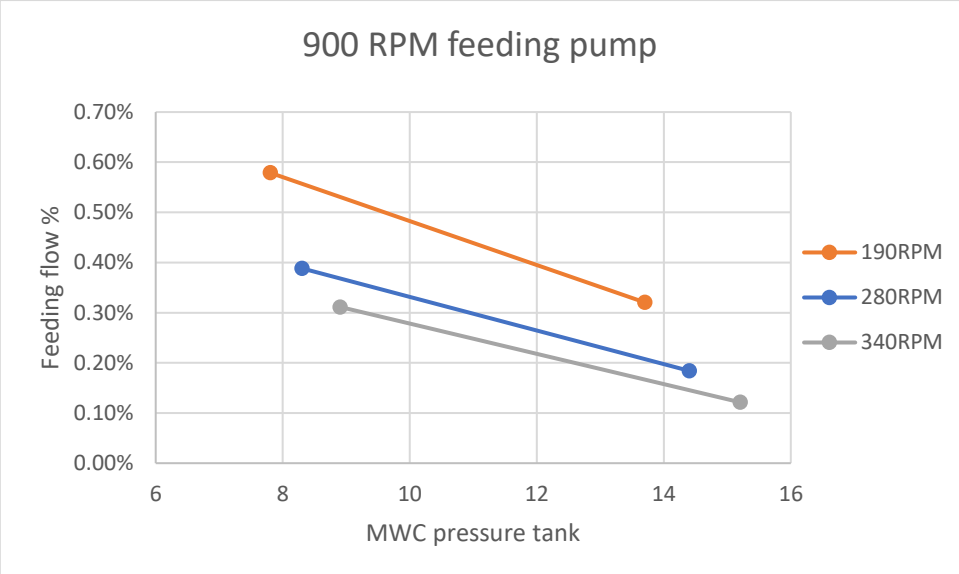


1350 RPM feeding pump

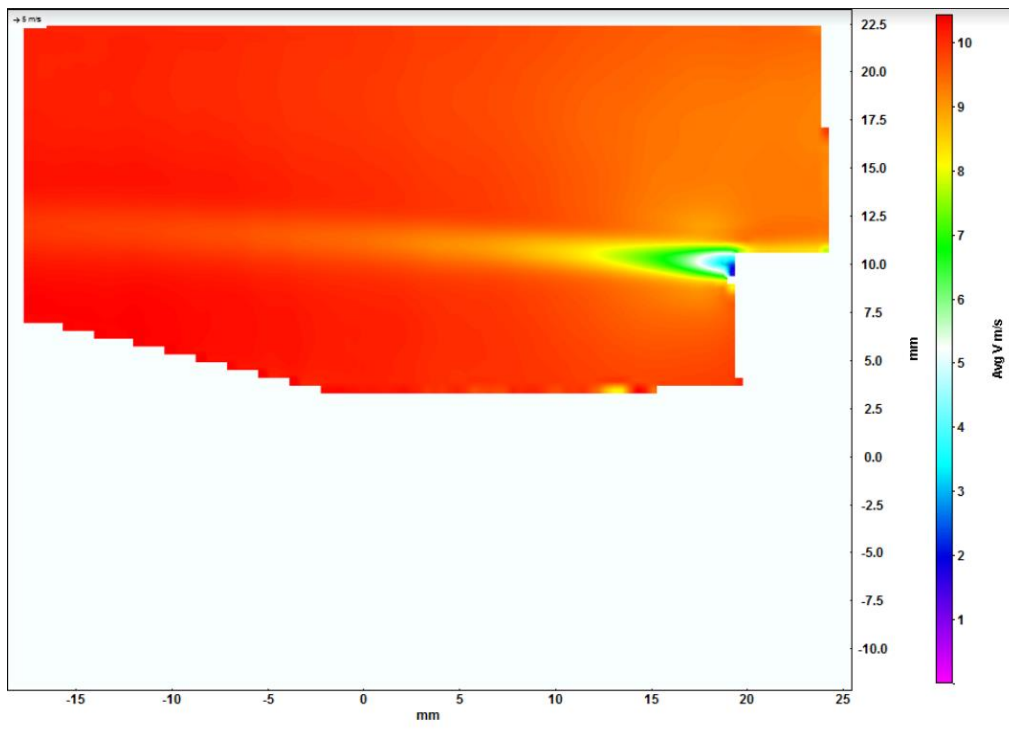


1800 RPM feeding pump

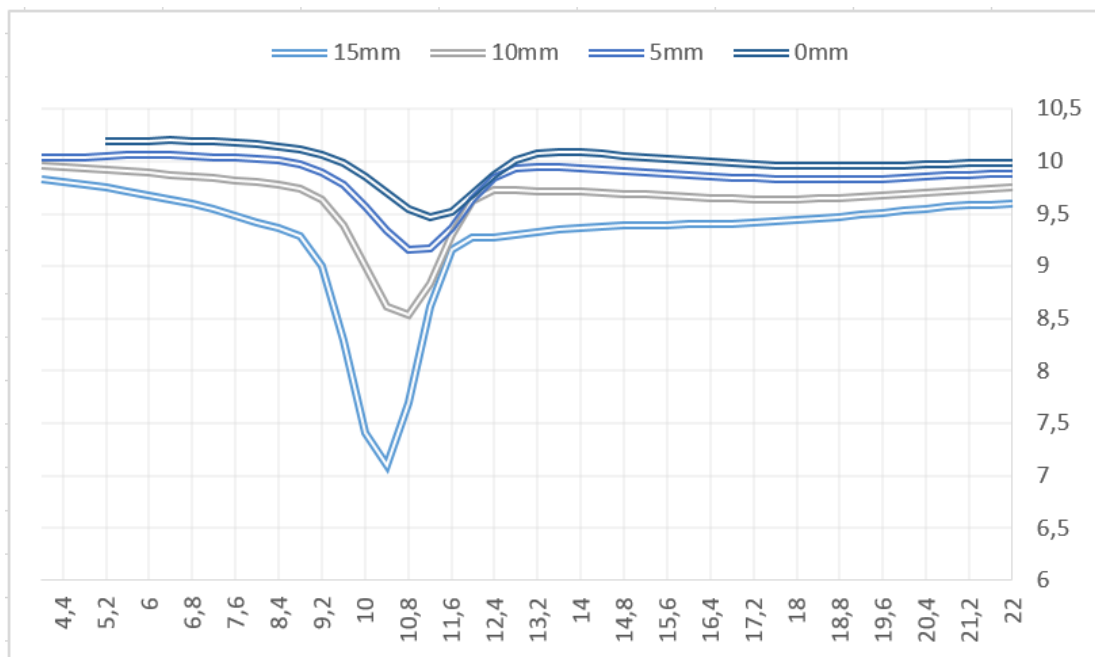




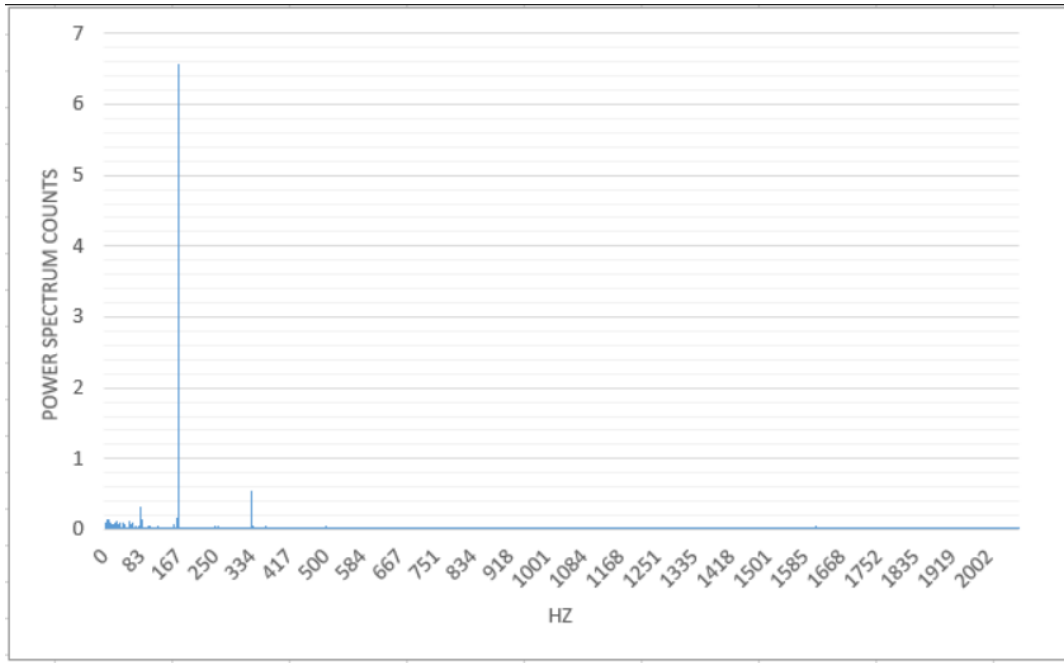
## Appendix B: Repeatability check



Average velocity field for ramp down dataset

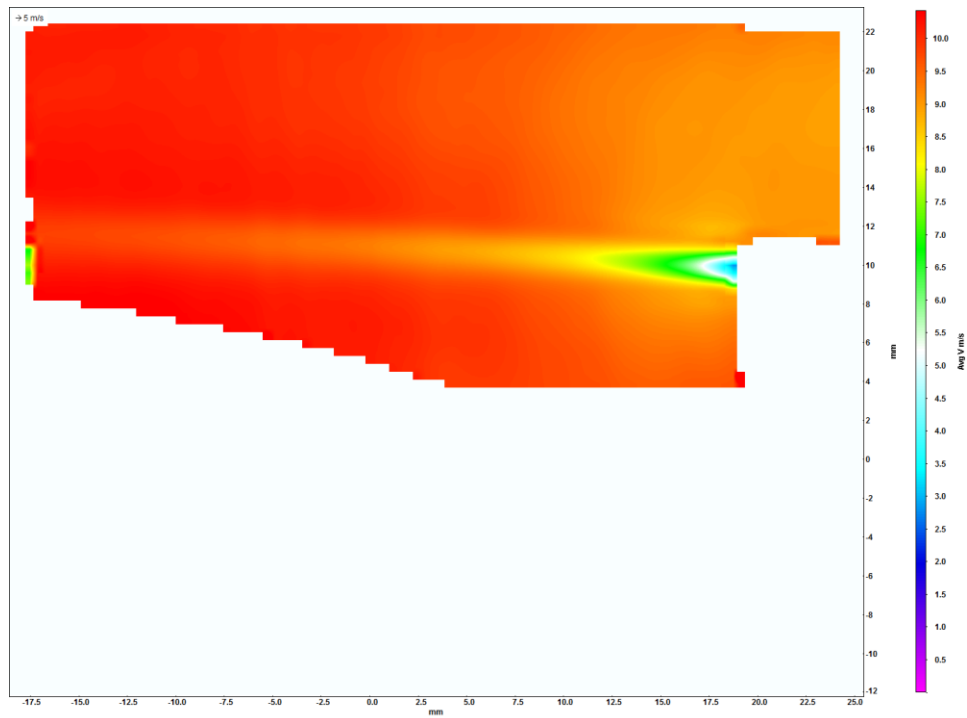


Cross wake velocity vectors for ramp down dataset

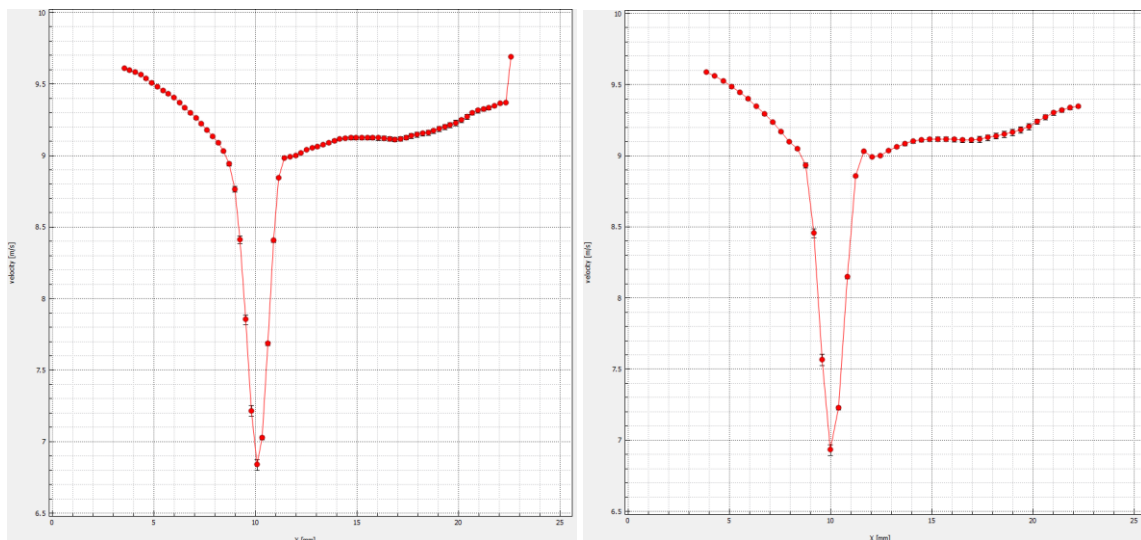


Power spectrum analysis at  $x=-5\text{mm}$ ,  $y=7.5\text{mm}$  for ramp down dataset. The higher peak is probably due to the discrete frequency interval aligning better with the true RSI frequency. Supported by the fact that RSI intensity was much closer between RU and RD datasets for e.g. figure 56.

## Appendix C: measurement results



Average velocity field for 16x16 pixel IA



Difference between vertical velocity line at  $x = 15\text{mm}$  for 16x16pixels (left) and 24x24pixels(right)

## Appendix D: Risk assessment

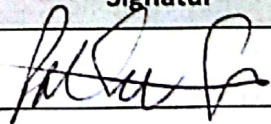
# Risk Assessment Report

## HiFrancis Blade Cascade

|                              |   |
|------------------------------|---|
| Project name                 | PIV measurements on blade cascade for HiFrancis project |
| Apparatus                    | Double-Cavity High speed laser, 2*10mJ, 1000Hz, 527nm   |
| Unit                         | EPT   |
| Equipment manager            | Bård Brandåstrø   |
| Project leader               | Pål Tore Storli   |
| HSE coordinator              | Morten Grønli   |
| HSE responsible (linjeleder) | Therese Løvås   |
| Location                     | Waterpower Laboratory                                   |
| Room number                  | 11  |
| Risk assessment performed by | Magne Tveit Bolstad                                     |

### Approval:

|   |           |
|---|-----------|
| Apparatur kort (UNIT CARD) valid for:                 | 12 months |
| Forsøk pågår kort (EXPERIMENT IN PROGRESS) valid for: | 12 months |

| Rolle                        | Navn            | Dato      | Signatur  |
|------------------------------|-----------------|-----------|---|
| Project leader               | Pål-Tore Storli | 24/8 2017 |  |
| HSE coordinator              | Morten Grønli   |           |   |
| HMS responsible (linjeleder) | Therese Løvås   |           |   |



## TABLE OF CONTENTS

|     |  |                              |
|-----|--|------------------------------|
| 1   | INTRODUCTION .....   | 1                            |
| 2   | CONCLUSION .....   | ERROR! BOOKMARK NOT DEFINED. |
| 3   | ORGANISATION .....   | 1                            |
| 4   | RISK MANAGEMENT IN THE PROJECT .....   | 1                            |
| 5   | DESCRIPTIONS OF EXPERIMENTAL SETUP .....   | 2                            |
| 6   | EVACUATION FROM THE EXPERIMENTAL AREA.....   | 2                            |
| 7   | WARNING .....  | 2                            |
| 7.1 | Before experiments.....  | 2                            |
| 7.2 | Non-conformance .....  | 2                            |
| 8   | ASSESSMENT OF TECHNICAL SAFETY .....   | 3                            |
| 8.1 | HAZOP .....  | 3                            |
| 8.2 | Flammable, reactive and pressurized substances and gas.....                        | 3                            |
| 8.3 | Pressurized equipment.....   | 4                            |
| 8.4 | Effects on the environment (emissions, noise, temperature, vibration, smell) ..... | 4                            |
| 8.5 | Radiation .....  | 4                            |
| 8.6 | Chemicals .....  | 4                            |
| 8.7 | Electricity safety (deviations from the norms/standards).....                      | 4                            |
| 9   | ASSESSMENT OF OPERATIONAL SAFETY .....   | 4                            |
| 9.1 | Procedure HAZOP .....  | 4                            |
| 9.2 | Operation and emergency shutdown procedure .....                                   | 4                            |
| 9.3 | Training of operators.....   | 5                            |
| 9.4 | Technical modifications.....   | 5                            |
| 9.5 | Personal protective equipment.....   | 5                            |
|     | 9.5.1 General Safety .....   | 5                            |
| 9.6 | Safety equipment .....   | 5                            |
| 9.7 | Special predations .....   | 5                            |
| 10  | QUANTIFYING OF RISK - RISK MATRIX.....   | 5                            |
| 11  | REGULATIONS AND GUIDELINES .....   | 6                            |
| 12  | DOCUMENTATION.....   | 6                            |
| 13  | GUIDANCE TO RISK ASSESSMENT TEMPLATE.....  | 7                            |

## 1 INTRODUCTION

PIV measurements will be performed on a Site Acceptance Test-rig in accordance with the new PIV equipment at the waterpower laboratory. Measurements will be performed in May-June 2017.

## 2 ORGANISATION

| Role                          |                 |
|-------------------------------|-----------------|
| Project leader                | Pål Tore Storli |
| Equipment manager             | Bård Brandåstrø |
| Room manager                  | Bård Brandåstrø |
| HSE coordinator               | Morten Grønli   |
| HSE responsible (linjeleder): | Therese Løvås   |

## 3 RISK MANAGEMENT IN THE PROJECT

| Hovedaktiviteter risikostyring  | Nødvendige tiltak, dokumentasjon   | DATE |
|---|--|------|
| Prosjekt initiering<br>Project initiation                               | Prosjekt initiering mal  | X    |
| Veiledningsmøte<br>Guidance Meeting                                     | Skjema for Veiledningsmøte med pre-risikovurdering                                   | x    |
| Innledende risikovurdering<br>Initial Assessment                        | Fareidentifikasjon – HAZID<br>Skjema grovanalyse                                     | x    |
| Vurdering av teknisk sikkerhet<br>Evaluation of technical security      | Prosess-HAZOP<br>Tekniske dokumentasjoner  | x    |
| Vurdering av operasjonell sikkerhet<br>Evaluation of operational safety | Prosedyre-HAZOP<br>Opplæringsplan for operatører                                     | x    |
| Sluttvurdering, kvalitetssikring<br>Final assessment, quality assurance | Uavhengig kontroll<br>Utstedelse av apparaturkort<br>Utstedelse av forsøk pågår kort | x    |

## 4 DESCRIPTIONS OF EXPERIMENTAL SETUP

- Drawings and photos describing the setup.
- Process and Instrumentation Diagram (PID) with list of components
- Location of the operator, gas bottles, shutdown valves for water / air.

## 5 EVACUATION FROM THE EXPERIMENTAL AREA

Evacuate at signal from the alarm system or local gas alarms with its own local alert with sound and light outside the room in question, see 6.2

Evacuation from the rigging area takes place through the marked emergency exits to the assembly point, (corner of Old Chemistry Kjelhuset or parking 1a-b.)

### Action on rig before evacuation:

Describe in which condition the rig should be left in case of evacuation (emergency shutdown procedure, water, gas, electric supply, etc.)

## 6 WARNING

### 6.1 Before experiments

Send an e-mail with information about the planned experiment to:  
[iept-experiments@ivt.ntnu.no](mailto:iept-experiments@ivt.ntnu.no)

### The e-mail must include the following information:

- Name of responsible person:
- Experimental setup/rig:
- Start Experiments: (date and time)
- Stop Experiments: (date and time)

You must get the approval back from the laboratory management before start up. All running experiments are notified in the activity calendar for the lab to be sure they are coordinated with other activity.

### 6.2 Non-conformance

#### **FIRE**

If you are NOT able to extinguish the fire, activate the nearest fire alarm and evacuate area. Be then available for fire brigade and building caretaker to detect fire place.

If possible, notify:

| NTNU                            | SINTEF                                   |
|---------------------------------|--|
| Morten Grønli, Mob: 918 97 515  | Harald Mæhlum, Mob: 930 14 986           |
| Therese Løvås, Mob: 91897007    | Anne Karin T. Hemmingsen Mob: 930 19 669 |
| NTNU – SINTEF Beredskapstelefon | 800 80 388                               |

**GAS ALARM**

If a gas alarm occurs, close gas bottles immediately and ventilate the area. If the level of the gas concentration does not decrease within a reasonable time, activate the fire alarm and evacuate the lab. Designated personnel or fire department checks the leak to determine whether it is possible to seal the leak and ventilate the area in a responsible manner.

**PERSONAL INJURY**

- First aid kit in the fire / first aid stations
- Shout for help
- Start life-saving first aid
- **CALL 113** if there is any doubt whether there is a serious injury

**OTHER NON-CONFORMANCE (AVVIK)**

**NTNU:**

You will find the reporting form for non-conformance on:  
<https://innsida.ntnu.no/wiki/-/wiki/Norsk/Melde+avvik>

**SINTEF:**

Synergi

**7 ASSESSMENT OF TECHNICAL SAFETY**

**7.1 HAZOP**

*See Chapter 13 "Guide to the report template".*

The experiment set up is divided into the following nodes:

|        |                |
|--------|----------------|
| Node 1 | Blade cascade  |
| Node 2 | Laser class IV |
| Node 3 | Tent/enclosure |
|        |                |

**Attachments, Form: Hazop\_mal**

**Conclusion**

**Node 1:**

- Pressure is supervised during operation

**Node 2:**

- Radiation area shielded
- Appropriate signalling and lights in place, light active during operation

**Node 3:**

- Appropriate signalling and lights in place, light active during operation

**7.2 Flammable, reactive and pressurized substances and gas**

*See Chapter 13 "Guide to the report template".*

|    |  |
|----|--|
| NO |  |
|----|--|

**7.3 Pressurized equipment**

*See Chapter 13 "Guide to the report template".*

|     |  |
|-----|--|
| YES |  |
|-----|--|

**7.4 Effects on the environment (emissions, noise, temperature, vibration, smell)**

*See Chapter 13 "Guide to the report template".*

|    |  |
|----|--|
| NO |  |
|----|--|

**7.5 Radiation**

*See Chapter 13 "Guide to the report template".*

|     |   |
|-----|---|
| YES | Radiation Sources need to have an own risk assessment |
|-----|---|

**Attachments: Radiation risk assessment**

**Conclusion:**

**7.6 Chemicals**

*See Chapter 13 "Guide to the report template".*

|    |  |
|----|--|
| NO |  |
|----|--|

**7.7 Electricity safety (deviations from the norms/standards)**

*See Chapter 13 "Guide to the report template".*

|    |  |
|----|--|
| NO |  |
|----|--|

**8 ASSESSMENT OF OPERATIONAL SAFETY**

Ensure that the procedures cover all identified risk factors that must be taken care of. Ensure that the operators and technical performance have sufficient expertise.

**8.1 Procedure HAZOP**

*See Chapter 13 "Guide to the report template".*

The method is a procedure to identify causes and sources of danger to operational problems.

**Attachments::** HAZOP\_MAL\_Proseedyre

**8.2 Operation procedure and emergency shutdown procedure**

*See Chapter 13 "Guide to the report template".*

The operating procedure is a checklist that must be filled out for each experiment.

Emergency procedure should attempt to set the experiment set up in a harmless state by unforeseen events.

**Attachments:** Procedure for running experiments  
Emergency shutdown procedure:

**8.3 Training of operators**

**8.4 Technical modifications**

**8.5 Personal protective equipment**

- *It is mandatory use of appropriate eye protection in the rig zone*

**8.6 General Safety**

- *The area around the staging attempts shielded.*
- *Operator has to be present during experiments.*

**8.7 Safety equipment**

- *Warning signs and warning light, see the Regulations on Safety signs and signalling in the workplace*

**8.8 Special predations**

**9 QUANTIFYING OF RISK - RISK MATRIX**

See Chapter 13 "Guide to the report template".

The risk matrix will provide visualization and an overview of activity risks so that management and users get the most complete picture of risk factors.

| IDnr | Aktivitet-hendelse   | Frekv-Sans | Kons | RV |
|------|--|------------|------|----|
| 1    | <i>Unintentional refraction/reflection of laser beam</i>         | 1          | A    | ■  |
| 2    | <i>People without protective goggles entering radiation area</i> | 1          | C    | 1C |
| 3    | <i>Damaging lab equipment</i>                                    | 2          | B    | ■  |
| 4    | <i>Water-damage on lab equipment</i>                             | 3          | B    | 3C |
| 5    | <i>Structural failure due to high pressure</i>                   | 1          | C    | 1C |

**Conclusion:** There is little remaining risk. The most prominent risk is that people unintentionally wander into the radiation area without protective goggles, but proper signalling and blocking should prevent this. The risk is therefore acceptable.

## 10 REGULATIONS AND GUIDELINES

Se <http://www.arbeidstilsynet.no/regelverk/index.html>

- Lov om tilsyn med elektriske anlegg og elektrisk utstyr (1929)
- Arbeidsmiljøloven
- Forskrift om systematisk helse-, miljø- og sikkerhetsarbeid (HMS Internkontrollforskrift)
- Forskrift om sikkerhet ved arbeid og drift av elektriske anlegg (FSE 2006)
- Forskrift om elektriske forsyningsanlegg (FEF 2006)
- Forskrift om utstyr og sikkerhetssystem til bruk i eksplosjonsfarlig område NEK 420
- Forskrift om håndtering av brannfarlig, reaksjonsfarlig og trykksatt stoff samt utstyr og anlegg som benyttes ved håndteringen
- Forskrift om Håndtering av eksplosjonsfarlig stoff
- Forskrift om bruk av arbeidsutstyr.
- Forskrift om Arbeidsplasser og arbeidslokaler
- Forskrift om Bruk av personlig verneutstyr på arbeidsplassen
- Forskrift om Helse og sikkerhet i eksplosjonsfarlige atmosfærer
- Forskrift om Høytrykksspyling
- Forskrift om Maskiner
- Forskrift om Sikkerhetsskilting og signalgivning på arbeidsplassen
- Forskrift om Stillaser, stiger og arbeid på tak m.m.
- Forskrift om Sveising, termisk skjæring, termisk sprøyting, kullbuemeisling, lodding og sliping (varmt arbeid)
- Forskrift om Tekniske innretninger
- Forskrift om Tungt og ensformig arbeid
- Forskrift om Vern mot eksponering for kjemikalier på arbeidsplassen (Kjemikalieforskriften)
- Forskrift om Vern mot kunstig optisk stråling på arbeidsplassen
- Forskrift om Vern mot mekaniske vibrasjoner
- Forskrift om Vern mot støy på arbeidsplassen

Veiledninger fra arbeidstilsynet

se: <http://www.arbeidstilsynet.no/regelverk/veiledninger.html>

## 11 DOCUMENTATION

- Tegninger, foto, beskrivelser av forsøksoppsetningen
- Hazop\_mal
- Sikker bruk av LASERE, retningslinje
- HAZOP\_MAL\_Prosedyre
- Forsøksprosedyre
- Opplæringsplan for operatører
- Skjema for sikker jobb analyse, (SJA)
- Apparatorkortet
- Forsøk pågår kort

## 12 GUIDANCE TO RISK ASSESSMENT TEMPLATE

### Chapter 7 Assessment of technical safety.

Ensure that the design of the experiment set up is optimized in terms of technical safety.

Identifying risk factors related to the selected design, and possibly to initiate re-design to ensure that risk is eliminated as much as possible through technical security.

This should describe what the experimental setup actually are able to manage and acceptance for emission.

#### 7.1 HAZOP

The experimental set up is divided into nodes (eg motor unit, pump unit, cooling unit.). By using guidewords to identify causes, consequences and safeguards, recommendations and conclusions are made according to if necessary safety is obtained. When actions are performed the HAZOP is completed.

(e.g. "No flow", cause: the pipe is deformed, consequence: pump runs hot, precaution: measurement of flow with a link to the emergency or if the consequence is not critical used manual monitoring and are written into the operational procedure.)

#### 7.2 Flammable, reactive and pressurized substances and gas.

*According to the Regulations for handling of flammable, reactive and pressurized substances and equipment and facilities used for this:*

**Flammable material:** Solid, liquid or gaseous substance, preparation, and substance with occurrence or combination of these conditions, by its flash point, contact with other substances, pressure, temperature or other chemical properties represent a danger of fire.

**Reactive substances:** Solid, liquid, or gaseous substances, preparations and substances that occur in combinations of these conditions, which on contact with water, by its pressure, temperature or chemical conditions, represents a potentially dangerous reaction, explosion or release of hazardous gas, steam, dust or fog.

**Pressurized :** Other solid, liquid or gaseous substance or mixes having fire or hazardous material response, when under pressure, and thus may represent a risk of uncontrolled emissions

Further criteria for the classification of flammable, reactive and pressurized substances are set out in Annex 1 of the Guide to the Regulations "Flammable, reactive and pressurized substances"

<http://www.dsb.no/Global/Publikasjoner/2009/Veiledning/Generell%20veiledning.pdf>

[http://www.dsb.no/Global/Publikasjoner/2010/Tema/Temaveiledning\\_bruk\\_av\\_farlig\\_stoff\\_Del\\_1.pdf](http://www.dsb.no/Global/Publikasjoner/2010/Tema/Temaveiledning_bruk_av_farlig_stoff_Del_1.pdf)

Experiment setup area should be reviewed with respect to the assessment of Ex zone

- Zone 0: Always explosive atmosphere, such as inside the tank with gas, flammable liquid.
- Zone 1: Primary zone, sometimes explosive atmosphere such as a complete drain point
- Zone 2: secondary discharge could cause an explosive atmosphere by accident, such as flanges, valves and connection points

#### 7.4 Effects on the environment



With pollution means: bringing solids, liquid or gas to air, water or ground, noise and vibrations, influence of temperature that may cause damage or inconvenience effect to the environment.

Regulations: <http://www.lovddata.no/all/hl-19810313-006.html#6>

NTNU guidance to handling of waste: <http://www.ntnu.no/hms/retningslinjer/HMSR18B.pdf>

### 7.5 Radiation

Definition of radiation

**Ionizing radiation:** Electromagnetic radiation (in radiation issues with wavelength <100 nm) or rapid atomic particles (e.g. alpha and beta particles) with the ability to stream ionized atoms or molecules.

**Non ionizing radiation:** Electromagnetic radiation (wavelength >100 nm), og ultrasound<sub>1</sub> with small or no capability to ionize.

**Radiation sources:** All ionizing and powerful non-ionizing radiation sources.

**Ionizing radiation sources:** Sources giving ionizing radiation e.g. all types of radiation sources, x-ray, and electron microscopes.

**Powerful non ionizing radiation sources:** Sources giving powerful non ionizing radiation which can harm health and/or environment, e.g. class 3B and 4. MR<sub>2</sub> systems, UVC<sub>3</sub> sources, powerful IR sources<sub>4</sub>.

<sub>1</sub>Ultrasound is an acoustic radiation ("sound") over the audible frequency range (> 20 kHz). In radiation protection regulations are referred to ultrasound with electromagnetic non-ionizing radiation.

<sub>2</sub>MR (e.g. NMR) - nuclear magnetic resonance method that is used to "depict" inner structures of different materials.

<sub>3</sub>UVC is electromagnetic radiation in the wavelength range 100-280 nm.

<sub>4</sub>IR is electromagnetic radiation in the wavelength range 700 nm - 1 mm.

For each laser there should be an information binder (HMSRV3404B) which shall include:

- General information
- Name of the instrument manager, deputy, and local radiation protection coordinator
- Key data on the apparatus
- Instrument-specific documentation
- References to (or copies of) data sheets, radiation protection regulations, etc.
- Assessments of risk factors
- Instructions for users
- Instructions for practical use, startup, operation, shutdown, safety precautions, logging, locking, or use of radiation sensor, etc.
- Emergency procedures
- See NTNU for laser: <http://www.ntnu.no/hms/retningslinjer/HMSR34B.pdf>

### 7.6 The use and handling of chemicals.

In the meaning chemicals, a element that can pose a danger to employee safety and health

See: <http://www.lovddata.no/cgi-wift/ldles?doc=/sf/sf/sf-20010430-0443.html>

Safety datasheet is to be kept in the HSE binder for the experiment set up and registered in the database for chemicals.

## Chapter 8 Assessment of operational procedures.

Ensures that established procedures meet all identified risk factors that must be taken care of through operational barriers and that the operators and technical performance have sufficient expertise.

**8.1 Procedure Hazop**

Procedural HAZOP is a systematic review of the current procedure, using the fixed HAZOP methodology and defined guidewords. The procedure is broken into individual operations (nodes) and analyzed using guidewords to identify possible nonconformity, confusion or sources of inadequate performance and failure.

**8.2 Procedure for running experiments and emergency shutdown.**

Have to be prepared for all experiment setups.

*The operating procedure has to describe stepwise preparation, startup, during and ending conditions of an experiment. The procedure should describe the assumptions and conditions for starting, operating parameters with the deviation allowed before aborting the experiment and the condition of the rig to be abandoned.*

*Emergency procedure describes how an emergency shutdown have to be done, (conducted by the uninitiated),*

*what happens when emergency shutdown, is activated. (electricity / gas supply) and which events will activate the emergency shutdown (fire, leakage).*

**Chapter 9 Quantifying of RISK**

Quantifying of the residue hazards, Risk matrix

To illustrate the overall risk, compared to the risk assessment, each activity is plotted with values for the probability and consequence into the matrix. Use task IDnr.

Example: If activity IDnr. 1 has been given a probability 3 and D for consequence the risk value become D3, red. This is done for all activities giving them risk values.

In the matrix are different degrees of risk highlighted in red, yellow or green. When an activity ends up on a red risk (= unacceptable risk), risk reducing action has to be taken

|                     |               |                    |          |          |        |        |
|---------------------|---------------|--------------------|----------|----------|--------|--------|
| <b>CONSEQUENCES</b> | Catastrophic  | E1                 | E2       | E3       | E4     | E5     |
|                     | Major         | D1                 | D2       | D3       | D4     | D5     |
|                     | Moderate      | C1                 | C2       | C3       | C4     | C5     |
|                     | Minor         | B1                 | B2       | B3       | B4     | B5     |
|                     | Insignificant | A1                 | A2       | A3       | A4     | A5     |
|                     |               | Rare               | Unlikely | Possible | Likely | Almost |
|                     |               | <b>PROBABILITY</b> |          |          |        |        |

Table 8. Risk's Matrix

*Table 9. The principle of the acceptance criterion. Explanation of the colors used in the matrix*

| COLOUR | DESCRIPTION  |
|--------|--|
| Red    | Unacceptable risk Action has to be taken to reduce risk      |
| Yellow | Assessment area. Actions has to be considered                |
| Green  | Acceptable risk. Action can be taken based on other criteria |

# Attachment to Risk Assessment report

## HiFrancis Blade Cascade PIV LDY300

|                                     |   |
|-------------------------------------|---|
| <b>Project name</b>                 | PIV measurements on blade cascade for HiFrancis project |
| <b>Apparatus</b>                    | Double-Cavity High speed laser, 2*10mJ, 1000Hz, 527nm   |
| <b>Unit</b>                         | EPT   |
| <b>Equipment manager</b>            | Bård Brandåstrø   |
| <b>Project leader</b>               | Pål Tore Storli   |
| <b>HSE coordinator</b>              | Morten Grønli   |
| <b>HSE responsible (linjeleder)</b> | Therese Løvås   |
| <b>Location</b>                     | Waterpower Laboratory                                   |
| <b>Room number</b>                  | 11  |
| <b>Risk assessment performed by</b> | Magne Tveit Bolstad / Steinar Straume                   |

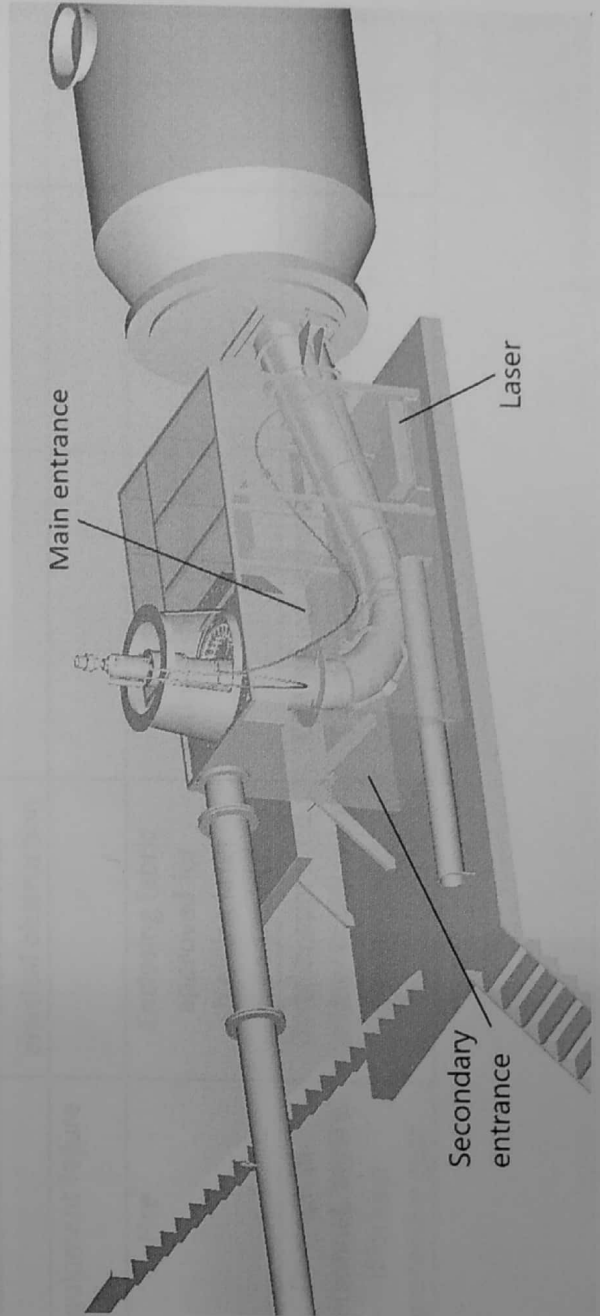
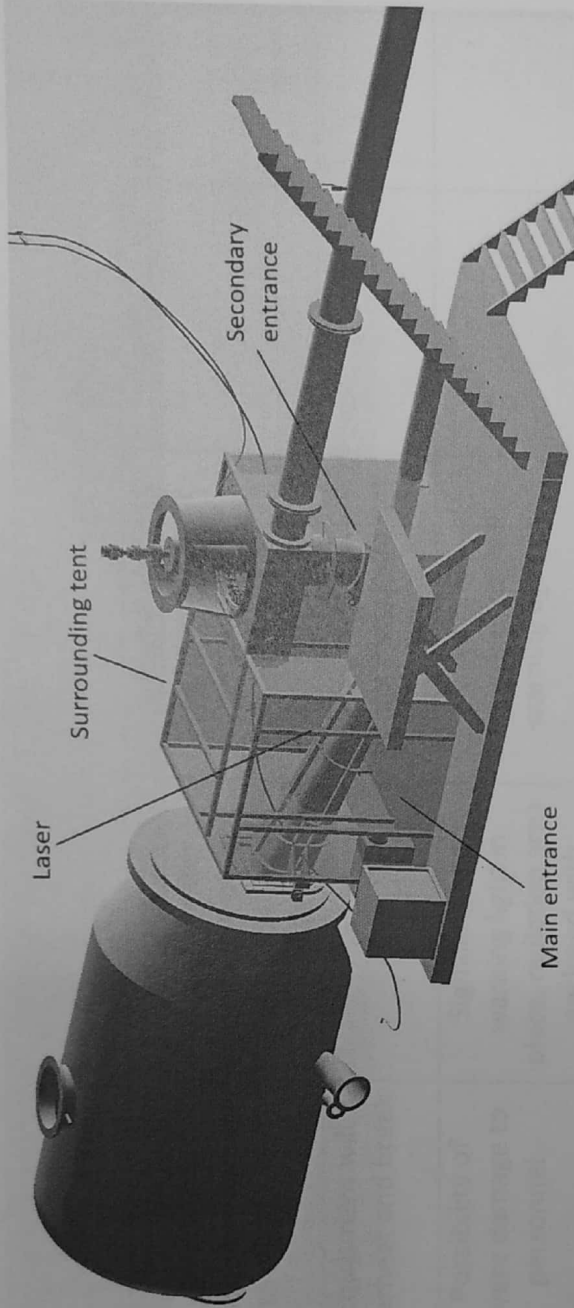
### TABLE OF CONTENTS

|   |    |
|---|----|
| ATTACHMENT A: PROCESS AND INSTRUMENTATION DIAGRAM .....         | 1  |
| ATTACHMENT B: HAZOP TEMPLATE .....                              | 2  |
| ATTACHMENT C: TEST CERTIFICATE FOR LOCAL PRESSURE TESTING ..... | 3  |
| ATTACHMENT D: HAZOP PROCEDURE (TEMPLATE).....                   | 4  |
| ATTACHMENT E: PROCEDURE FOR RUNNING EXPERIMENTS.....            | 5  |
| ATTACHMENT F: TRAINING OF OPERATORS .....                       | 7  |
| ATTACHMENT G: FORM FOR SAFE JOB ANALYSIS.....                   | 8  |
| APPARATURKORT / UNITCARD.....                                   | 10 |
| FORSØK PÅGÅR /EXPERIMENT IN PROGRESS .....                      | 11 |

**ATTACHMENT A: PROCESS AND INSTRUMENTATION DIAGRAM**

Radiation area is blocked on all sides by light-blocking fabric (this includes a roof), working as a sealed tent. The entrance is overlapping fabric.

A warning light by the entrance will activate when the laser is on.



### ATTACHMENT B: HAZOP TEMPLATE

| Project:<br>Node: Laser |   | Page   |  |  |   |        |           |
|-------------------------|---|--|--|--|---|--------|-----------|
| Ref                     | Guideword                                     | Causes   | Consequences   | Safeguards   | Recommendations                                   | Action | Date/Sign |
|                         | Unintentional rarefaction of beam             | Poor alignment of laser beam, unintentional beam obstruction | Damage to personnel, damage to equipment               | Laser emitter latched in place, radiation area enclosed                                  | Careful instrument handling                       |        |           |
|                         | Laser generation unit temperature rise        | Cooling system failure                                       | Equipment will overheat and break                      | -  | Be aware of equipment condition                   |        |           |
|                         | Unprotected personnel entering radiation area | Insufficient signalling, radiation area too accessible       | Possibility of severe damage to personnel              | Signalling and warning light in place, radiation area enclosed with physical obstruction | Always run experiments with warning light on      |        |           |
|                         | Electrical failures in apparatuses            | Wear, poor construction                                      | Equipment failure                                      |  |   |        |           |
|                         | Fire hazard                                   | Laser beam hitting flammable material                        | Fire   | Enclosing fabric approved for shielding laser experiments.                               | Make sure a fire extinguisher is easily available |        |           |
|                         | Beam interception by operator                 | Careless equipment handling, obstructed work area            | Damage to personnel, severe if lacking protective gear | Goggles approved for laser in use worn by operator                                       | Careful instrument handling                       |        |           |

**ATTACHMENT C: TEST CERTIFICATE FOR LOCAL PRESSURE TESTING**

|  |       |
|--|-------|
| Trykkpåkjent utstyr:   | Rør   |
| Benyttes i rigg:   |       |
| Design trykk for utstyr (bara):                                  | 10bar |
| Maksimum tillatt trykk (bara):<br>(i.e. burst pressure om kjent) | 10bar |
| Maksimum driftstrykk i denne rigg:                               | 10bar |


**Prøvetrykket skal fastlegges i følge standarden og med hensyn til maksimum tillatt trykk.**

|   |           |               |  |
|---|-----------|---------------|--|
| Prøvetrykk (bara):                          | 10bar     |               |  |
| X maksimum driftstrykk:<br>I følge standard |           |               |  |
| Test medium:                                | Vann      |               |  |
| Temperatur (°C)                             |           |               |  |
| Start tid:                                  | Fall 2016 | Trykk (bara): |  |
| Slutt tid:                                  | Fall 2016 | Trykk (bara): |  |
| Maksimum driftstrykk i denne rigg:          |           |               |  |

Eventuelle repetisjoner fra atm. trykk til maksimum prøvetrykk:.....

Test trykket, dato for testing og maksimum tillatt driftstrykk skal markers på (skilt eller innslått)

Trondheim      29.05.2017  
Sted og dato

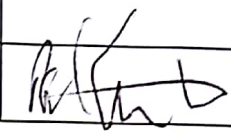
  
Signatur

### ATTACHMENT D: HAZOP PROCEDURE (TEMPLATE)

| Project Name |                                  | Page  |              |            |                 |        |           |
|--------------|----------------------------------|---|--------------|------------|-----------------|--------|-----------|
| Ref          | Guideword                        | Causes  | Consequences | Safeguards | Recommendations | Action | Date/Sign |
|              | Not clear procedure              | Procedure is to ambitious, or confusingly                               |              |            |                 |        |           |
|              | Step in the wrong place          | The procedure can lead to actions done in the wrong pattern or sequence |              |            |                 |        |           |
|              | Wrong actions                    | Procedure improperly specified  |              |            |                 |        |           |
|              | Incorrect information            | Information provided in advance of the specified action is wrong        |              |            |                 |        |           |
|              | Step missing                     | Missing step, or step requires too much of operator                     |              |            |                 |        |           |
|              | Step unsuccessful                | Step has a high probability of failure                                  |              |            |                 |        |           |
|              | Influence and effects from other | Procedure's performance can be affected by other sources                |              |            |                 |        |           |



### ATTACHMENT E: PROCEDURE FOR RUNNING EXPERIMENTS

|   |           |   |
|---|-----------|---|
| PIV measurements on blade cascade for HiFrancis project                   | Dato      | Signatur  |
| <b>Apparatur</b><br>Double-Cavity High speed laser, 2*10mJ, 1000Hz, 527nm |           |   |
| <b>Prosjektleder</b><br>Pål Tore Storli                                   | 20/8/2017 |  |

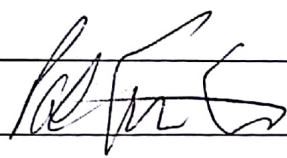
| Conditions for the experiment:   | Completed   |
|--|-------------|
| Experiments should be run in normal working hours, 08:00-16:00 during winter time and 08.00-15.00 during summer time.<br>Experiments outside normal working hours shall be approved. |             |
| One person must always be present while running experiments, and should be approved as an experimental leader.   |             |
| An early warning is given according to the lab rules, and accepted by authorized personnel.  |             |
| Be sure that everyone taking part of the experiment is wearing the necessary protecting equipment and is aware of the shut down procedure and escape routes.                         |             |
| Preparations   | Carried out |
| 1. Make sure the tent is closed.   |             |
| 2. Post the "Experiment in progress" sign.   |             |
| 3. Rotate emergency button so that it clicks in the out position.  |             |
| 4. Turn the system key to "on".  |             |
| 5. Turn the pump on in either internal or external mode.   |             |
| 6. Turn on the warning light to open this laser interlock.   |             |
| 7. Put on laser goggles.   |             |
| 8. Block the entrance to the experimental area using warning chains.   |             |
| 9. Turn the laser on in either internal or external mode.  |             |
| 10. Open the shutter when ready to operate safely.   |             |
|  |             |
|  |             |
| During the experiment  |             |
| <i>Keep unauthorized personnel out of radiation area</i>   |             |
| <i>Avoid wearing jewellery and/or shiny objects</i>  |             |
| End of experiment  |             |
| <i>Close the shutter.</i>  |             |

|  |   |  |
|--|---|--|
|  | Turn the LASER OFF.   |  |
|  | Turn the warning light off.   |  |
|  | Allow the pump to run for approximately 2 minutes to avoid excess heat to damage the equipment.                       |  |
|  | Turn the pump off   |  |
|  | Turn the system off   |  |
|  | Press the emergency button  |  |
|  | <b>To reflect on before the next experiment and experience useful for others</b>                                      |  |
|  | Was the experiment completed as planned and on scheduled in professional terms?                                       |  |
|  | Was the competence which was needed for security and completion of the experiment available to you?                   |  |
|  | Do you have any information/ knowledge from the experiment that you should document and share with fellow colleagues? |  |

**Operator(s):**

| Name                | Date     | Signature                  |
|---------------------|----------|----------------------------|
| Magne Tveit Bolstad | 21.08.17 | <i>Magne Tveit Bolstad</i> |
| Kristian Sagmo      | 21.08.17 | <i>Kristian Sagmo</i>      |
|                     |          |                            |
|                     |          |                            |
|                     |          |                            |

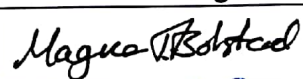
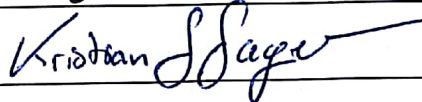
**ATTACHMENT F: TRAINING OF OPERATORS**

| Project   | Date    | Signature   |
|---|---------|---|
| PIV measurements on blade cascade for HiFrancis project                   |         |   |
| <b>Apparatus</b><br>Double-Cavity High speed laser, 2*10mJ, 1000Hz, 527nm |         |   |
| <b>Project Leader</b><br>Pål Tore Storli                                  | 20/8-17 |  |

|  |  |  |
|--|--|--|
|  | <b>Knowledge about EPT LAB in general</b>  |  |
|  | Lab <ul style="list-style-type: none"> <li>• Access</li> <li>• routines and rules</li> <li>• working hour</li> </ul> |  |
|  | Knowledge about the evacuation procedures.   |  |
|  | Activity calendar for the Lab  |  |
|  | Early warning, <a href="mailto:iept-experiments@ivt.ntnu.no">iept-experiments@ivt.ntnu.no</a>                        |  |
|  |  |  |
|  | <b>Knowledge about the experiments</b>   |  |
|  | Procedures for the experiments   |  |
|  | Emergency shutdown.  |  |
|  | Nearest fire and first aid station.  |  |

I hereby declare that I have read and understood the regulatory requirements has received appropriate training to run this experiment and are aware of my personal responsibility by working in EPT laboratories.

**Operator(s):**

| Name                | Date     | Signature  |
|---------------------|----------|--|
| Magne Tveit Bolstad | 21.08.17 |  |
| Kristian Sagmo      | 21.08.17 |  |
|                     |          |  |
|                     |          |  |
|                     |          |  |

| HSE aspect   | Yes | No | NA | Comments / actions | Resp. |
|--|-----|----|----|--------------------|-------|
| <b>Documentation, experience, qualifications</b>               |     |    |    |                    |       |
| Known operation or work?                                       | X   |    |    |                    |       |
| Knowledge of experiences / incidents from similar operations?  |     | X  |    |                    |       |
| Necessary personnel?   | X   |    |    |                    |       |
| <b>Communication and coordinating</b>                          |     |    |    |                    |       |
| Potential conflicts with other operations?                     |     | X  |    |                    |       |
| Handling of an eventually incident (alarm, evacuation)?        |     | X  |    |                    |       |
| Need for extra assistance / watch?                             |     | X  |    |                    |       |
| <b>Working area</b>  |     |    |    |                    |       |
| Unusual working position                                       |     | X  |    |                    |       |
| Work in tanks, manhole?  |     | X  |    |                    |       |
| Work in ditch, shaft or pit?                                   |     | X  |    |                    |       |
| Clean and tidy?  | X   |    |    |                    |       |
| Protective equipment beyond the personal?                      |     | X  |    |                    |       |
| Weather, wind, visibility, lighting, ventilation?              | X   |    |    |                    |       |
| Usage of scaffolding/lifts/belts/ straps, anti-falling device? |     | X  |    |                    |       |
| Work at heights?   |     | X  |    |                    |       |
| Ionizing radiation?  |     | X  |    |                    |       |
| Influence of escape routes?                                    |     | X  |    |                    |       |
| <b>Chemical hazards</b>  |     |    |    |                    |       |
| Usage of hazardous/toxic/corrosive chemicals?                  |     | X  |    |                    |       |
| Usage of flammable or explosive chemicals?                     |     | X  |    |                    |       |
| Risk assessment of usage?                                      | X   |    |    |                    |       |
| Biological materials/substances?                               |     | X  |    |                    |       |
| Dust/asbestos/dust from insulation?                            |     | X  |    |                    |       |
| <b>Mechanical hazards</b>                                      |     |    |    |                    |       |
| Stability/strength/tension?                                    |     | X  |    |                    |       |
| Crush/clamp/cut/hit?   |     | X  |    |                    |       |
| Dust/pressure/temperature?                                     |     | X  |    |                    |       |
| Handling of waste disposal?                                    |     | X  |    |                    |       |
| Need of special tools?   |     | X  |    |                    |       |
| <b>Electrical hazards</b>                                      |     |    |    |                    |       |
| Current/Voltage/over 1000V?                                    |     | X  |    |                    |       |
| Current surge, short circuit?                                  |     | X  |    |                    |       |
| Loss of current supply?  |     | X  |    |                    |       |
| <b>Area</b>  |     |    |    |                    |       |
| Need for inspection?   | X   |    |    |                    |       |
| Marking/system of signs/rope off?                              | X   |    |    |                    |       |
| Environmental consequences?                                    |     | X  |    |                    |       |
| <b>Key physical security systems</b>                           |     |    |    |                    |       |
| Work on or demounting of safety systems?                       |     | X  |    |                    |       |
| <b>Other</b>   |     |    |    |                    |       |

## APPARATURKORT / UNITCARD

**Dette kortet SKAL henges godt synlig på apparaturen!**  
*This card MUST be posted on a visible place on the unit!*

|  |  |
|--|--|
| <b>Apparatur (Unit)</b><br>PIV measurements in the vaneless space of the Francis turbine   |  |
| <b>Prosjektleder (Project Leader)</b><br>Pål Tore Storli   | <b>Telefon mobil/privat (Phone no. mobile/private)</b><br>735 92 518 |
| <b>Apparaturansvarlig (Unit Responsible)</b><br>Bård Brandåstrø  | <b>Telefon mobil/privat (Phone no. mobile/private)</b><br>918 97 257 |
| <b>Sikkerhetsrisikoer (Safety hazards)</b><br>Flashing laser light   |  |
| <b>Sikkerhetsregler (Safety rules)</b><br>-Wear appropriate safety goggles for laser wavelength<br>-No shiny objects (eg. Jewellery) worn<br>-Cover skin and wear gloves when laser is close to 100% to intensity. |  |
| <b>Nødstop prosedyre (Emergency shutdown)</b><br>Turn off laser using emergency stop or turn off warning light to the left of the tent-entrance.   |  |

**Her finner du (Here you will find):**

|                                      |                                      |
|--------------------------------------|--------------------------------------|
| <b>Prosedyrer (Procedures)</b>       | Apparaturperm i skap ved cascaderigg |
| <b>Bruksanvisning (Users manual)</b> | Apparaturperm i skap ved cascaderigg |

**Nærmeste (Nearest)**

|  |   |
|--|---|
| <b>Brannslukningsapparat (fire extinguisher)</b> | Ved inngangen til laboratoriet i 1.etg. |
| <b>Førstehjelpsskap (first aid cabinet)</b>      | Ved inngangen til laboratoriet i 1.etg. |

**NTNU**  
**Institutt for energi og prosessteknikk**

**SINTEF Energi**  
**Avdeling energiprosesser**

**Dato**

**Dato**

**Signert**

**Signert**

# FORSØK PÅGÅR / EXPERIMENT IN PROGRESS

**Dette kortet SKAL henges opp før forsøk kan starte!**  
*This card MUST be posted on the unit before the experiment startup!*

|   |  |
|---|--|
| <b>Apparatur (Unit)</b><br>PIV measurements in the vaneless space of the Francis turbine  |  |
| <b>Prosjektleder (Project Leader)</b><br>Pål-Tore Storli  | <b>Telefon mobil/privat (Phone no. mobile/private)</b><br>735 92 518               |
| <b>Apparaturansvarlig (Unit Responsible)</b><br>Bård Brandåstrø   | <b>Telefon mobil/privat (Phone no. mobile/private)</b><br>918 97 257               |
| <b>Godkjente operatører (Approved Operators)</b><br>Steinar Straume<br>Kristian Sagmo   | <b>Telefon mobil/privat (Phone no. mobile/private)</b><br>481 23 078<br>452 44 270 |
| <b>Prosjekt (Project)</b><br>PIV measurements in the vaneless space of the Francis turbine  |  |
| <b>Forsøksstid / Experimental time (start - stop)</b><br>01.06.18-01.06.2020  |  |
| <b>Kort beskrivelse av forsøket og relaterte farer (Short description of the experiment and related hazards)</b><br><br>Laser measurements with class IV laser on a Francis turbine. Danger of eye injury and skin injury. Radiation area clearly marked. The flashing laser light can cause eye damage as well as trigger epilepsy in some cases if proper goggles are not worn. |  |

**NTNU**  
**Institutt for energi og prosessteknikk**

**SINTEF Energi**  
**Avdeling energiprosesser**

**Dato**

---

**Dato**

---

**Signert**

---

**Signert**

---

# Emergency situations:

## **Eye damage:**

In the case of an accident that may have caused eye damage, the person should be sent for an examination within 24 hours of the accident.

For emergency help outside of regular work hours, call 113 or call St. Olav's hospital directly, 06800. During regular work hours, contact Occupational Health Services for referral to an eye doctor.

In the case of probable or proven chronic injury, the occupational physician should refer the employee or student to the eye doctor for an examination.

**Note that it may take some time before eye damage becomes noticeable. If there is any doubt as to whether you have been injured, contact a doctor or eye doctor.**

## **Fire:**

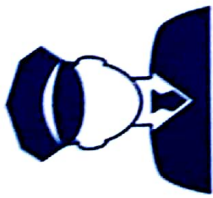
**Fire extinguishers and fire hoses are available in the laboratory, and they are clearly marked. Remove power from equipment, if possible.**

## **Shock injury:**

**A person who has suffered an electric shock may have very little external evidence of injury. It therefore important to have a check-up so that a doctor may determine if any significant unseen injury exist.**



☎ 110



☎ 112



☎ 113

## Viktige telefonnummer / Important phone numbers

NTNU vakt / NTNU Security Guards ☎ 918 97 373

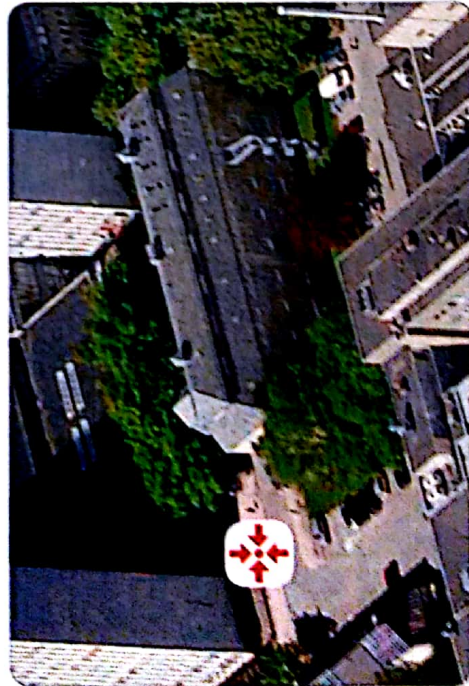
Beredskap / Emergency ☎ 800 80 388

Legevakt / Medical Emergency ☎ 116 117

Adresse / Location  
**Gatenavn**

postnummer Poststed

Møteplass / Assembly point



Bygg 324: Vannkraftlaboratoriet

Revisjonsdato: 16.mars 2018

## Branninstruks / Fire regulations



### Hvis brann oppstår

- Utløst manuell brannmelder
- Ring brannvesenets på telefon 110

### Ved alarm

- Lukk dører og vinduer
- Forlat bygningen
- Gå til møteplass
- Meld fra dersom du vet årsak til utløst alarm

### Gjør deg kjent med

- Rømningsveiene
- Nærmeste brannmelder
- Sløkkeutstyrets plassering og virkemåte

**Heis skal ikke benyttes  
ved brannalarm**



### If a fire starts

- Activate the manual fire alarms
- Call the Fire Department at tel. 110

### If the alarm sounds

- Shut doors and windows
- Leave the building
- Go to the assembly point
- Please report if you know what caused the alarm

### Make yourself familiar with

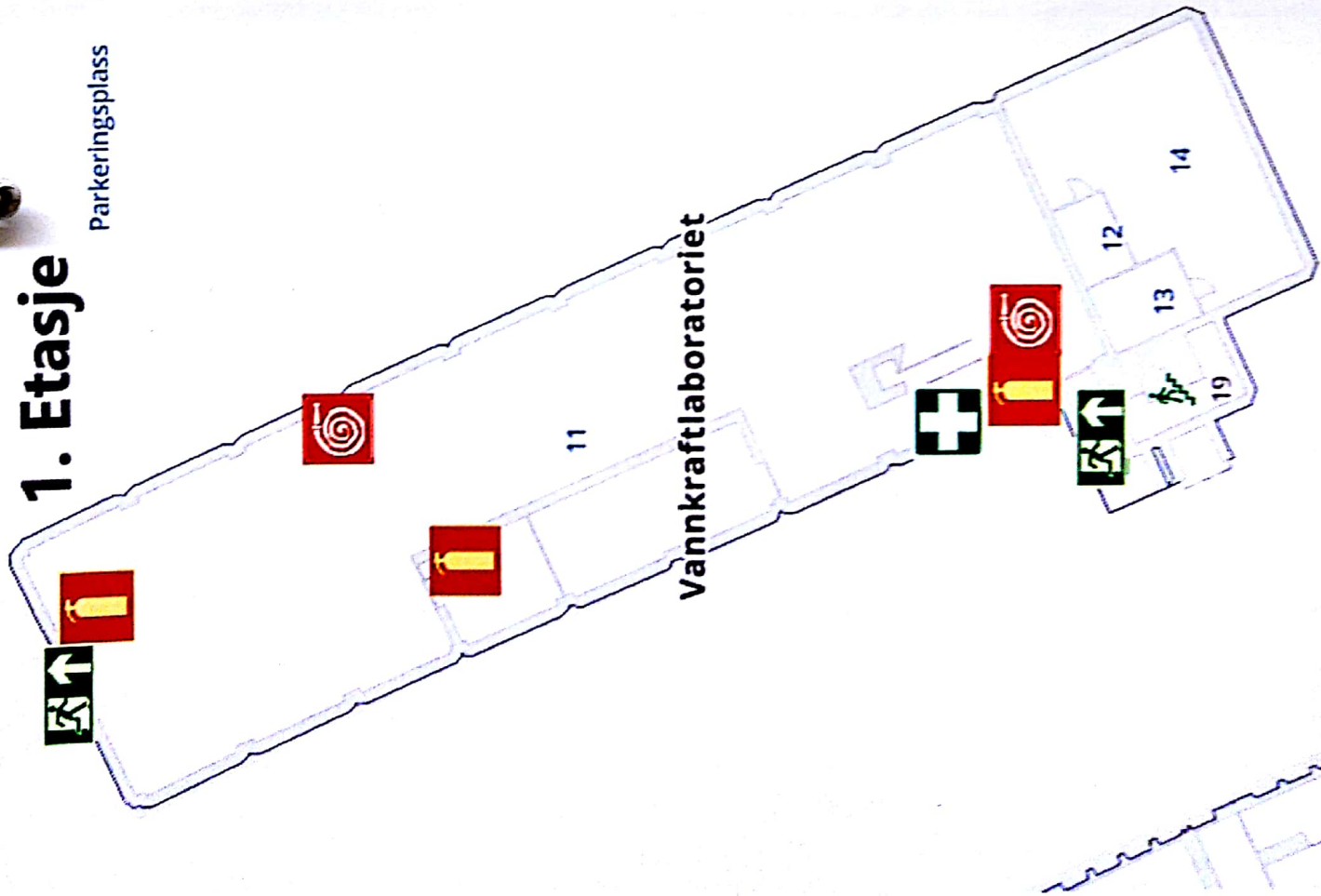
- Evacuation routes
- Nearest fire alarm
- Location of extinguishers and how they work

**Lifts must not be used  
during fire alarms**



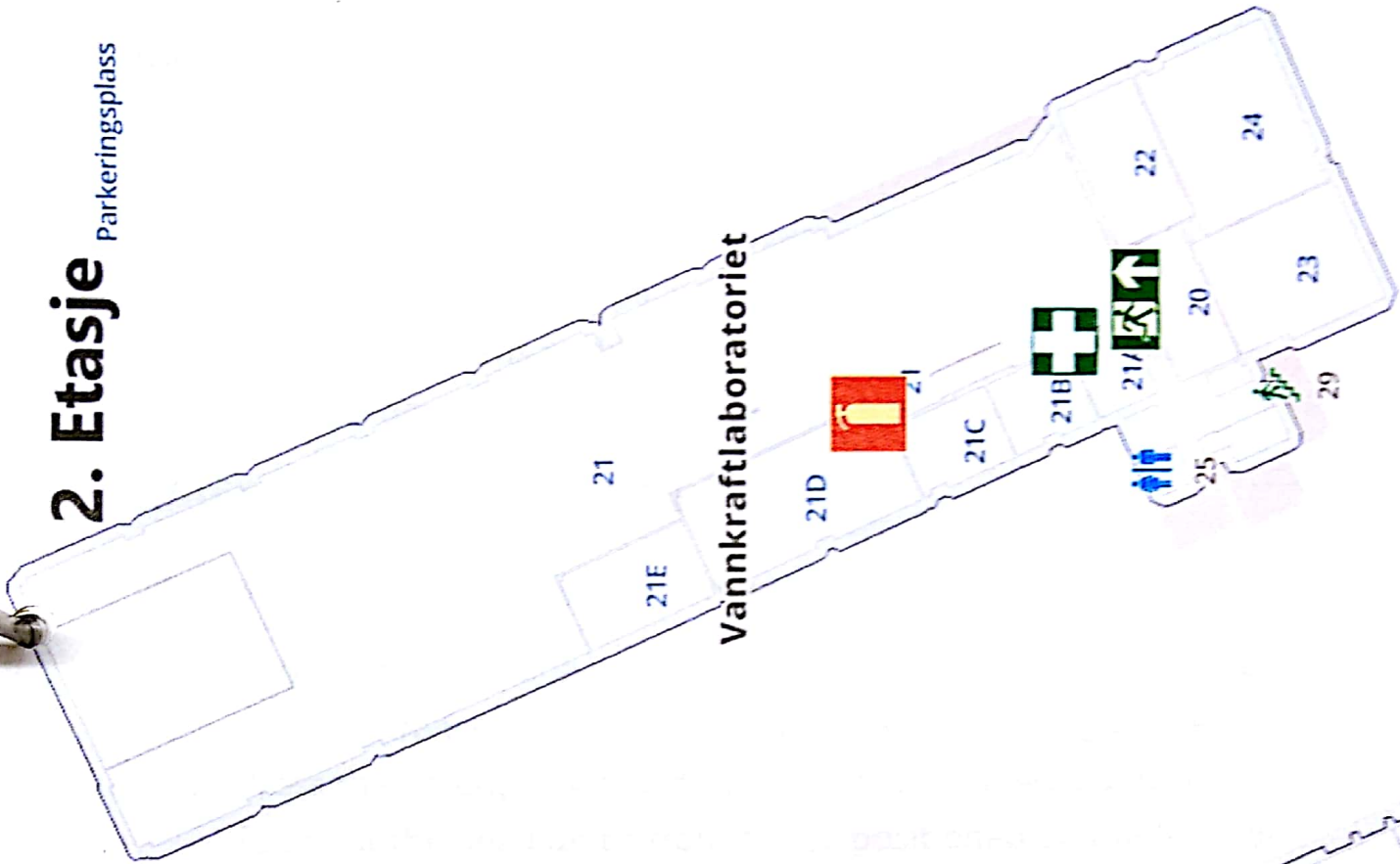
# 1. Etasje

Parkeringsplass



# 2. Etasje

Parkeringsplass



## **NØDSTOPP**



Lasersystemet kan stenges på følgende to måter:

1. Skru av varsellampen merket "Warning" ved inngangen til teltet. Knappen finnes på lysboksens høyre side.
2. Trykk inn laserens nødstop. Denne er å finne på fremsiden av laserens hovedenhet, plasser på venstre side av teltet.

## **EMERGENCY SHUTDOWN**

The laser system may be shut down in the following two ways:

1. Turn off the warning light marked "warning" to the left of the tent's entrance. The switch is found at the light's right side.
2. Press the emergency shutdown on the laser's head unit. This is found at the head unit's front panel, positioned on the left side of the tent.

|   |   |               |             |            |   |
|---|---|---------------|-------------|------------|---|
| NTNU  | Godkjenning som<br>autorisert bruker av laser<br>klasse 4 | Utarbeidet av | Nummer      | Dato       |  |
|  |   | HMS-avd.      | HMSRV-3403b | 10.04.2014 |   |
| HMS   |   | Godkjent av   | side        | Erstatter  |   |
|   |   | Rektor        | 1 av 1      | 31.03.2011 |   |

Navn: Steinar Straume

Fødselsdato: 19.09.91

Stilling/status: Masterstudent

Enhet: Vannkraftlaboratoriet

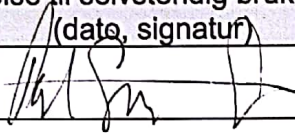
#### Autorisert bruker av laser klasse 4:

Autoriserte brukere av lasere klasse 4 skal ha tilstrekkelig kompetanse til å kunne foreta selvstendige vurderinger av sikker bruk av laserkilden. Tilstrekkelig kompetanse tilsier instrumentspesifikk kunnskap om oppstartsprosedyrer, instrumentinnstillinger, sikkerhetsanordninger, avstengning, evt. nødprosedyrer, innhold i informasjonsperm, evt. strålingsmålinger, m.m.

Vurdering av om den autoriserte brukeren har tilstrekkelig kompetanse og tillatelse til selvstendig bruk av de enkelte laserne klasse 4, gis av faglig ansvarlig.

Faglig ansvarlig gir ved signatur i tabellen under vedkommende bruker tillatelse til selvstendig bruk av de oppførte lasere/lasersystem klasse 4.

#### Oversikt over gitt tillatelse til selvstendig bruk av lasere/lasersystem klasse 4

| Laser/lasersystem      | Rom | Tillatelse til selvstendig bruk gitt av<br>(date, signatur)                                  |
|------------------------|-----|--|
| Flowmaster LDY300 PIV. | 11  | 12/4-18  |
|                        |     |  |
|                        |     |  |
|                        |     |  |
|                        |     |  |
|                        |     |  |
|                        |     |  |

Skjemaet oppbevares ved enheten i 10 år etter at vedkommende har sluttet ved NTNU. Lokal strålevernskoordinator skal ha kopi av skjemaet.